In vivo ^{13}C-MR spectroscopy for human investigations

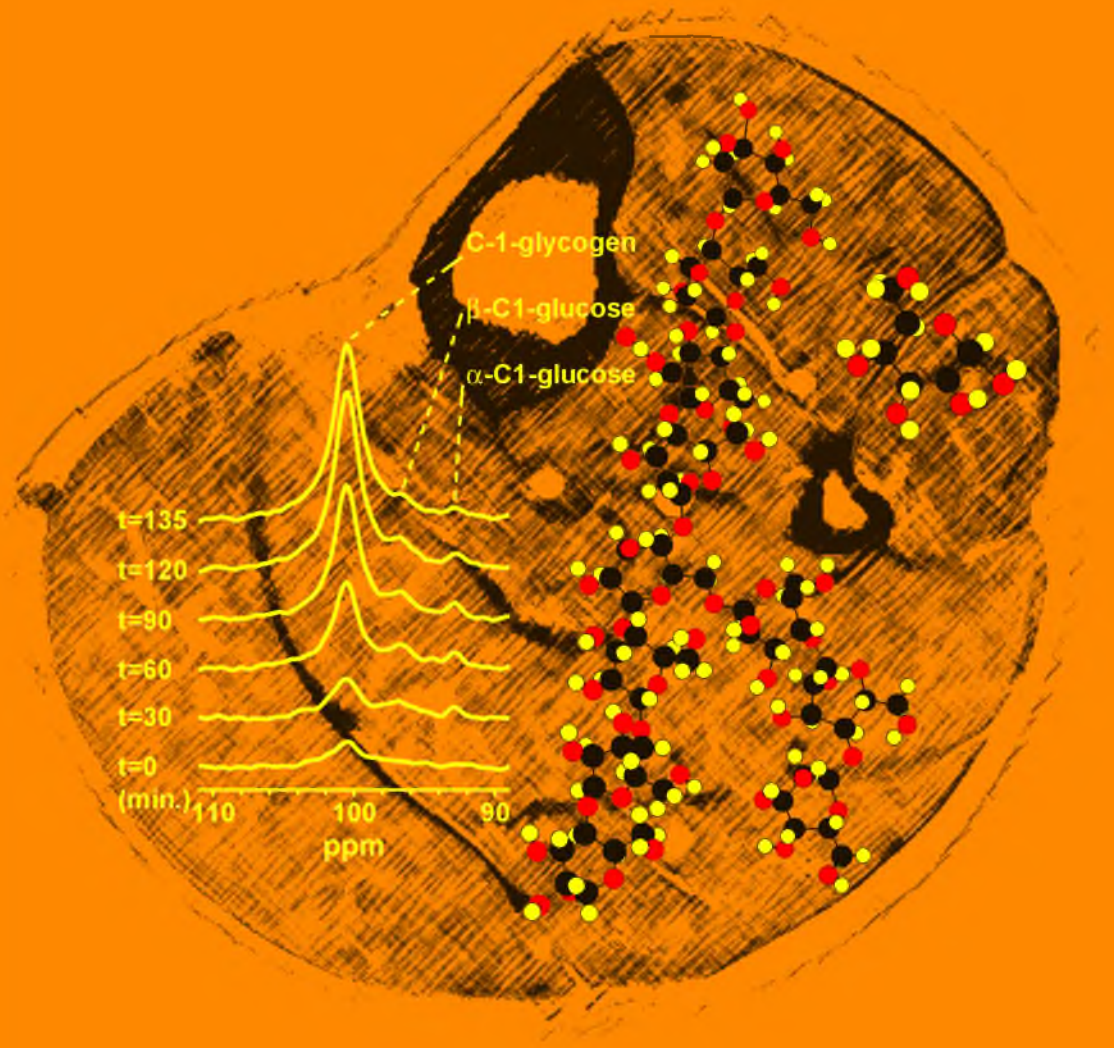

A.J. van den Bergh

Stellingen

behorende bij het proefschrift:

In vivo ^{13}C MR spectroscopy for human investigations

1. De associatie van het getal 13 met ongeluk is niet altijd terecht, het voorkomen van een koolstofvariant met 13 kerndeeltjes is voor de MR spectroscopist een geluk te noemen (dit proefschrift).

2. De toepassing van protonontkoppeling ten behoeve van humaan onderzoek kan geschieden binnen de geldende limieten voor RF depositie (dit proefschrift).

3. Op basis van temperatuur en vermogens metingen gedurende proton ontkoppeling kan geconcludeerd worden dat de richtlijnen voor specifieke absorptie ratio te conservatief zijn (dit proefschrift).

4. Signaalruisverbetering door middel van heteronucleaire polarizatie transfer geeft *in vivo* ^{13}C MR spectroscopie een meer dynamisch karakter (dit proefschrift).

5. Glucosevoeding resulteert in een sneller spierglycogeenherstel dan fructosevoeding (dit proefschrift).

6. De spierglycogeenvorming en de totale spier glucoseconcentratie tijdens een hyperinsulinemische euglycemische clamp zijn beide goede parameters voor insuline sensitiviteit (dit proefschrift).

7. Afrikaanse percussie wordt het best benaderd door de kakofonie van de gradiënten tijdens een map shim sequentie (eigen waarneming).

8. Het illegale CDcircuit zorgt niet alleen voor inkomstenderving van vele artiesten maar ook voor een grotere naamsbekendheid.

9. Bij het beklimmen van een steile heuvel met de ATB speelt niet zozeer gewicht een rol maar eerder de verdeling daarvan (eigen waarneming).

10. Door het plaatsen van meerdere spectroscopisten in één werkkamer neemt niet alleen de ruis toe, maar ook het signaal af (anonieme kamergenoot).

Nijmegen, 13 april 1999

A.J. van den Bergh

In vivo ^{13}C MR spectroscopy for human investigations

Een wetenschappelijke proeve op het gebied van de Medische Wetenschappen

Proefschrift

ter verkrijging van de graad van doctor
aan de Katholieke Universiteit Nijmegen,
volgens het besluit van het College van Decanen
in het openbaar te verdedigen
op dinsdag 13 april 1999
des namiddags te 3.30 uur precies

door

Adrianus Johannes van den Bergh
geboren op 20 oktober 1966
te Breda

Promotor: Prof. Dr. A. Heerschap

Manuscriptcommissie: Prof. Dr. J.M.F. Trijbels
Prof. Dr. C.W. Hilbers
Dr. A. Hermus

ISBN: 90 - 9012516 - 7

Financial support by:
- Glaxo Wellcome
- Campro Scientific
- Stichting Radiologisch Onderzoek Nijmegen (Rad-ON)
- Diabetes Fonds Nederland

is greatfully acknowledged.

善行無轍跡
(Lao Tzu)

Al zwervende vergaar ik
(Jan P. Strijbos)

Contents

^{18}FDG	2-fluoro-2-deoxy-D-glucose
B_0	static magnetic field
B_1	pulsed magnetic field generated by transmit coil
B_2	pulsed magnetic field generated by transmit coil 2nd RF channel
CHO	carbohydrate
CSI	chemical shift imaging
CW decoupling	continuous wave decoupling
Cyclpot-Vosing	cyclic polarization transfer - volume selective editing
DC	duty cycle
DEPT	distortionless enhancement by polarization transfer
FDA	food and drug administration
FID	free induction decay
FF	fructose feeding
G6P	glucose-6-phosphate
ge-HMQC	gradient enhanced heteronuclear multiple quantum coherence
GF	glucose feeding
GRR	glycogen recovery rate
INEPT	Insensitive Nucleus Enhancement by Polarization Transfer
ISIS	image selected *in vivo* spectroscopy
Luise	lovely user interface spectroscopy evaluation
MQF	multiple quantum filter
MR	magnetic resonance
MRI	magnetic resonance imaging
MRS	magnetic resonance spectroscopy
m-VL	muscle vastus lateralis
NIDDM	non insulin dependent diabetes mellitus
NMR	nuclear magnetic resonance
NOE	nuclear Overhauser enhancement
PET	positron emission tomography

POCE	proton observed carbon edited
ppm	parts per million
PRECISELY	PRoton Excited C-13 Image-SElected *in vivo* Localized spectroscopY
PRESS	point resolved spectroscopy
P_{90}^{sup}	power required to generate a 90° flip angle at the surface
P^{total}	power applied to coil
P^{used}	peak power applied to coil
Q_l	quality factor loaded
Q_u	quality factor unloaded
RGC	relative glycogen content
RF	radio frequency
rpm	revolutions per minute
SAR	specific absorption rate
SINEPT	sine-dependent polarization transfer
SNR	signal to noise ratio
S^{sup}	superficial specific absorption rate
S^{tis}	tissue specific absorption rate
T_1	spin lattice relaxation time
T_2	longitudinal or transverse relaxation time
Tend	end temperature reached after decoupling protocol
Tmax	maximum temperature reached during decoupling protocol
VOI	volume of interest
WALTZ	Wideband Alternating-phase Low-power Technique for Zero-residual splitting
WBGU	whole body glucose uptake
Wmax	maximum power output
W^{total}	total tissue weight within coil
γ	gyromagnetic ratio
ν	precession frequency
σ	screening factor

1 Introduction

A.J. van den Bergh

Department of Radiology, University of Nijmegen, The Netherlands

History of MR

The phenomenon of nuclear magnetic resonance (NMR) was demonstrated for the first time in 1946 independently by Bloch *et al.* and Purcell *et al.*; in 1952 they received the Nobel prize for their discovery (1, 2). The chemical shift, the property of a small but specific displacement of the resonance frequency of a particular nucleus in a different chemical compound made NMR to one of the most powerful analytical tools in chemistry and biochemistry. Since the 1950's NMR is used as a tool for studying chemical structure, configuration, and chemical reaction processes.

In 1973, it was Lauterbur, who gave the first demonstration of the concept of magnetic resonance imaging (3). Pictures of fruit, animals and finally humans were obtained later during the 70's. In the same period Hoult *et al.* reported in 1974 on the application of NMR spectroscopy to intact, freshly excised muscle from the leg of a rat (4). More studies followed on the isolated heart, liver and other organs. Subsequently, the logical step from these tissue studies to *in vivo* NMR spectroscopy of whole animals was made (5).

Since the first commercial MR scanners for human examinations became available around 1981, both magnetic resonance imaging (MRI), and *in vivo* magnetic resonance spectroscopy (MRS) rapidly evolved. MRI has become a major imaging modality in radiology. Besides the use of MRI as a tool to study the internal anatomy of the body, it has also been used to obtain functional

information; i.e. of brain activity, several recent review articles have summarized the current status on this topic (6-9).

With MRS one can have access to physiology and biochemistry of living human tissue. The biochemical status of the human body can be assessed in a non-invasive manner, which makes it possible to perform longitudinal examinations to study the dynamics of biochemical processes in the human body.

Basics of MR

A nucleus is composed of protons and neutrons. These nucleons have spins, and the spin of a nucleus as a whole is the vector sum of the spins of the individual nucleons. This vector sum varies from one nucleus to another, and depends on the way nucleons are coupled to each other. If this vector sum is not equal to zero, than the nucleus has a magnetic moment. A nucleus that possess a magnetic moment can be used to perform an NMR experiment. The hydrogen atom ^{1}H, with one proton in its nucleus is one of the most important nuclei in biological MR.

Without the presence of an external magnetic field the spins of these nuclei are randomly oriented, so there will be no net magnetization. In the presence of a magnetic field, the nuclei will align parallel or anti-parallel along the applied field axis. The parallel orientation has a slightly lower energy state, therefore more nuclei will align parallel and produce a net magnetic moment (macroscopic magnetization).

This magnetic moment is not exactly aligned with the external magnetic field but it precesses around it. The frequency with which it precesses is given by the Larmor equation.

$$\nu_0 = \gamma B_0/2\pi \qquad [1]$$

In which γ is the gyromagnetic ratio (dependent on the type of nucleus), B_0 is the strength of the applied external magnetic field, and ν_0 is the frequency of precession (Larmor frequency). Both γ and B_0 determine the energy difference

between the parallel and anti parallel states. A higher energy difference (higher product of γB_0) leads to a larger population difference between the states, and thus to a proportionally higher sensitivity. This is one of the reasons why MR spectroscopists keep buying more powerful magnets. Another advantage is the improved spectral resolution at higher field strengths. This can be explained by looking at equation 2.

$$\nu = \gamma(B_0 - \sigma B_0)/2\pi \qquad [2]$$

The screening factor σ is introduced, it depends on the chemical environment of each nucleus. From the equation it is clear that the frequency ν is proportional the external magnetic field B_0. The effect of γ on the frequency is large compared to the effect of σ. So resonance frequencies differ strongly going from one nuclear species to another, and slight differences occur within one nuclear species, these differences in frequency depending on the chemical environment are called chemical shift.

In order to create an MR image or spectrum, the resonance condition must be fulfilled. There must be a situation of alternating absorption and dissipation of energy. By applying a radio frequency (RF) magnetic field at the Larmor frequency “on resonance”, the nuclei can be placed in a higher energy state by the absorption of the RF energy. When returning back to the low energy state, the spins emit RF energy to the environment, which can be picked up by a receiver coil. The application of different RF pulses and RF acquisition schemes in combination with the use of magnetic field gradients can result in MR images or spectra.

Isotopes of interest for clinical *in vivo* MR spectroscopy

The atomic nuclei that are potentially useful for biomedical *in vivo* MR spectroscopy applications are given in table 1. with their MR related properties.

Brief descriptions of the most commonly applied nuclei for *in vivo* MR spectroscopy studies are given below.

^{1}H: this nucleus has almost 100% natural abundance and is present in most biochemicals. It has the highest intrinsic sensitivity of all stable nuclei, and it is therefore a very interesting nucleus for *in vivo* MR spectroscopy. Some important metabolites detectable by ^{1}H MR spectroscopy are: choline compounds, citrate, creatine, glutamate, glutamine, lactate, myo-inositol and N-acetyl-aspartate. It has two drawbacks, the limited chemical shift range and the need for water and lipid signal suppression. Its main applications are in brain, muscle and prostate spectroscopy. (10-13)

^{31}P: phosphorus has a 100% natural abundance and a reasonable sensitivity. It is very suitable for the study of high energy phosphate metabolites and other phosphorus containing metabolites such as phospho mono- and di-esters. Applications of *in vivo* ^{31}P MR spectroscopy are in the study of muscle, cardiac, and brain metabolism and also in monitoring tumor therapy (14-24). Besides the study of metabolites, ^{31}P MR spectroscopy can be used as a noninvasive technique to monitor the intracellular pH (25-27).

^{13}C: ^{13}C has only 1.1% natural abundance (^{12}C has an occurrence of over 98% and no magnetic moment) and a low intrinsic sensitivity. It can be detected in a large number of biochemically important compounds in a broad spectral range. Furthermore, the ability to use selectively enriched substrates for the study of metabolic pathways makes this nucleus interesting for *in vivo* applications.

^{19}F: the abundance of the ^{19}F nucleus is 100% and its sensitivity almost equals that of protons. Because of its presence in tumor therapeutics, this nucleus has a particular clinical interest (28-33).

In spite of the low sensitivity of ^{13}C, this nucleus is very well suited for obtaining biochemically important information. This thesis is focused on the application of *in vivo* ^{13}C MR spectroscopy in human investigations. In the next sections, the current status of human *in vivo* ^{13}C MR spectroscopy is reviewed.

Nucleus	Spin	$\gamma/2\pi$ (MHz/Tesla)	Natural Abundance (%)	Sensitivity vs. ^{1}H
^{1}H	$^{1}/_{2}$	42.57	99.98	1
^{13}C	$^{1}/_{2}$	10.71	1.108	0.00025
^{14}N	1	3.08	99.63	0.0019
^{15}N	$^{1}/_{2}$	-4.31	0.37	0.0000068
^{17}O	$^{5}/_{2}$	-5.77	0.037	0.000019
^{19}F	$^{1}/_{2}$	40.05	100	0.85
^{23}Na	$^{3}/_{2}$	11.26	100	0.13
^{31}P	$^{1}/_{2}$	17.24	100	0.83
^{39}K	$^{3}/_{2}$	1.99	93.1	0.001

Table 1.

Spin, gyromagnetic ratios, natural abundance and relative sensitivity compared to proton, of biological interesting nuclei.

Human metabolism studied by *in vivo* ^{13}C MR spectroscopy

Natural abundance:

Natural abundance ^{13}C MR spectroscopy is limited to highly concentrated compounds such as triglycerides and glucose units in glycogen, because of the low intrinsic sensitivity of this technique.

The resonances of triglycerides are dispersed over a broad spectral range. Signals that co-resonate in the ^{1}H spectrum can be resolved in the ^{13}C spectrum, which makes ^{13}C the favorable technique for the study of triglycerides, despite its lower sensitivity. Special interest goes to the degree of saturation of lipids (34). It has been shown that in neonatal development the amount of unsaturated fatty acids increase with maturity (35). In this study similar differences were found for

gestational age. Preterm infants showed a relatively lower unsaturated fatty acid content compared to full term infants. The relation between diet and adipose tissue fatty acid composition was also studied. The ratio of unsaturated to total fatty acid composition in adipose tissue correlated with the same ratio as in diet fat, after a minimal diet period lasting half a year (36). Another study revealed differences in the adipose tissue composition of vegans compared to vegetarians and omnivores (37). Vegans showed a higher level of unsaturated fatty acids. Differences in the degree of saturation of fatty acids were reported of carcinoma compared to non-cancerous tissue of human breast (38). The comparison of cystic fibrosis patients with healthy volunteers by *in vivo* ^{13}C MR spectroscopy revealed a difference in the amount of polyunsaturated fatty acid content (39).

More challenging in natural abundance *in vivo* ^{13}C MR spectroscopy is the detection of metabolites such as glycogen, creatine, citrate, myo-inositol. Jue *et al.* demonstrated that the C-1 signal of glycogen is observable in humans, the other glycogen signals are less well resolved (40). ^{13}C MR spectroscopy has emerged as an appropriate noninvasive alternative for biopsy methods for the detection of muscle glycogen (41). Several studies report on muscle glycogen depletion and repletion after exercise (42-48). Price *et al.* investigated the glycogen resynthesis after depletion and found an insulin dependent and insulin independent phase after depletion up to 25% (45). Other studies focused on the glycogen resynthesis with carbohydrate intake during the recovery period (46-48). Glucose feeding during recovery resulted in a faster resynthesis rate compared to fructose ingestion (47).

Natural abundance detection of glycogen is also possible *in vivo* in the human liver (42, 49-53).

A more clinical application of the study of glycogen metabolism is in glycogen storage disease, in which muscular or liver glycogen content can be studied non-invasively by natural abundance ^{13}C MR spectroscopy (54-57).

Other potentially clinical important metabolites that can be detected by *in vivo* natural abundance ^{13}C MR spectroscopy are citrate (58), myo-inositol (59-61) and creatine (42, 47, 62).

^{13}C labeling:

One can benefit from the low natural abundance of the ^{13}C nucleus in the human body and that is by the application of selectively ^{13}C enriched substrates. After the administration of ^{13}C labeled substrates the observation of the applied label and its metabolic intermediates or end products can be used to study fluxes through metabolic pathways. These techniques can be applied to study brain, liver and muscle metabolism.

Beckmann *et al.* demonstrated in 1991 that labeled C-1 glucose and its labeled metabolic products C-2, C-4 and C-3 glutamate/glutamine and lactate could be detected in the human brain *in vivo* during hyperglycemic glucose clamping (63). In the same year, it was shown by ^{1}H detected ^{13}C MR spectroscopy that glucose was actively metabolized to lactate in a patient with a 32 day old cortical infarct (64). Glucose steady state concentrations and glucose transport activity into the brain were also determined with the use of labeled ^{13}C-1-glucose in combination with *in vivo* brain MR spectroscopy (65, 66). Other *in vivo* brain MR spectroscopy studies demonstrated that this technique can provide more information than positron emission tomography (PET) regarding the metabolic processes beyond the uptake of glucose into the brain, the metabolic flux from glucose to glutamate could be followed (67, 68). Using a mathematical model, several metabolic rates for the human neocortex could be determined from *in vivo* ^{13}C MR spectroscopy data (69). Shulman *et al.* discussed the role of MR spectroscopy and other MR techniques in the study of brain function (70).

The incorporation of labeled C-1-glucose has also been studied in the liver (71, 72). It was demonstrated that liver glycogen synthesis and breakdown occur simultaneously during net glycogen synthesis (73). Studies comparing healthy subjects with patients with poorly controlled insulin dependent diabetes mellitus

(NIDDM) demonstrate that these patients have an increased hepatic gluconeogenesis and relative decreased rates of hepatic pyruvate oxidation (74). The fate of infused labeled ^{13}C-1-glucose in muscle tissue is important in the study of exercise and diabetes. In 1989, Jue *et al.* showed that under conditions of hyperglycemia and hyperinsulinemia, a majority of the infused glucose was converted to muscle glycogen in normal man (76). Using the same method it was shown that defects in muscle glycogen synthesis have a dominant role in the insulin resistance that occurs in patients with NIDDM (77). It was demonstrated that the degradation and synthesis of muscle glycogen can occur simultaneously during prolonged low-intensity exercise (75). Combined ^{13}C / ^{31}P MR spectroscopy suggests that the post-transport steps do not play a significant role in the control of muscle glucose disposal, and that glucose transport/hexokinase activity maybe impaired in patients with NIDDM (78-81). Similar conclusions were drawn for insulin resistant obese subjects (82).

All of the human *in vivo* ^{13}C MR spectroscopy studies mentioned above used labeled glucose as a substrate for infusion. There is a great potential in the use of other labeled compounds as currently in use in *in vivo* animal studies or isolated organ studies. For example to study the pharmacology of certain types of drugs (83-86). Also the use of multi-labeled compounds can be of clinical interest because of the additional information that can be obtained due to the spin spin interaction of adjacent ^{13}C nuclei (87-90).

In vivo ^{13}C MR spectroscopy: double resonance

Most of the metabolites studied by *in vivo* ^{13}C MR spectroscopy have attached protons. The spin spin interaction that exists between neighboring ^{1}H and ^{13}C nuclei results in a multiplet splitting in the ^{13}C spectrum. The multiplet structure obtained in the ^{13}C spectrum is dependent on the number of attached protons to the ^{13}C nucleus. If the number of attached protons equals n, than the multiplet consists of n+1 peaks, thus information about the molecular structure can be

obtained. However, these multiplets complicate spectrum analysis and decrease sensitivity. In order to utilize the full potential of *in vivo* ^{13}C MR spectroscopy it is necessary to remove these ^{1}H-^{13}C multiplet splittings by proton decoupling during the ^{13}C signal acquisition period. The spectrum obtained with ^{1}H decoupling is simplified and sensitivity is enhanced by gathering all the intensity of a multiplet into a singlet.

^{1}H-^{13}C decoupling and other double resonance techniques require some special hardware which is not standard installed on a clinical imaging system, such as a second radio frequency channel, filters to ensure signal separation and a dual frequency high sensitivity coil (see below).

The application of a radio frequency decoupling field for *in vivo* studies in humans is of concern since it could lead to tissue heating (91). At the present time, two levels of concern are issued by the US Food and Drug Administration (FDA): guidelines for specific absorption rate (SAR) and temperature increase induced by RF (92).

Selective decoupling of a single proton frequency requires minimal energy, this method is often applied for the detection of the C-1 resonance of glycogen in liver and muscle (43, 49). This approach is very useful if one is interested in one particular metabolite signal, other signals present in the spectrum remain proton coupled.

Broadband proton decoupling results in higher SAR levels, but it may help to reveal additional metabolite signals and to uncover resonances otherwise obscured by the intense triglyceride signals. Studies performed at the clinical field strength of 1.5T indicate that broadband proton decoupling using WALTZ sequences is possible within FDA guidelines (42, 54). Broadband decoupling at higher field strength requires more power, not only because of the broader chemical shift range to be covered, but also due to the higher frequency (f), according to Röschmann [SAR] $\propto f^{2.145}$ (93). Bomsdorf *et al.* suggested that broadband proton decoupling at 4T would violate safety guidelines (51). Recently, Gruetter *et al.* demonstrated the possibility of broadband proton

decoupling at 4T using a quadrature proton coil (94, 95). For these measurements at 4T the relationship between SAR and frequency holds true. However, recently this relationship has been refuted for ultra high magnetic field strengths on a whole body 8T system (96).

The RF field inhomogeneity of surface coils leads to an inefficient use of RF power required for decoupling (97, 98). B_2 insensitive hyperbolic secant pulses used for decoupling can result in lower SAR values for broadband decoupling compared to WALTZ type sequences (99, 100).

Application of a decoupling RF field can also result in Nuclear Overhauser Enhancement (NOE), so sensitivity is further improved. The effect of NOE and decoupling were investigated for phantoms and lipid tissue of the human calf and breast (101). Bi-level irradiation for optimal NOE and decoupling as used in *in vivo* ^{31}P MR spectroscopy are not often used in ^{13}C MR spectroscopy because of the increased SAR level (102, 103).

Another means of signal enhancement by double resonance techniques is transfer of polarization. Polarization transfer from ^{1}H to ^{13}C can result in a signal enhancement of $\gamma^{1}H/\gamma^{13}C \approx 4$. The highest possible signal can be obtained when excitation and detection are performed on the sensitive proton nucleus, this is the so-called indirect detection, enhancements of $(\gamma^{1}H/\gamma^{13}C)^{5/2} \approx 32$ can be achieved theoretically. Only a limited number of studies report on indirect detection of ^{13}C in humans *in vivo*. Knüttel *et al.* demonstrated that indirect detection of the unsaturated fatty acid carbon signals and glycogen is possible *in vivo* using Cyclpot-Vosing (104, 105). This volume selective technique is based on multiple-quantum filtering (MQF) and cyclic polarization transfer. Indirect detection was also applied in the study of labeled compounds in normal brain metabolism and in a patient with stroke (64, 67). A modified proton observe carbon edited (POCE) sequence was recently used for the natural abundance detection of brain N-acetyl aspartate (106). As for the use of labels, the development in techniques is ahead in animal studies. A very promising technique which has yet only been applied *in vivo* in cat brain to monitor ^{13}C-1-

glucose and its metabolites is the gradient-enhanced heteronuclear multiple quantum coherence (ge-HMQC) technique (107).

As shown by the studies mentioned above, indirect detection offers high sensitivity, but it also has some disadvantages, it requires a good water suppression and it has a lower resolution compared to detection at the carbon nucleus.

Several methods are in use for the transfer of polarization from ^{1}H to ^{13}C for sensitivity enhancement. The sine-dependent polarization transfer (SINEPT) technique was applied to humans *in vivo* for the detection of glycogen and fatty acid resonances (108, 109). This sequence requires no 180° pulses and due to its sequential arrangement of RF pulses it can be implemented on a single-channel MR system. Distortionless enhancement by polarization transfer (DEPT) has also been applied *in vivo* to humans (95, 110). First attempts of Insensitive Nucleus Enhancement by Polarization Transfer (INEPT) were shown by Kreis *et al.* (111). An alternative approach, not based on pulse interrupted free precession, but by which transfer of magnetization is achieved by heteronuclear isotropic mixing, has recently been reported to be feasible in animals and humans (112, 113). An adiabatic variant of this heteronuclear cross polarization has been proposed for *in vivo* applications (114).

These recent developments and improvements in double resonance *in vivo* ^{13}C MR spectroscopy will facilitate the applications of these techniques in the clinical situation. Due to these developments a debate started comparing ^{18}FDG PET with ^{13}C-glucose MR spectroscopy (115, 116). Both techniques have their advantages and disadvantages and it is the research question that should determine the technique of choice.

Radio Frequency coils for *in vivo* ^{13}C MR spectroscopy

Radio frequency coils are used for transmitting and/or receiving. A crucial problem for *in vivo* ^{13}C MR spectroscopy applied to humans is the need for

proton decoupling with limited RF deposition so that safety guidelines are not exceeded. To perform a ^{13}C *in vivo* experiment, a coil configuration is required with the highest possible sensitivity for ^{13}C, and an efficient ^{1}H coil for decoupling, while interactions between coils must be minimized.

Therefore, surface coils are often used for ^{13}C because of their good filling factor which yields a good signal to noise ratio. In addition, these types of coils allow a crude form of localization because of their inhomogeneous B_1 field. For the proton decoupler coil several arrangements are possible in combination with the carbon surface coil. A circular concentric coplanar configuration with a inner ^{13}C coil and an outer ^{1}H coil has been used in several studies (49, 54, 101, 117). A problem that arises with these type of coils is the strong interaction between the coils, the RF of the proton coil is partially blocked by the ^{13}C inner coil which can result in excessive power requirements for decoupling.

To reduce coil interactions, an orthogonal arrangement can be used. Figure-8 and butterfly shaped coils are reported to obtain orthogonality in coil configurations (42, 47, 109, 118). The rapidly decreasing B_2 field along the ^{13}C coil axis can result in high local SAR values which is of concern with human application (98).

Alternatively, double tuned coils can be used which lack the blockage of the proton RF (119). Another advantage of these type of coils is the matching of the RF fields which is important in polarization transfer techniques (112). A disadvantage of double tuned coils is that it is difficult to achieve optimal performance for both nuclei and sufficient channel separation.

A more recent development, is a quadrature proton coil combined with a circular ^{13}C coil (94). This coil combines the two important properties of a high sensitivity for ^{13}C and an efficient proton decoupling.

Volume coils provide a homogeneous RF field and are therefore interesting for polarization transfer experiments. A combination of a volume proton coil with a ^{13}C surface coil was used for polarization transfer by SINEPT (108). A birdcage transmit coil in combination with a double tuned surface receiver coil was used in

the VOSING technique (104). Heteronuclear cross polarization was performed with a combination of a birdcage proton coil and a half volume ^{13}C coil (113).

Spatial localization for ^{13}C MRS

As mentioned above, surface coils provide excellent signal to noise ratios and a crude form of localization. However, the volume sampled by a surface coil is not well defined. Therefore, additional techniques are required to obtain spectra from a volume of interest (VOI), without contamination with signal from outside the selected VOI.

In *in vivo* ^{13}C MR spectroscopy the intense signals originating from superficial lipid tissue are often unwanted. Suppression of these signals from outside the VOI can be performed in several ways. A simple method is by the application of a rectangular pulse with a high flip angle 180°- 200° in the plane of the surface coil (54). An alternative for this method is the use of an adiabatic rapid half passage excitation preceded by a low flip angle rectangular pulse followed by a dephasing gradient (42, 47). Tailored pulses for the detection of wanted signals and suppression of unwanted can also be used (49).

In the above described techniques the VOI is not sharply delineated, only unwanted signals form the surface are suppressed. A well defined VOI can be obtained by the application of frequency selective RF pulses in combination with B_0 gradients. ISIS (image selected *in vivo* spectroscopy) (120) is a suitable single voxel technique for ^{13}C because T_2 relaxation losses are limited, another advantage is that signals are not adversely affected by J modulation as in spin-echo sequences. ISIS was successfully used to obtain a 3D localized spectrum of the human brain (59). Due to the large chemical shift range of the ^{13}C nucleus a chemical shift displacement error occurs when the technique of frequency selective excitation in combination with a B_0 gradient is applied for localization. In localization by chemical shift imaging (CSI), this chemical shift displacement error is much smaller (121). Another advantage of CSI is that multiple voxels are

obtained within a single measurement. The use of ^{13}C 1D CSI was demonstrated *in vivo* in humans (122). The detection of myo-inositol in the human brain was performed by ^{13}C 3D CSI, showing that low concentrated compounds can be detected in a well defined volume (61).

Another way to circumvent the large chemical shift displacement error in ^{13}C MR spectroscopy is by excitation of the ^{1}H nucleus followed by polarization transfer to ^{13}C. In this way, the precise localization on ^{1}H, the signal gain by polarization transfer and the high spectral resolution of the ^{13}C nucleus are combined. Using this approach, localized spectra of the human calf muscle could be obtained (110). Gruetter *et al.* used localization based on ISIS, followed by DEPT polarization transfer on the human brain, the acronym PRECISELY is proposed (PRoton Excited C-13 Image-SElected *in vivo* Localized spectroscopY) (95). Kreis *et al.* demonstrated that the combination of PRESS and INEPT was feasible (111). Indirect detection methods (see double resonance section) also allow for the precise localization via the ^{1}H nucleus.

Quantification

In *in vivo* ^{13}C MR spectroscopy often relative changes of metabolite levels are monitored. However, in many cases absolute quantification of metabolite levels is desired. Absolute quantification can be performed by using an external reference solution of known concentration. Taylor *et al.* compared muscle glycogen concentrations obtained with MR using external referencing with biopsy results and demonstrated a high accuracy for the MR spectroscopy determination (41). Absolute quantification by comparing data with a phantom has been demonstrated to be feasible for brain myo-inositol (59), for muscle glucose (80) and liver glycogen (57).

Tissue concentration determination of metabolites can also be made by internal referencing, using a biochemical compound of known concentration. The advantage of this method is that the reference signal originates from the same

volume. The compounds under study should be homogeneously distributed over the tissue and completely MR visible. Creatine was used as an internal reference to quantify muscle glycogen (47, 123)

Absolute quantification of metabolites is difficult in spectra obtained with polarization transfer techniques. Whether an internal or external reference is used, the efficiency of polarization transfer of the metabolite under study and of the reference must be known exactly, *in vivo* efficiency levels are difficult to obtain.

Research goals

For clinical acceptance of *in vivo* ^{13}C MR spectroscopy it is important that techniques for data collection and analysis become possible in the clinical environment. Nearly all the research in *in vivo* ^{13}C MR spectroscopy on humans has been performed on experimental MR systems at high magnetic field strengths > 2T. However, the standard clinical MR system, available in most clinical research institutes operates at 1.5T. The work presented in the next chapters was performed on a modified clinical imaging system; equipped with a second RF transmit channel. The main purposes of the current work are: 1) to optimize the ^{13}C MR spectroscopy technique for human applications while ensuring patient safety; 2) to explore the utilization of this technique in human physiology and pathology related to glycogenesis.

Outline of this thesis

chapter 2: A method was developed to optimize decoupling power settings for surface coils by which RF deposition in the body could be reduced. Information obtained by this method was also used to calculate the amount of energy deposited in the tissue at the position of the highest RF field.

Chapter 3: The thermoregulatory response of the skin was investigated during exposure to RF radiation with a surface coil at several power levels. The skin temperature of the calf muscle was monitored in healthy male subjects.

Chapter 4: The potential of heteronuclear cross polarization was investigated. Phantom studies were performed, and *in vivo* studies on the human leg and on a neonatal piglet brain. The latter study was performed in combination with the introduction of labeled ^{13}C-1-glucose.

Chapter 5: Glycogen recovery rates were studied in healthy male subjects after depletion. A comparison was made between glucose and fructose feeding during the recovery period.

Chapter 6: Insulin stimulated glycogenesis in muscle was studied in subjects ranging from insulin sensitive to insulin resistant, by the combination of *in vivo* ^{13}C MR spectroscopy and infusion of ^{13}C labeled glucose. In addition, the effect of treatment with troglitazone on insulin resistance was investigated.

References

1. E. M. Purcell, H. C. Torrey, R. V. Pound, Resonance absorption by nuclear magnetic moments in a solid. *Phys. Rev.,* **69,** 37-38, (1946).
2. F. Bloch, W. W. Hansen, M. Packard, The nuclear induction experiment. *Phys. Rev.,* **70,** 474-485, (1946).
3. P. C. Lauterbur, Image formation by induced local interactions: examples employing nuclear magnetic resonance. *Nature,* **242,** 190-191, (1973).
4. D. I. Hoult, S. J. Busby, D. G. Gadian, G. K. Radda, R. E. Richards, P. J. Seeley, Observation of tissue metabolites using 31P nuclear magnetic resonance. *Nature,* **252,** 285-287, (1974).
5. J. J. Ackerman, T. H. Grove, G. G. Wong, D. G. Gadian, G. K. Radda, Mapping of metabolites in whole animals by 31P NMR using surface coils. *Nature,* **283,** 167-170, (1980).

6. S. G. Kim, K. Ugurbil, Functional magnetic resonance imaging of the human brain. *J. Neurosci. Methods,* **74,** 229-243, (1997).
7. P. A. Bandettini, E. C. Wong, Magnetic resonance imaging of human brain function. Principles, practicalities, and possibilities. *Neurosurg. Clin. N. Am.,* **8,** 345-371, (1997).
8. S. Rabe-Hesketh, E. T. Bullmore, M. J. Brammer, The analysis of functional magnetic resonance images. *Stat. Methods. Med. Res.,* **6,** 215-237, (1997).
9. S. Ogawa, R. S. Menon, S. G. Kim, K. Ugurbil, On the characteristics of functional magnetic resonance imaging of the brain. *Annu. Rev. Biophys. Biomol. Struct.,* **27,** 447-474, (1998).
10. F. A. Howe, R. J. Maxwell, D. E. Saunders, M. M. Brown, J. R. Griffiths, Proton spectroscopy in vivo. *Magn.Reson.Q.,* **9,** 31-59, (1993).
11. B. D. Ross, S. Bluml, R. Cowan, E. Danielsen, N. Farrow, R. Gruetter, In vivo magnetic resonance spectroscopy of human brain: the biophysical basis of dementia. *Biophys. Chem.,* **68,** 161-172, (1997).
12. A. Heerschap, G. J. Jager, M. van der Graaf, J. O. Barentsz, J. J. de la Rosette, G. O. Oosterhof, E. T. Ruijter, S. H. Ruijs, In vivo proton MR spectroscopy reveals altered metabolite content in malignant prostate tissue. *Anticancer Res.,* **17,** 1455-1460, (1997).
13. J. Kurhanewicz, D. B. Vigneron, S. J. Nelson, H. Hricak, J. M. MacDonald, B. Konety, P. Narayan, Citrate as an in vivo marker to discriminate prostate cancer from benign prostatic hyperplasia and normal prostate peripheral zone: detection via localized proton spectroscopy. *Urology,* **45,** 459-466, (1995).
14. D. J. Bryant, G. M. Bydder, H. A. Case, A. G. Collins, I. J. Cox, A. Makepeace, J. M. Pennock, Use of phosphorus-31 MR spectroscopy to monitor response to chemotherapy in non-Hodgkin lymphoma. *J. Comput. Assist. Tomogr.,* **12,** 770-774, (1988).
15. B. Chance, Applications of 31P NMR to clinical biochemistry. *Ann. N. Y. Acad. Sci.,* **428,** 318-332, (1984).
16. C. B. Higgins, M. Saeed, M. Wendland, W. M. Chew, Magnetic resonance spectroscopy of the heart. Overview of studies in animals and man. *Invest. Radiol.,* **24,** 962-968, (1989).

17. E. F. Hoffenberg, P. Kozlowski, T. A. Salerno, R. Deslauriers, Evaluation of cardiac 31P magnetic resonance spectroscopy: reviewing NMR principles. *J. Surg. Res.,* **62,** 135-143, (1996).
18. X. Maldonado, J. Alonso, J. Giralt, M. G. Cucurella, J. M. del Campo, A. Rovira, E. Felip, J. Capellades, E. Grive, D. Rubio, J. Gili, 31Phosphorus magnetic resonance spectroscopy in the assessment of head and neck tumors. *Int. J. Radiat. Oncol. Biol. Phys.,* **40,** 309-312, (1998).
19. L. f. R, R. Sauter, H. Kolem, A. Haase, M. von Kienlin, Localized Spectroscopy from Anatomically Matched Compartments: Improved Sensitivity and Localization for Cardiac 31P MRS in Humans. *J. Magn. Reson.,* **134,** 287-299, (1998).
20. G. K. Radda, R. D. Oberhaensli, D. J. Taylor, The biochemistry of human diseases as studied by 31P NMR in man and animal models. *Ann. N. Y. Acad. Sci.,* **508,** 300-308, (1987).
21. O. M. Redmond, J. P. Stack, O. C. NG, D. N. Carney, P. A. Dervan, B. J. Hurson, J. T. Ennis, 31P MRS as an early prognostic indicator of patient response to chemotherapy. *Magn. Reson. Med.,* **25,** 30-44, (1992).
22. S. R. Smith, P. A. Martin, J. M. Davies, R. H. Edwards, A. N. Stevens, The assessment of treatment response in non-Hodgkin's lymphoma by image guided 31P magnetic resonance spectroscopy. *Br. J. Cancer,* **61,** 485-490, (1990).
23. M. Delivoria Papadopoulos, J. E. DiGiacomo, 31P nuclear magnetic resonance spectroscopy in the human neonatal brain. *Semin. Perinatol.,* **14,** 248-257, (1990).
24. R. Gruetter, C. Fusch, E. Martin, C. Boesch, Determination of saturation factors in 31P NMR spectra of developing human brain. *Magn. Reson. Med.,* **29(1),** 7-11, (1993).
25. W. Negendank, Studies of human tumors by MRS: a review. *NMR Biomed.,* **5,** 303-324, (1992).
26. K. E. Jensen, C. Thomsen, O. Henriksen, In vivo measurement of intracellular pH in human brain during different tensions of carbon dioxide in arterial blood. A 31P-NMR study. *Acta. Physiol. Scand.,* **134,** 295-298, (1988).
27. K. Iwanaga, M. Sakurai, T. Minami, Y. Kato, K. Sairyo, Y. Kikuchi, Is the intracellular pH threshold an anaerobic threshold from the view point of intracellular events?: a brief review. *Appl. Human. Sci.,* **15,** 59-65, (1996).

28. C. W. Li, O. Gonen, Simultaneous 3D NMR spectroscopy of fluorine and phosphorus in human liver during 5-fluorouracil chemotherapy. *Magn. Reson. Med.,* **35,** 841-847, (1996).
29. J. Murphy-Boesch, C. W. Li, L. He, K. A. Padavic-Shaller, W. Negendank, T. R. Brown, Proton-decoupled 19F spectroscopy of 5-FU catabolites in human liver. *Magn. Reson. Med.,* **37,** 321-326, (1997).
30. H. P. Schlemmer, P. Bachert, W. Semmler, P. Hohenberger, P. Schlag, W. J. Lorenz, G. van Kaick, Drug monitoring of 5-fluorouracil: in vivo 19F NMR study during 5-FU chemotherapy in patients with metastases of colorectal adenocarcinoma. *Magn. Reson. Imaging,* **12,** 497-511, (1994).
31. W. Wolf, M. J. Albright, M. S. Silver, H. Weber, U. Reichardt, R. Sauer, Fluorine-19 NMR spectroscopic studies of the metabolism of 5- fluorouracil in the liver of patients undergoing chemotherapy. *Magn. Reson. Imaging,* **5,** 165-169, (1987).
32. Y. J. Kamm, A. Heerschap, G. Rosenbusch, I. M. Rietjens, J. Vervoort, D. J. Wagener, 5-Fluorouracil metabolite patterns in viable and necrotic tumor areas of murine colon carcinoma determined by 19F NMR spectroscopy. *Magn. Reson. Med.,* **36,** 445-450, (1996).
33. V. J. Kamm, I. M. Rietjens, J. Vervoort, A. Heerschap, G. Rosenbusch, H. P. Hofs, D. J. Wagener, Effect of modulators on 5-fluorouracil metabolite patterns in murine colon carcinoma determined by in vitro 19F nuclear magnetic resonance spectroscopy. *Cancer Res.,* **54,** 4321-4326, (1994).
34. C. T. Moonen, R. J. Dimand, K. L. Cox, The noninvasive determination of linoleic acid content of human adipose tissue by natural abundance carbon-13 nuclear magnetic resonance. *Magn. Reson. Med.,* **6,** 140-157, (1988).
35. E. L. Thomas, J. D. Hanrahan, M. Ala-Korpela, G. Jenkinson, D. Azzopardi, R. A. Iles, J. D. Bell, Noninvasive characterization of neonatal adipose tissue by 13C magnetic resonance spectroscopy. *Lipids,* **32,** 645-651, (1997).
36. N. Beckmann, J. J. Brocard, U. Keller, J. Seelig, Relationship between the degree of unsaturation of dietary fatty acids and adipose tissue fatty acids assessed by natural-abundance 13C magnetic resonance spectroscopy in man [published erratum appears in Magn. Reson. Med., 1993 Apr;29(4):581]. *Magn. Reson. Med.,* **27,** 97-106, (1992).

37. E. L. Thomas, G. Frost, M. L. Barnard, D. J. Bryant, S. D. Taylor-Robinson, J. Simbrunner, G. A. Coutts, M. Burl, S. R. Bloom, K. D. Sales, J. D. Bell, An in vivo 13C magnetic resonance spectroscopic study of the relationship between diet and adipose tissue composition. *Lipids,* **31,** 145-151, (1996).
38. T. A. Victor, A. Bergman, R. H. Knop, Detecting fatty acids of dietary origin in normal and cancerous human breast tissue by 13C nuclear magnetic resonance spectroscopy. *Br. J. Cancer,* **68,** 336-341, (1993).
39. R. J. Dimand, C. T. Moonen, S. C. Chu, E. M. Bradbury, G. Kurland, K. L. Cox, Adipose tissue abnormalities in cystic fibrosis: noninvasive determination of mono- and polyunsaturated fatty acids by carbon-13 topical magnetic resonance spectroscopy. *Pediatr. Res.* **24,** 243-246, (1988).
40. T. Jue, J. A. Lohman, R. J. Ordidge, R. G. Shulman, Natural abundance 13C NMR spectrum of glycogen in humans. *Magn. Reson. Med.,* **5,** 377-379, (1987).
41. R. Taylor, T. B. Price, D. L. Rothman, R. G. Shulman, G. I. Shulman, Validation of 13C NMR measurement of human skeletal muscle glycogen by direct biochemical assay of needle biopsy samples. *Magn. Reson. Med.,* **27,** 13-20, (1992).
42. A. Heerschap, P. R. Luyten, J. I. van der Heyden, L. J. Oosterwaal, J. A. den Hollander, Broadband proton decoupled natural abundance 13C NMR spectroscopy of humans at 1.5 T. *NMR Biomed.,* **2,** 124-132, (1989).
43. M. J. Avison, D. L. Rothman, E. Nadel, R. G. Shulman, Detection of human muscle glycogen by natural abundance 13C NMR. *Proc. Natl. Acad. Sci. USA,* **85,** 1634-1636, (1988).
44. T. B. Price, D. L. Rothman, M. J. Avison, P. Buonamico, R. G. Shulman, 13C-NMR measurements of muscle glycogen during low-intensity exercise. *J. Appl. Physiol.,* **70,** 1836-1844, (1991).
45. T. B. Price, D. L. Rothman, R. Taylor, M. J. Avison, G. I. Shulman, R. G. Shulman, Human muscle glycogen resynthesis after exercise: insulin- dependent and -independent phases. *J. Appl. Physiol.,* **76,** 104-111, (1994).
46. K. T. Moriarty, D. G. O. McIntryre, K. Bingham, R. Coxon, P. M. Glover, P. L. Greenhaff, I. A. Macdonald, H. S. Bachelard, P. G. Morris, Glycogen resynthesis in liver and muscle after exercise: measurement of the rate of resynthesis by 13C magnetic resonance spectroscopy. *Magma.,* **2,** 429-432, (1994).

47. A. J. van den Bergh, S. Houtman, A. Heerschap, N. J. Rehrer, H. J. van den Boogert, B. Oeseburg, M. T. Hopman, Muscle glycogen recovery after exercise during glucose and fructose intake monitored by 13C-NMR. *J. Appl. Physiol.,* **81,** 1495-1500, (1996).
48. R. Taylor, T. B. Price, L. D. Katz, R. G. Shulman, G. I. Shulman, Direct measurement of change in muscle glycogen concentration after a mixed meal in normal subjects. *Am. J. Physiol.,* **265,** E224-E229, (1993).
49. T. Jue, D. L. Rothman, B. A. Tavitian, R. G. Shulman, Natural-abundance 13C NMR study of glycogen repletion in human liver and muscle. *Proc. Natl. Acad. Sci. USA,* **86,** 1439-1442, (1989).
50. P. Jehenson, G. Bloch, Elimination of surface signals by a surface-spoiling magnetic field gradient. Theoretical optimization and application to human in vivo NMR spectroscopy. *J. Magn. Reson.,* **94,** 59-72, (1991).
51. H. Bomsdorf, T. Helzel, D. Kunz, P. Roschmann, O. Tschendel, J. Wieland, Spectroscopy and imaging with a 4 tesla whole-body MR system. *NMR Biomed.,* **1,** 151-158, (1988).
52. H. Ikehira, T. Obata, M. Koga, K. Yoshida, Human hepatic carbohydrate metabolism. Dynamic observation using 13C MRS without proton decoupling. *Acta. Radiol.,* **38,** 998-1002, (1997).
53. H. Barfuss, H. Fischer, D. Hentschel, R. Ladebeck, A. Oppelt, R. Wittig, W. Duerr, R. Oppelt, In vivo magnetic resonance imaging and spectroscopy of humans with a 4 T whole-body magnet. *NMR Biomed.,* **3,** 31-45, (1990).
54. N. Beckmann, J. Seelig, H. Wick, Analysis of glycogen storage disease by in vivo 13C NMR: comparison of normal volunteers with a patient. *Magn. Reson. Med.,* **16,** 150-160, (1990).
55. P. Jehenson, D. Duboc, G. Bloch, M. Fardeau, A. Syrota, Diagnosis of muscular glycogenosis by in vivo natural abundance 13C NMR spectroscopy. *Neuromuscul. Disord.,* **1,** 99-101, (1991).
56. P. Labrune, P. Jehenson, A. Syrota, M. Odievre, In vivo 13C-NMR evaluation of glycogen content in a patient with glycogen storage disease. *J. Inherit. Metab. Dis.,* **15,** 723-726, (1992).

57. W. Roser, N. Beckmann, U. Wiesmann, J. Seelig, Absolute quantification of the hepatic glycogen content in a patient with glycogen storage disease by 13C magnetic resonance spectroscopy. *Magn. Reson. Imaging.,* **14,** 1217-1220, (1996).
58. L. O. Sillerud, K. R. Halliday, R. H. Griffey, C. Fenoglio Preiser, S. Sheppard, In vivo 13C NMR spectroscopy of the human prostate. *Magn. Reson. Med.,* **8,** 224-230, (1988).
59. R. Gruetter, D. L. Rothman, E. J. Novotny, R. G. Shulman, Localized 13C NMR spectroscopy of myo-inositol in the human brain in vivo. *Magn. Reson. Med.,* **25,** 204-210, (1992).
60. A. J. van den Bergh, H. J. van den Boogert, H. Heerschap. Natural abundance 13C CSI of the human brain, *in* "SMR 2nd Meeting, San Francisco, 1994," p. 567
61. A. J. van den Bergh, H. J. van den Boogert, H. Heerschap. In vivo three dimensional 13C chemical shift imaging of the human brain, *in* "ISMRM 4th Annual Meeting, New York, 1996," p. 1215
62. N. Beckmann, In vivo 13C spectroscopy in humans, *in* "NMR basic principles and progress vol. 28", 74-99, Springer-Verlag, Berlin Heidelberg,1992.
63. N. Beckmann, I. Turkalj, J. Seelig, U. Keller, 13C NMR for the assessment of human brain glucose metabolism in vivo. *Biochemistry.,* **30,** 6362-6366, (1991).
64. D. L. Rothman, A. M. Howseman, G. D. Graham, O. A. Petroff, G. Lantos, P. B. Fayad, L. M. Brass, G. I. Shulman, R. G. Shulman, J. W. Prichard, Localized proton NMR observation of [3-13C]lactate in stroke after [1-13C]glucose infusion. *Magn. Reson. Med.,* **21,** 302-307, (1991).
65. R. Gruetter, E. J. Novotny, S. D. Boulware, D. L. Rothman, G. F. Mason, G. I. Shulman, R. G. Shulman, W. V. Tamborlane, Direct measurement of brain glucose concentrations in humans by 13C NMR spectroscopy. *Proc. Natl. Acad. Sci USA,* **89,** 1109-1112, (1992).
66. R. Gruetter, E. J. Novotny, S. D. Boulware, D. L. Rothman, G. F. Mason, G. I. Shulman, W. V. Tamborlane, R. G. Shulman, Non-invasive measurements of the cerebral steady-state glucose concentration and transport in humans by 13C nuclear magnetic resonance. *Adv. Exp. Med. Bio.,I* **331,** 35-40, (1993).
67. D. L. Rothman, E. J. Novotny, G. I. Shulman, A. M. Howseman, O. A. Petroff, G. Mason, T. Nixon, C. C. Hanstock, J. W. Prichard, R. G. Shulman, 1H-[13C] NMR

measurements of [4-13C]glutamate turnover in human brain. *Proc. Natl. Acad. Sci. USA,* **89,** 9603-9606, (1992).

68. R. Gruetter, E. J. Novotny, S. D. Boulware, G. F. Mason, D. L. Rothman, G. I. Shulman, J. W. Prichard, R. G. Shulman, Localized 13C NMR spectroscopy in the human brain of amino acid labeling from D-[1-13C]glucose. *J. Neurochem.,* **63,** 1377-1385, (1994).
69. G. F. Mason, R. Gruetter, D. L. Rothman, K. L. Behar, R. G. Shulman, E. J. Novotny, Simultaneous determination of the rates of the TCA cycle, glucose utilization, alpha-ketoglutarate/glutamate exchange, and glutamine synthesis in human brain by NMR. *J. Cereb. Blood. Flow. Metab.,* **15,** 12-25, (1995).
70. R. G. Shulman, A. M. Blamire, D. L. Rothman, G. McCarthy, Nuclear magnetic resonance imaging and spectroscopy of human brain function. *Proc. Natl. Acad. Sci. USA,* **90,** 3127-3133, (1993).
71. M. Ishihara, H. Ikehira, S. Nishikawa, T. Hashimoto, K. Yamada, F. Shishido, T. Ogino, K. Cho, S. Kobayashi, M. Kawana, et al., Dynamic human glycogen and glucose metabolism detection utilizing in vivo 13C NMR. *Am. J. Physiol. Imaging,* **7,** 32-35, (1992).
72. N. Beckmann, R. Fried, I. Turkalj, J. Seelig, U. Keller, G. Stalder, Noninvasive observation of hepatic glycogen formation in man by 13C MRS after oral and intravenous glucose administration. *Magn. Reson. Med.,* **29,** 583-590, (1993).
73. I. Magnusson, D. L. Rothman, B. Jucker, G. W. Cline, R. G. Shulman, G. I. Shulman, Liver glycogen turnover in fed and fasted humans. *Am. J. Physiol.,* **266,** E796-E803, (1994).
74. G. W. Cline, D. L. Rothman, I. Magnusson, L. D. Katz, G. I. Shulman, 13C-nuclear magnetic resonance spectroscopy studies of hepatic glucose metabolism in normal subjects and subjects with insulin- dependent diabetes mellitus. *J. Clin. Invest.,* **94,** 2369-2376, (1994).
75. T. B. Price, R. Taylor, G. F. Mason, D. L. Rothman, G. I. Shulman, R. G. Shulman, Turnover of human muscle glycogen with low-intensity exercise. *Med. Sci. Sports. Exerc.,* **26,** 983-991, (1994).
76. T. Jue, D. L. Rothman, G. I. Shulman, B. A. Tavitian, R. A. DeFronzo, R. G. Shulman, Direct observation of glycogen synthesis in human muscle with 13C NMR. *Proc. Natl. Acad. Sci. USA,* **86,** 4489-4491, (1989).

77. G. I. Shulman, D. L. Rothman, T. Jue, P. Stein, R. A. DeFronzo, R. G. Shulman, Quantitation of muscle glycogen synthesis in normal subjects and subjects with non-insulin-dependent diabetes by 13C nuclear magnetic resonance spectroscopy. *N. Engl. J. Med.,* **322,** 223-228, (1990).
78. D. L. Rothman, I. Magnusson, G. Cline, D. Gerard, C. R. Kahn, R. G. Shulman, G. I. Shulman, Decreased muscle glucose transport/phosphorylation is an early defect in the pathogenesis of non-insulin-dependent diabetes mellitus. *Proc. Natl. Acad. Sci. USA,* **92,** 983-987, (1995).
79. R. Roussel, G. Velho, P. G. Carlier, L. Jouvensal, G. Bloch, In vivo NMR evidence for moderate glucose accumulation in human skeletal muscle during hyperglycemia. *Am. J. Physiol.,* **271,** E434-438, (1996).
80. R. Roussel, P. G. Carlier, C. Wary, G. Velho, G. Bloch, Evidence for 100% 13C NMR visibility of glucose in human skeletal muscle. *Magn. Reson. Med.,* **37,** 821-824, (1997).
81. R. G. Shulman, D. L. Rothman, T. B. Price, Nuclear magnetic resonance studies of muscle and applications to exercise and diabetes. *Diabetes,* **45 Suppl 1,** S93-98, (1996).
82. K. F. Petersen, R. Hendler, T. Price, G. Perseghin, D. L. Rothman, N. Held, J. M. Amatruda, G. I. Shulman, 13C/31P NMR studies on the mechanism of insulin resistance in obesity. *Diabetes,* **47,** 381-386, (1998).
83. E. J. Novotny, Jr., T. Ogino, D. L. Rothman, O. A. Petroff, J. W. Prichard, R. G. Shulman, Direct carbon versus proton heteronuclear editing of 2-13C ethanol in rabbit brain in vivo: a sensitivity comparison. *Magn. Reson. Med.,* **16,** 431-443, (1990).
84. H. J. Muller, D. Lanens, T. J. De Cock Buning, F. L. Van de Vyver, F. C. Alderweireldt, R. Dommisse, M. Spanoghe, G. J. Mulder, J. Lugtenburg, Noninvasive in vivo 13C-NMR spectroscopy in the rat to study the pharmacokinetics of 13C-labeled xenobiotics. *Drug. Metab. Dispos.,* **20,** 507-509, (1992).
85. D. Artemov, Z. M. Bhujwalla, R. J. Maxwell, J. R. Griffiths, I. R. Judson, M. O. Leach, J. D. Glickson, Pharmacokinetics of the 13C labeled anticancer agent temozolomide detected in vivo by selective cross-polarization transfer. *Magn. Reson. Med.,* **34,** 338-342, (1995).

86. K. Albert, G. Kruppa, K. P. Zeller, E. Bayer, F. Hartmann, In vivo metabolism of [4-13C]phenacetin in an isolated perfused rat liver measured by continuous flow 13C NMR spectroscopy. *Z. Naturforsch.,* **39,** 859-862, (1984).
87. A. Lapidot, A. Gopher, Cerebral metabolic compartmentation. Estimation of glucose flux via pyruvate carboxylase/pyruvate dehydrogenase by 13C NMR isotopomer analysis of D-[U-13C]glucose metabolites. *J. Biol. Chem.,* **269,** 27198-27208, (1994).
88. C. R. Malloy, A. D. Sherry, F. M. Jeffrey, Analysis of tricarboxylic acid cycle of the heart using 13C isotope isomers. *Am. J. Physiol.,* **259,** H987-H995, (1990).
89. S. Cerdan, B. Kunnecke, J. Seelig, Cerebral metabolism of 1,2-13C2acetate as detected by in vivo and in vitro 13C NMR. *J. Biol. Chem.,* **265,** 12916-12926, (1990).
90. E. Kustermann, J. Seelig, B. Kunnecke, Ascorbic acid, a vitamin, is observed by in vivo 13C nuclear magnetic resonance spectroscopy of rat liver. *Am. J. Physiol.,* **274,** E65-71, (1998).
91. P. A. Bottomley, P. B. Roemer, Homogeneous tissue model estimates of RF power deposition in human NMR studies. Local elevations predicted in surface coil decoupling. *Ann. N.Y. Acad. Sci.,* **649,** 144-159, (1992).
92. FDA, *Guidence for Content and Review of a Magnetic Rosonance Diagnostic Device 510(k) Application*, US Food and Drug Administration: Rockville, MD.
93. P. Roschmann, Radiofrequency penetration and absorption in the human body: limitations to high-field whole-body nuclear magnetic resonance imaging. *Med. Phys.,* **14,** 922-931, (1987).
94. G. Adriany, R. Gruetter, A half volume coil for efficient proton decoupling in humans at 4 Tesla. *J. Magn. Reson.,* **125,** 178-184, (1997).
95. R. Gruetter, G. Adriany, H. Merkle, P. M. Andersen, Broadband decoupled, 1H-localized 13C MRS of the human brain at 4 Tesla. *Magn. Reson. Med.,* **36,** 659-664, (1996).
96. P. M. L. Robitaille, A. Kangarlu, A. M. Abduljalil. On RF power requirements in magnetic resonance imaging, *in* "ESMRMB, Geneva, 1998," p. 96
97. J. Mispelter, B. Tiffon, E. Quiniou, J. M. Lhoste, Optimization of 13C-{1H} double coplanar surface-coil design for the WATLZ-16 decoupling sequence. *J. Magn. Reson.,* **82,** 622-628, (1989).

98. A. J. van den Bergh, H. J. van den Boogert, A. Heerschap, Calibration of the 1H decoupling field strength and experimental evaluation of the specific RF absorption rate in 1H-decoupled human 13C- MRS. *Magn. Reson. Med.,* **39,** 642-646, (1998).
99. A. J. van den Bergh, H. J. van den Boogert, H. Heerschap. In vivo 13C-NMR spectroscopy of humans: a comparison between WALTZ-4 and adiabatic broadband 1H decoupling schemes, *in* "ISMRM 5th Annual Meeting, Vancouver, 1997," p. 1347
100. P. R. Luyten, G. Bruntink, F. M. Sloff, J. W. Vermeulen, J. I. van der Heijden, J. A. den Hollander, A. Heerschap, Broadband proton decoupling in human 31P NMR spectroscopy. *NMR Biomed.,* **1,** 177-183, (1989).
101. G. Ende, P. Bachert, Dynamic 13C-1H nuclear polarization of lipid methylene resonances applied to broadband proton-decoupled in vivo 13C MR spectroscopy of human breast and calf tissue. *Magn. Reson. Med.,* **30,** 415-423, (1993).
102. R. van Sluis, G. S. Payne, M. O. Leach, Increased NOE enhancement in 1H decoupled 31P MRS. *Magn. Reson. Med.,* **34,** 893-897, (1995).
103. T. R. Brown, R. Stoyanova, T. Greenberg, R. Srinivasan, J. Murphy-Boesch, NOE enhancements and T1 relaxation times of phosphorylated metabolites in human calf muscle at 1.5 Tesla. *Magn. Reson. Med.,* **33,** 417-421, (1995).
104. A. Knuttel, R. Kimmich, K.-H. Spohn, Indirect 13C tomography and volume-selective spectroscopy via proton NMR. I Spectroscopic Techniques. *J. Magn. Reson.,* **86,** 526-541, (1990).
105. A. Knuttel, R. Kimmich, K. H. Spohn, Motion-insensitive volume-selective pulse sequences for direct and proton-detected 13C spectroscopy: detection of glycogen in the human liver in vivo. *Magn. Reson. Med.,* **17,** 470-482, (1991).
106. W. Chen, G. Adriany, X. H. Zhu, R. Gruetter, K. Ugurbil, Detecting natural abundance carbon signal of NAA metabolite within 12- cm3 localized volume of human brain using 1H-13C NMR spectroscopy [In Process Citation]. *Magn. Reson. Med.,* **40,** 180-184, (1998).
107. P. C. van Zijl, A. S. Chesnick, D. DesPres, C. T. Moonen, J. Ruiz Cabello, P. van Gelderen, In vivo proton spectroscopy and spectroscopic imaging of [1-13C]-glucose and its metabolic products. *Magn. Reson. Med.,* **30,** 544-551, (1993).

108. M. Saner, G. McKinnon, P. Boesiger, Glycogen detection by in vivo 13C NMR: A comparison of proton decoupling and polarization transfer. *Magn. Reson. Med.,* **28,** 65-73, (1992).

109. H. Bomsdorf, P. Roschmann, J. Wieland, Sensitivity enhancement in whole-body natural abundance 13C spectroscopy using 13C/1H double-resonance techniques at 4 Tesla. *Magn. Reson. Med.,* **22,** 10-22, (1991).

110. N. Beckmann, S. Muller, Analysis of localized polarization transfer for 13C volume-selective spectroscopy with surface coils. *J. Magn. Reson.,* **93,** 299-318, (1991).

111. R. Kreis, J. Slotboom, J. Felblinger, C. Boesch. 13C-MR spectroscopy on a 1.5T scanner with 1H-localization using PRESS, INEPT polarization transfer, adiabatic pulses and WALTZ decoupling, *in* "ISMRM 5th Annual Meeting, Vancouver, 1997," p. 1438

112. D. Artemov, Z. M. Bhujwalla, J. D. Glickson, In vivo selective measurement of (1-13C)-glucose metabolism in tumors by heteronuclear cross polarization. *Magn. Reson. Med.,* **33,** 151-155, (1995).

113. A. J. van den Bergh, H. J. van den Boogert, A. Heerschap, Heteronuclear cross polarization for enhanced sensitivity of in vivo 13C MR spectroscopy on a clinical 1.5 T MR system. *J. Magn. Reson.,* **135,** 93-98, (1998).

114. H. Kostler, R. Kimmich, Adiabatic J cross polarization for localized direct and proton-detected 13C spectroscopy. *J. Magn. Reson.,* **Series B 102,** 285-292, (1993).

115. M. E. Bellemann, G. Brix, NMR studies of brain 13C-glucose uptake and metabolism: present status [letter; comment]. *Magn. Reson. Imaging,* **15,** 997-1003, (1997).

116. P. C. van Zijl, D. Rothman, NMR studies of brain 13C-glucose uptake and metabolism: present status [see comments]. *Magn. Reson. Imaging,* **13,** 1213-1221, (1995).

117. B. Tiffon, J. Mispelter, J.-M. Lhoste, A Carbon-13 in vivo double surface-coil NMR probe with efficient low-power proton decoupling at 400 MHz using Waltz-16 sequence. *J. Magn. Reson.,* **68,** 544-550, (1986).

118. P. A. Bottomley, C. J. Hardy, P. B. Roemer, O. M. Mueller, Proton-decoupled, Overhauser-enhanced, spatially localized carbon-13 spectroscopy in humans. *Magn. Reson. Med.,* **12,** 348-363, (1989).

119. J. A. den Hollander, K. L. Beha9, R. G. Shulman, Use of double-tuned surface coils for the application of 13C NMR to brain metabolism. *J. Magn. Reson.,, (199*2).

120. R. J. Ordidge, A. Connelly, J. A. B. Lohman, Image-selected in vivo spectroscopy (ISIS). A New technique for spatially selective NMR spectroscopy. *J. Magn. Reson.,* **66,** 283-294, (1986).

121. T. R. Brown, B. M. Kincaid, K. Ugurbil, NMR chemical shift imaging in three dimensions. *Proc. Natl. Acad. Sci. USA,* **79,** 3523-3526, (1982).

122. N. Beckmann, S. Muller, Natural-abundance 13C spectroscopic imaging applied to humans. *J. Magn. Reson.,* **93,** 186-194, (1991).

123. S. Rotman, J. Slotboom, C. Boesch, E. Jequier. Muscle glycogen recovery after exercise measured by 13C-NMR in humans: Effect of nutritional solutions, *in* "ESMRMB, Geneva, 1998," p. 562

2 Calibration of the ^{1}H decoupling field strength and experimental evaluation of the specific RF absorption rate in ^{1}H decoupled human ^{13}C MRS

A.J. van den Bergh, H.J. van den Boogert and A. Heerschap

Department of Radiology, University of Nijmegen, The Netherlands

Abstract

For patient safety in human ^{1}H decoupled ^{13}C-MRS, it is absolutely necessary to evaluate the specific RF absorption rate (SAR) of the tissue exposed to ^{1}H frequency irradiation. With the use of surface coils, the local SAR at the body surface is of most concern due to the inherent RF field inhomogeneity. An empirical procedure to spatially calibrate the decoupler power level and to evaluate the local SAR at the body surface is described. For head, liver, muscle gastrocnemius and muscle vastus lateralis the SAR at the body surface was estimated for an $^{1}H/^{13}C$ double surface coil setup. Optimized duty cycle values obtained with this procedure show that broadband ^{1}H decoupled ^{13}C-MR spectroscopy is clinically feasible at 1.5 T for such a coil configuration within safety guidelines.

This chapter is based on the publication: Calibration of the ^{1}H decoupling field strength and experimental evaluation of the specific RF absorption rate in ^{1}H-decoupled human ^{13}C-MRS. A.J. van den Bergh, H.J. van den Boogert, A. Heerschap, Magn Reson Med, 39: 642-646 (1998).

Introduction

The use of radio frequency (RF) fields in magnetic resonance applied to humans is of concern since it could lead to tissue heating (1-5). In ^{31}P and ^{13}C-MR spectroscopy an ^{1}H decoupling RF field often is applied during the data acquisition period to remove multiplet splittings for improved sensitivity and resolution (6-8). Especially in ^{13}C-MRS where relatively large ^{1}H-^{13}C couplings have to be removed this may pose problems as the specific RF absorption rate (SAR) may exceed safety limits.

To estimate the SAR for volume coils their spatial RF distribution can be evaluated by computational techniques. The impedance method which uses anatomical models has been described for the human torso (9, 10) and for the human head (11). In another approach geometrical models have been used (5, 12).

For ^{1}H decoupling in ^{13}C-MRS mostly surface type coils are used. In contrast to volume coils, calculation of the local SAR is complex with these coils. Because of the inherent RF field inhomogeneity of surface coils, the local SAR will sooner exceed the safety guidelines (2) than the average SAR in the sensitive region of the coil. Several attempts have been made to estimate the SAR by computational techniques for the use of surface coils (12-16).

For patient safety, it is absolutely necessary to evaluate the local SAR for every applied experimental condition of ^{1}H decoupling in ^{13}C-MRS. In this study we describe an experimental approach that matches the experimental conditions applied during decoupling to estimate the local SAR instead of using a computational model.

The basis of our approach is a pulse sequence which is well known in high resolution ^{13}C NMR to calibrate the decoupler field strength (17). Extended with phase encoding this sequence provides spatial information about the RF field distribution of the decoupler coil (18). The spatial information of the decoupler RF field strength obtained by this technique, can be used to optimize the decoupler field strength and to calculate the local (surface) SAR.

Materials and Methods

Measurements were performed on an 1.5 T Magnetom SP 4000 (Siemens, Erlangen, Germany) equipped with a second RF transmit channel. Double resonance experiments were performed using a double surface coil consisting of an 11 cm diameter ^{13}C surface coil and a 17 x 23 cm ^{1}H butterfly coil. The slightly "V" shaped ^{1}H coil was placed below the ^{13}C coil to avoid the high flux regions of the coil wires near the patient. The patient to coil distance was 32 mm in the center and 16 mm at the outside of the coil. Dielectric losses in the distant patient volume were further minimized by using a transmission line resonater coil with distributed tuning capacitance (19). The ^{1}H coil was cooled by airflow to prevent possible mismatching caused by heating the coil due to power deposited in the coil during decoupling.

To evaluate whether the SAR remains within safety guidelines it is necessary to know the highest local SAR. The highest local SAR with the use of surface coils is assumed to occur at the body surface closest to the surface coil. To estimate this time averaged superficial SAR (S^{sup}) we used equation 1 (7).

During a decoupling experiment the peak power actually applied to the surface

$$S^{sup} = [\, P^{used} / P_{90}^{sup} \,] \times S^{tis} \times DC \qquad [1]$$

coil (P^{used}) and the pulse duty cycle (DC) are known. So the time averaged SAR at the body surface (S^{sup}) can be calculated if the P_{90}^{sup}, which is the peak power applied to the surface coil to obtain a 90° pulse at the body surface and S^{tis} the specific power absorbed by the tissue are known.

The latter one was determined for a 90° pulse of 500 µs (WALTZ element) in a homogeneous RF field using equation 2.

$$S^{tis} = (1-Q_l/Q_u) \times P^{total} / W^{total} \qquad [2]$$

To obtain the S^{tis} value we used a regular knee coil linearly polarized, and placed a certain amount of fresh meat (weight: W^{total}) in it. The quality factor (Q) of the coil was determined loaded (Q_l) and unloaded (Q_u) with a network analyzer model 8752A (Hewlett Packard, Santa Rosa, California). Power applied to the coil (P^{total}) was measured using a powermeter model 8542B supplied with

80350A peak power sensors (Giga-tronics Inc., San Ramon, California). Cable losses were measured and corrected for.

With the use of efficient transmitter coils, as done in this study, dielectric losses are considered to be negligible, and thus the power absorbed by the tissue is mainly due to the induced electric field which arises from the magnetic field (2, 5, 12). It is assumed that whenever the B_1 field strength is equal at a location in the homogeneous coil and at a location in the sensitive region of the surface coil the SAR will also be equal. To assess P_{90}, the pulse power needed for a 90° ^{1}H flip angle at a certain location, we modified a sequence previously described by Bax (17). The original sequence enables one to calibrate the decoupler RF field strength. However, this calibration is not spatially resolved. In our modified sequence we use phase encoding to perform localized calibration of the decoupler RF field strength (18).

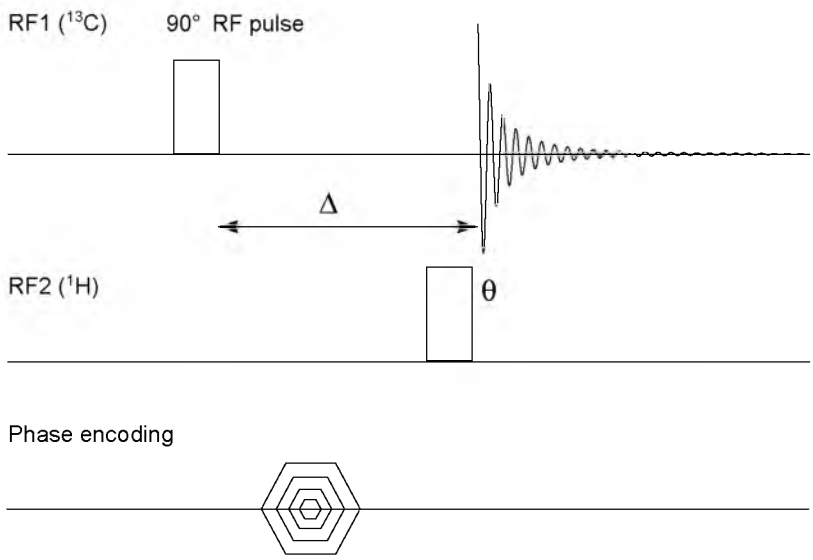

Figure 1

Schematic representation of the spatial RF field calibration sequence. The delay Δ has to be set 1/(2J) of a directly bonded ^{13}C-^{1}H pair. At the location where the proton pulse flip angle Θ equals π/2, no carbon magnetization will be observed for the ^{13}C resonance of the ^{13}C-^{1}H pair.

A schematic representation of this modified sequence is given in figure 1. The delay Δ has to be adjusted to 1/(2J), where J is the ^{1}H carbon spin coupling constant for a directly bonded ^{13}C-^{1}H pair. In the region where the proton pulse flip angle Θ equals $\pi/2$, no carbon magnetization will be observed for the carbon resonance of the ^{13}C-^{1}H pair, so it's easy to assess the P_{90} for this region.

The ^{13}C doublet signals at ± 128 ppm of unsaturated triglycerides in superficial adipose tissue were used as the ^{13}C-^{1}H pair for *in vivo* estimations of the superficial 90° peak power. In order to obtain these P_{90}^{sup} values, we acquired at least four 1D-CSI measurements with different peak powers applied to the surface coil. These measurements were performed for the head, liver, muscle gastrocnemius and muscle vastus lateralis from 5 different healthy volunteers after receiving a written informed consent. Mean age of the subjects was 28 yr. (range 22-46 yr.), body mass 73 kg (63-90 kg).

Measurement parameters of the calibration 1D-CSI were as follows, 32 phase encoding steps, a field of view of 160 mm resulting in slices of 5 mm, a repetition time of 400 ms, total number of acquisitions 1280, 1024 datapoints were acquired, Δ was set to 3.289 ms which corresponds to 1/(2J) of the unsaturated triglycerides. The pulse duration of the ^{1}H pulse on the second RF channel was 500 µs.

On a cylindrical phantom with diameter 14 cm, containing sunflower oil, 3D-CSI calibration measurements were performed and in addition B_1 field map images (11) were made in three orthogonal planes of a rectangular container 14 x 27 x 37 cm (h x w x l) filled with water, both to obtain information about the RF field distribution of the ^{1}H decoupling coil in 3 dimensions.

To verify the correlation between the calibration and decoupling performance we used the cylindrical phantom. The settings for the decoupling 1D-CSI matched the settings of the calibration sequence, decoupling was performed with WALTZ-4 with a basic 90° pulse of 500 µs, corresponding to a decoupling field $\gamma B_2/2\pi$ = 500 Hz. The proton bandwidth with these settings over which the ^{13}C-MRS resonance peak from unsaturated triglycerides remains within 85% of its fully

decoupled value was determined to be ±400 Hz which is sufficient for ^{1}H decoupling at 1.5 T.

Spectral data were analyzed using the Luise software (Siemens, Erlangen, Germany). CSI data were zerofilled in spatial as well as spectral dimension to a 64 x 2048 matrix. The CSI voxels were shifted to match with the superficial adipose tissue. Unsaturated triglyceride signals of superficial adipose tissue were fitted and integrated. Integrated areas of resonances multiplied by their peak sign were plotted against the RF peak power applied to the decoupler surface coil and the zero-crossing was chosen as the value for the $P^{sup}_{90.}$

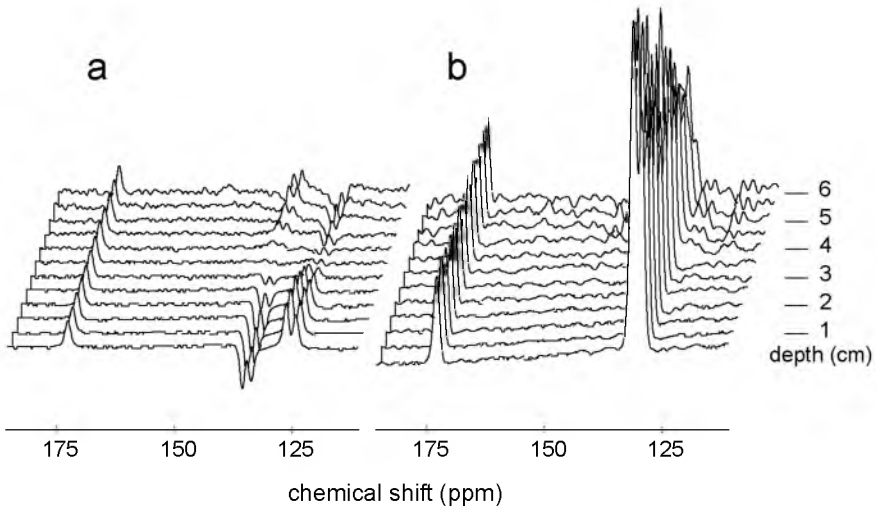

Figure 2

(a) Stack plot of spectra obtained with the 1D-CSI RF field calibration sequence from a cylindrical phantom filled with sunflower oil. The delay Δ was set to 1/(2J) of the unsaturated ^{13}C-^{1}H pair of triglycerides from sunflower oil. ^{13}C-MR spectra were collected from 0.5 cm slices. (b) Stack plot of spectra collected with a corresponding 1D-CSI using WALTZ-4 decoupling. The same peak power was applied to the decoupler coil in the calibration sequence and during WALTZ-4 decoupling.

Results

Figure 2a. shows 1D-CSI ^{13}C-MR spectra obtained with the spatial RF calibration sequence from the cylindrical phantom filled with sunflower oil. In this stack plot

one can clearly see that in the slice at a depth of 4 cm there is almost no magnetization left, the ^{1}H pulse flip angle Θ in this region is approximately $\pi/2$. In the region closer to the coil the ^{1}H pulse angle $\Theta > \pi/2$. Further away from the coil (4.5 cm) the pulse angle generated by the decoupler coil is less than $\pi/2$. If we look at the corresponding 1D-CSI ^{13}C-MRS measurement with WALTZ-4 decoupling at the same proton RF peak power (figure 2b.) one can see that the decoupling performance close to the coil is excellent. Beyond the region where the ^{1}H pulse angle Θ is estimated to be $\pi/2$ with the use of the 1D-CSI calibration sequence, we can see sidebands appearing due to insufficient decoupling power. This shows that RF calibration and decoupling performance are in good agreement.

The average S^{tis} (equation 2.) measured with a regular knee coil of fresh meat samples was found to be 9.09 Watt/kg (SD= 1.36, n=4).

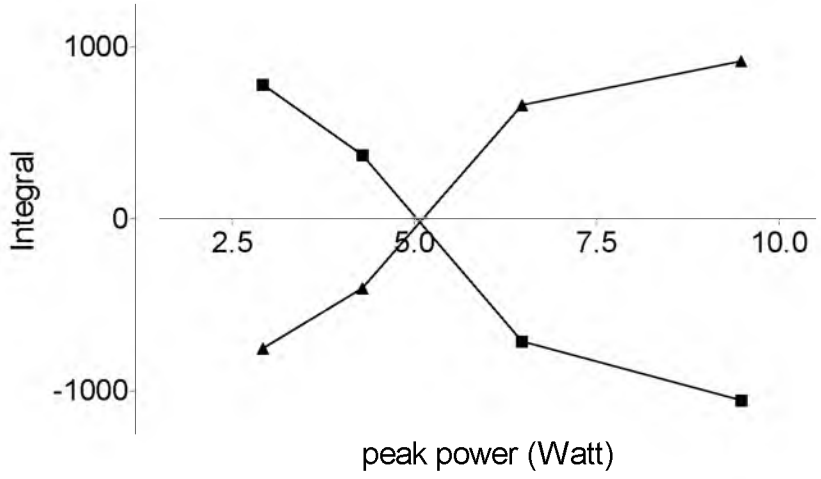

Figure 3

Integrated areas of the unsaturated triglyceride signals multiplied with their peak sign plotted against the RF amplitude of the decoupling channel.

Spectra were obtained from the head of a healthy subject, placed with the occipitoparietal region facing the surface coil. Four 1D-CSI measurements were performed with different peak power on the decoupler RF channel. Spectra originating from the subcutaneous adipose tissue were analyzed.

In figure 3 the results of a RF calibration of the ^{1}H decoupling coil loaded with the human head are presented. The data are obtained from four different 1D-CSI calibration measurements, all with different peak power on the decoupler RF channel, taken from the slice matching with the superficial lipid tissue (in this case of the human head). From this graph one can easily derive a value for P_{90}^{sup}. Similar studies were performed for liver and skeletal muscle. Averaged values from 5 healthy volunteers of the P_{90}^{sup} for these tissues are given in table 1.
The data obtained from the cylindrical phantom, filled with sunflower oil, with the 3D-CSI calibration sequence showed a much larger variation in pulse angle as a function of distance from the coil compared to variations in pulse angle in a plane parallel to the coil.

Tissue	min.	max.	mean (n=5)	SD
head	5.01	5.85	5.49	0.35
liver	9.06	14.95	11.79	2.35
muscle vastus lateralis	7.15	11.78	9.01	1.99
muscle gastrocnemius	5.28	6.80	6.06	0.71

Table 1.

Mean P_{90}^{sup} (Watt) values from 5 healthy subjects, obtained with the 1D-CSI calibration sequence from the head, liver, muscle vastus lateralis and muscle gastrocnemius.

When the power was set to achieve an excitation pulse angle of 90° in the second plane parallel to the coil with the use of the 1D-CSI calibration, the voxels in the bottom plane all showed excitation angles larger than 90°. The voxels in the second plane all showed very small signals or no signal at all for the ^{13}C-^{1}H pair, meaning an excitation angle close to 90°. The voxels in the third plane all showed an excitation angle less than 90°.

B_1 field maps reconstructed from images of the large rectangular phantom, filled with water and placed on top of the ^{13}C surface coil gave a more detailed picture of the relative field strength within the excitation volume of the decoupling coil. The field maps perpendicular to the plane of the coil showed a decreasing B_1 field moving away from the coil as in figure 2. A "butterfly" shaped field map image was obtained in a 6 mm thick slice adjacent and parallel to the ^{13}C coil. The latter field map showed three regions with slightly increased intensity. These regions were connected with each other, with one at the center above the ^{13}C surface coil and with two side lobs above both loops of the ^{1}H coil. Setting the pixel with the highest B_1 field strength to 100 % resulted in an average B_1 field strength of 91.8 % (SD = 2.45 %) for a large rectangle, 212 x 100 mm covering the 3 regions, which indicates a fairly uniform B_1 field distribution. The average B_1 field of the decoupler coil within the sensitive area of the ^{13}C coil (a circle with diameter 100 mm) was 90.6 % (SD = 2.41).

The actual power used (P^{used}) to acquire broadband decoupled ^{13}C-MR spectra of the tissues studied in this paper, resulted in P^{used}/ P^{sup}_{90} values ranging from 1 for superficial lipid to 11 for the liver. Using formula 1 one can calculate duty cycle values to remain within safety guidelines for the local SAR (2) to be 0.88 and 0.08 respectively. For signals like the C_1 of glycogen in muscle or liver an adequate signal to noise ratio can be achieved with these duty cycles within acceptable measurement times (20).

Discussion

In this paper an experimental method to obtain spatial information of the ^{1}H decoupling RF field strength in ^{1}H decoupled ^{13}C-MRS is presented. With this method the minimum power needed to obtain adequately decoupled spectra can be determined. Furthermore the calibration procedure makes it possible to obtain exact values of the power needed to generate a 90° excitation angle at the surface and thereby enabling a local (surface) SAR calculation.

Localization for this calibration procedure was performed in only one direction parallel to the surface coil. With phase encoding in only one direction we were able to acquire four data sets with a good signal to noise ratio with respect to the unsaturated triglyceride signals within acceptable measurement times. To justify the use of 1D-CSI calibration of the decoupling RF field strength, we had to assume that the RF field strength of our decoupling coil varies more in depth than in a plane parallel to the coil. This assumption was verified with a 3D-CSI calibration experiment performed on the cylindrical phantom containing sunflower oil. The results from this 3D-CSI experiment showed that the in plane variation was small compared to the variation between planes parallel to the coil. Similar results were obtained by using a B_1 field map imaging technique.

These B_1 field map images show some similarity with the computer contour plots of the magnitude of the transverse RF field produced by a 8 x 13 cm figure eight surface coil (12), notwithstanding the difference in coil sizes and shape.

Although the B_1 field map imaging technique can give quick access to the RF field distribution of a coil in several orientations, it only gives relative information about the RF field distribution. In this study we need to know the amount of power to apply to the surface coil to generate a 90° pulse at a certain location and this information can exactly be obtained with the calibration procedure.

A possible limitation of the SAR estimation procedure is that it evaluates the sensitive area of the ^{13}C surface coil, and thus may overlook higher field strengths of the decoupler coil outside this area to which the subject may be exposed. However, the B_1 field maps obtained in a plane adjacent to the ^{13}C coil from a phantom extending well beyond the viewing area of the ^{1}H coil showed that, for the current used coil configuration, the B_1 field strength the in region used for the SAR estimation deviated less than 10 % from the most intense spot of the B_1 field of the decoupler coil. Furthermore, in actual *in vivo* ^{1}H decoupling experiments the subjects tissue is positioned in such a way that its only exposed to the central region of the B_1 field of the decoupler coil.

In this study we used the superficial adipose tissue to estimate the P_{90}^{sup} and used equations 1 and 2 to calculate the local (surface) SAR. To obtain S^{tis} we used

fresh meat which mainly contains muscle tissue whose conductivity is higher than that of adipose tissue (10). In this way we may overestimate the local SAR for superficial adipose tissue. However care should be taken because of the skin adjacent to the superficial lipid (closer to the surface coil) whose conductivity is similar to that of muscle.

The RF field inhomogeneity of circular surface coils leads to an inefficient use of RF power used for decoupling (21). This is also true for the butterfly coil used in the present experiments, as shown by the high P^{used}/ P^{sup}_{90} ratios. With different coil configuration types it maybe possible to make more efficient use of the power applied to the decoupling coil(22).

Acknowledgment

The authors thank dr. Leon, Th. E. O van Erning for critically reading the manuscript.

References

1. T. F. Budinger, Emerging nuclear magnetic resonance technologies. Health and safety. *Ann. N. Y. Acad. Sci.,* **649,** 1-18, (1992).
2. F. G. Shellock, E. Kanal, "Magnetic Resonance bioeffects, safety, and patient managment," Raven Press, New York, 1994.
3. F. G. Shellock, E. Kanal, Policies, guidelines, and recommendations for MR imaging safety and patient management. SMRI Safety Committee. *J. Magn. Reson. Imag.,* **1,** 97-101, (1991).
4. R. E. Gangarosa, J. E. Minnis, J. Nobbe, D. Praschan, R. W. Genberg, Operational safety issues in MRI. *Magn. Reson. Imag.,* **5,** 287-292, (1987).
5. P. A. Bottomley, R. W. Redington, W. A. Edelstein, J. F. Schenck, Estimating radiofrequency power deposition in body NMR imaging. *Magn. Reson. Med.,* **2,** 336-349, (1985).
6. P. R. Luyten, G. Bruntink, F. M. Sloff, J. W. Vermeulen, J. I. van der Heijden, J. A. den Hollander, A. Heerschap, Broadband proton decoupling in human 31P NMR spectroscopy. *NMR Biomed.,* **1,** 177-183, (1989).

7. A. Heerschap, P. R. Luyten, J. I. van der Heyden, L. J. Oosterwaal, J. A. den Hollander, Broadband proton decoupled natural abundance 13C NMR spectroscopy of humans at 1.5 T. *NMR Biomed.,* **2,** 124-132, (1989).
8. N. Beckmann, In vivo 13C spectroscopy in humans, *in* "NMR basic principles and progress vol. 28", 74-99, Springer-Verlag, Berlin Heidelberg,1992.
9. M. Grandolfo, A. Polichetti, P. Vecchia, O. P. Gandhi, Spatial distribution of RF power in critical organs during magnetic resonance imaging. *Ann. N. Y. Acad. Sci.,* **649,** 176-187, (1992).
10. O. P. Gandhi, J. Y. Chen, Absorption and distribution patterns of RF fields. *Ann. N. Y. Acad. Sci.,* **649,** 131-143, (1992).
11. D. Simunic, P. Wach, W. Renhart, R. Stollberger, Spatial distribution of high-frequency electromagnetic energy in human head during MRI: numerical results and measurements. *IEEE. Trans. Biomed. Eng.,* **43,** 88-94, (1996).
12. P. A. Bottomley, P. B. Roemer, Homogeneous tissue model estimates of RF power deposition in human NMR studies. Local elevations predicted in surface coil decoupling. *Ann. N. Y. Acad. Sci.,* **649,** 144-159, (1992).
13. J. R. Keltner, J. W. Carlson, M. S. Roos, S. T. Wong, T. L. Wong, T. F. Budinger, Electromagnetic fields of surface coil in vivo NMR at high frequencies. *Magn. Reson. Med.,* **22,** 467-480, (1991).
14. D. J. Schaefer. Estimation of current limits for RF power deposition from planar, transmit surface coils, *in* "Proc., ISMRM 4th Scientific Meeting, New York, 1996," p. 1446
15. R. J. Strilka, S. Li, M. B. Smith. A numerical study of RF deposition using surface coils in high field MRI, *in* "Proc., ISMRM 4th Scientific Meeting, New York, 1996," p. 1448
16. M. E. Bellemann, F. Hauert, P. Bachert, H.-J. Zabel, W. J. Lorenz. Local RF power deposition in broadband 1H decoupling experiments with transmission line resonators, *in* "Proc., SMRM, 10th annual meeting, San Francisco, 1991," p. 972
17. A. Bax, A simple method for the calibration of decoupler radiofrequency field strength. *J. Magn. Reson.,* **52,** 76-80, (1983).
18. A. J. van den Bergh, H. J. van den Boogert, H. Heerschap. Spatially localized calibration of the decoupler radio frequency field strength, *in* "Proc.,SMR 2nd Meeting,San Francisco, 1994," p. 760
19. C.-N. Chen, D. I. Hoult, The visualization of RF probe electric fields. *Magn. Reson.*

Med., **29,** 386-390, (1993).

20. A. J. van den Bergh, S. Houtman, A. Heerschap, N. J. Rehrer, H. J. van den Boogert, B. Oeseburg, M. T. Hopman, Muscle glycogen recovery after exercise during glucose and fructose intake monitored by 13C-NMR. *J. Appl. Physiol.,* **81,** (4), 1495-1500, (1996).
21. J. Mispelter, B. Tiffon, E. Quiniou, J. M. Lhoste, Optimization of 13C-{1H} double coplanar surface-coil design for the WATLZ-16 decoupling sequence. *J. Magn. Reson.,* **82,** 622-628, (1989).
22. G. Adriany, R. Gruetter, A half volume coil for efficient proton decoupling in humans at 4 Tesla. *J. Magn. Reson.,* **125,** (1), 178-184, (1997).

3 Skin temperature increase during local exposure to high power RF levels in humans

A.J. van den Bergh, H.J. van den Boogert and A. Heerschap

Department of Radiology, University of Nijmegen, The Netherlands

Abstract

The thermoregulatory response of the skin was investigated in 5 healthy volunteers during prolonged exposure to RF radiation by a surface coil. Temperature changes induced by RF radiation were measured at the skin of the calf muscle by a fluoroptic probe. Exposure to superficial SAR levels of 6.5, 12 and 22 Watt/kg resulted in skin temperature increases, the highest temperature recorded was 38.3 °C. Although the maximum values of each temperature curve correlated with the applied superficial SAR levels, these values did not exceed the recommended temperature limit for the extremities such as given by the FDA. None of the subjects experienced the changes in skin temperature. For subjects with normal thermoregulatory function, these findings suggest that the recommended SAR limit for the extremities may be too conservative.

This chapter is based on a paper submitted to Magnetic Resonance in Medicine.

Introduction

Proton decoupling and nuclear Overhauser enhancement (NOE) are often applied in *in vivo* ^{13}C and ^{31}P MR spectroscopy in humans (1-6). Benefits of these techniques are, improvement of spectral resolution (spectrum simplification) and improvement in signal to noise ratio. A better signal to noise ratio means that measurement time can be reduced, which is important for patient comfort.

However, proton decoupling and NOE require relatively high level RF radiation often applied with high duty cycles. Heating, induced by this RF radiation during a MR examination, is of concern because of possible tissue damage (7-11). Precautions should be taken in experimental procedures, especially in ^{13}C MRS, in which relatively large ^{1}H-^{13}C couplings have to be removed (1, 2, 5, 12, 13).

To perform a ^{13}C *in vivo* MR spectroscopy experiment, a coil configuration is required with the highest possible sensitivity for ^{13}C, and an efficient ^{1}H coil for decoupling. Therefore, often surface coils are used (1, 4, 14-16). Because of the inherent RF field inhomogeneity of these type of coils, they produce a high local specific absorption rate (SAR) and a low total body SAR. Recently, we developed an empirical procedure to predict the local SAR at the body surface, for surface coils using the unsaturated carbon signals of subcutaneous lipid tissue (17). However, power deposition in the skin is not directly evaluated by this method. The skin probably reflects the worst case because of its properties and its position in the RF field of the surface coil.

Either SAR levels or temperature criteria can be used as guidelines for safety precautions (18). Several animal and human studies have been performed to study the temperature increase at different locations on the body during imaging protocols using a body coil (19-22). Temperature changes by a proton decoupling protocol using a surface coil were reported by Morvan *et al.* (23). In the latter study temperature changes were measured by an imaging technique, based on the temperature dependence of the diffusion coefficient of water. Temperature change was measured in muscle tissue after 20 minutes of

decoupling. To our knowledge, measurements of absolute skin temperature during decoupling have not yet been reported.

The aim of the present study was to investigate if exposure to high local SAR levels applied with a surface coil could result in skin temperatures above the recommended criteria for safe MR operation (18).

Experimental

Subjects. Five healthy male subjects participated in this study. Subjects were screened for contra-indications to undergo a MR procedure. All subjects were experienced MR investigators and were well aware of the possible tissue heating effects of high level RF radiation. The subjects were in contact with the MR operator during decoupling experiments; experiments could be terminated at any time.

System. Experiments were performed at 1.5 T using a Siemens Vision whole body system (Siemens, Erlangen, Germany) supplied with a second RF transmit channel. We used a double surface coil configuration consisting of an 11 cm diameter ^{13}C coil and a 17 x 23 cm butterfly proton coil. The slightly V-shaped proton coil was placed below the ^{13}C coil to avoid the high flux regions of the coil wires near the patient. This coil was cooled by air flow to prevent possible mismatching caused by heating the coil due to power deposited in the coil during decoupling. The ambient conditions were: room temperature 21 ± 1.0 ° C, relative humidity between 50 % and 70 %.

Subjects laid in a supine position with the calf muscle of the right leg positioned on the double surface coil. In total 4 experiments were performed on each subject. The first experiment was to determine the P_{90}^{sup}, which is the power applied to the surface coil to obtain a 90° pulse at the body surface (superficial lipid tissue). This was done by a spatially resolved calibration sequence according to (17). In order to obtain information of the thermoregulatory function of the skin during exposure to RF radiation, 3 subsequent experiments were performed at different occasions with respectively 6.5, 12 and 22 Watt/kg local

SAR (S^{sup}) deposited as determined for subcutaneous adipose tissue. This superficial SAR value for each individual was calculated using Eq. 1 (1, 17).

$$S^{sup} = [P^{used} / P^{sup}_{90}] \times S^{tis} \times DC \quad [1]$$

The specific absorption of muscle tissue S^{tis} was determined to be 9.09 Watt/kg for a 500 μs rectangular 90° pulse (17). The value for P^{used} and the duty cycle (DC) can be set to desired values. In the current study, the DC was fixed at 27 % and P^{used} was changed to achieve the required superficial SAR value.

The subjects were inside the magnet for approximately 10 minutes prior to the start of decoupling. During this period imaging and shimming was performed and the temperature of the skin could stabilize.

During the 60 minutes that each decoupling experiment lasted the skin temperature of the muscle gastrocnemius at the center of both coils, which reflects the worst case, was monitored with a fluoroptic thermometry system (Luxtron 712, California, USA). A control fluoroptic probe was attached to the skin of the same leg at the muscle quadriceps femoris outside the RF field of the double surface coil. Temperature was sampled with 30 second time intervals. The fluoroptic probes were attached to the skin with micropore tape.

Temperatures at the start of each experiment were determined for both temperature probes. The maximum skin temperature (T_{max}) and the temperature at the end of each experiment (T_{end}) were derived from the temperature curves.

Results

The amplitude required for a 500 μs 90° pulse at the body surface ranged from 6.7 to 7.8 Watt (mean ± SD; 7.2 ± 0.47 Watt).

The mean skin temperature at the start of the decoupling periods was 30.23 ± 0.63 °C. This temperature was lower than the mean control temperature at the start of the decoupling experiments, which was 33.56 ± 0.78 °C. This difference was due to the cooling of the coil on which the leg was positioned.

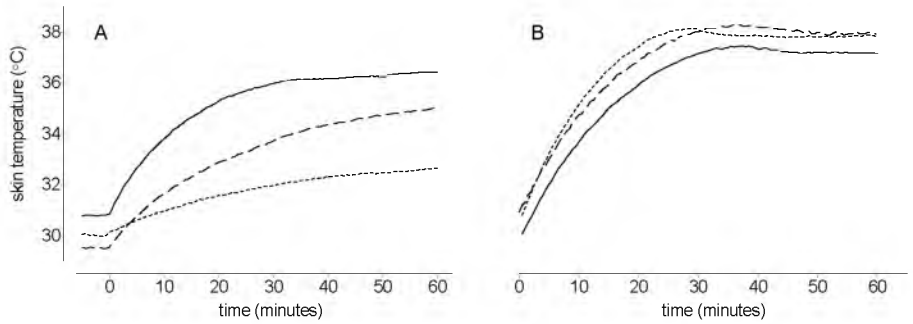

Figure 1.

Figure A, experimental data of subject 2, skin temperature increase of the calf muscle during 60 minutes of decoupling with different local (superficial) SAR levels, ----- 6.5, — — 12 and —— 22 Watt/kg. Figure B, experimental data of skin temperature overshoot at 22W/kg local SAR of three subjects: ----- subject 3, — — subject 4, and —— subject 5. Temperature was monitored with time intervals of 30 seconds using a fluoroptic probe attached to the skin.

At the onset of decoupling the skin temperature within the RF field rapidly increased in all experiments, at all power levels. During further decoupling the temperature rise slowed down. In most experiments the temperature curve occurred as an one phase exponential as illustrated in figure 1A for an individual subject. Fitting the experimental data of this subject with an one phase exponential function resulted in R^2 values > 0.99. In these cases the T_{end} corresponds with T_{max}. The relation between the applied power level and the maximum temperature reached is clearly visible in this figure. The initial temperature rise is also higher at higher local SAR levels.

In three experiments, all with the highest local SAR applied, the temperature curves followed a different shape, see figure 1B. Skin temperature first increased, followed by a decrease after which it stabilized.

Summarized results for each individual and for each SAR level are given in the table 1. In figure 2, the relationship between the applied superficial SAR and the T_{max} is shown. This relation between local SAR and T_{max} is not linear. Since for

three individuals the T_{end} at the superficial SAR level of 22 Watt/kg was different from the T_{max}, this value is also shown in figure 2.

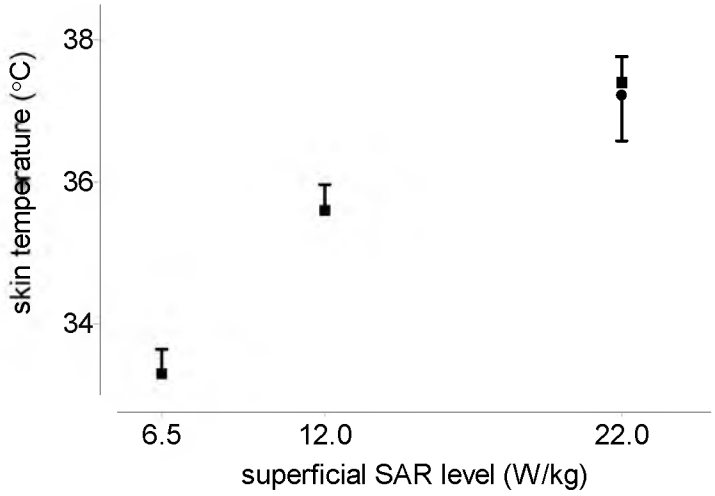

Figure 2.

Mean and standard deviation (n=5) of the T_{max} (■) during a proton decoupling protocol applied to the calf muscle plotted against superficial SAR level. T_{end} value (●) is shown for the superficial SAR level of 22 Watt/kg.

None of the subjects experienced any tissue heating effects, nor did they report any other discomfort during the decoupling procedures.

In 12 out of 15 experiments the control skin temperature recorded outside the RF field of the proton decoupler coil fluctuated in a range of ± 0.5 °C, with no clear increase or decrease. Three cases showed a clear rise of the control temperature during decoupling, of which the largest was 1.8 °C, during an experiment with 6.5 Watt/kg superficial SAR.

Subject	Age (year)	body weight (kg)	P_{90}^{sup} (Watt)	22 W/kg T_{max}	22 W/kg T_{end}	12 W/kg T_{max}	6.5 W/kg T_{max}
1	31	85	7.1	36.8	36.8	37.0	34.6
2	26	75	6.8	36.4	36.4	35.1	32.6
3	49	87	7.9	38.1	37.8	35.6	33.1
4	33	65	7.5	38.3	37.9	35.1	33.1
5	26	87	6.7	37.4	37.2	35.2	33.1

Table 1.

Subject information and summarized results of the calibration and decoupling experiments. P_{90}^{sup} values are given for each individual as well as T_{max} and T_{end} values for the three applied superficial SAR levels.

Discussion

In this study the effect of RF radiation by an ^{1}H decoupling coil on the skin temperature was investigated. The duration of the applied decoupling is representative for several consecutive ^{1}H decoupled ^{13}C MR spectroscopy examinations such as in dynamic studies.

The RF radiation by the ^{1}H surface coil during decoupling induced changes in temperature that could be described by an one phase exponential increase in all except for three experiments. In three subjects, at the highest superficial SAR level the temperature curve showed an overshoot. The T_{max} in these three subjects was higher than 37 °C, in the other two subjects the T_{max} remained below 37 °C at the same superficial SAR level.

Thermophysiological responses are difficult to predict; several studies report on whole body thermophysiology (24-27). Studies on local tissue temperature stress suggest that the heat removed from or supplied to the tissue by blood circulation is one of the most important factors in thermoregulation (28-30). Heat induced by

RF and heat loss to the environment also play a major role in the local tissue heat balance, conductive heat transfer through tissue and metabolic heat production are less important (28, 29, 31).

It goes beyond the scope of this study to model the temperature curves. Similar increments in skin temperature as observed in this study could be accounted for by Buse *et al.* in an one-dimensional mathematical model study (32). Overshoots above the core temperature as in the present study were also described. The weighting factor of the skin temperature feedback and the depth of the skin receptors could be modeled to match the experimental data (32).

A steady state skin temperature is reached in most experiments, at that time, there is an equilibrium between heat induced by RF irradiation and the total heat loss. Higher local SAR levels result in higher equilibrium skin temperatures. When skin temperature rises above the core temperature, heat removal by the blood circulation and (local) sweat production starts to play an important role, and a non-linear relation between the locally applied SAR and the equilibrium skin temperature is expected as seen in figure 2.

Morvan *et al*. reported a temperature increase in muscle tissue close to the skin of 5 °C after 20 minutes of decoupling at a level of 6 Watt input power (23). It is not clear to what level of superficial SAR this corresponds. As shown in figure 1, the temperature increase did not reach a steady state within 20 minutes in our experiments. The temperature overshoot, as observed in our experiments, demonstrate that it is also important to monitor temperature during decoupling. Furthermore, the temperature registered by imaging was obtained within 1 minute after cessation of decoupling, our data (not shown here) showed a decrease in temperature of 0.5 °C within the first minute after cessation of decoupling.

Locally we measured a rather large temperature increase as a result of RF radiation applied with a surface coil. It is not likely that these experiments will result in an increase in core temperature. The highest total average body SAR in our experiments was 0.15 W/kg. No statistically significant differences in mean

body temperatures were reported by Shellock *et al.* during a 30 minute MR imaging protocol with up to 4.0 W/kg mean SAR (20).

Despite the relatively large increase in skin temperature, none of the subjects sensed these changes. Skin temperature can change during the circadian rhythm or in response to the environment in a broader range than detected during this study (33).

These findings that at SAR levels above the spatial peak power level of 8 W/kg recommended by the FDA do not result in temperature increase above 40 °C which is temperature limit for the extremities (18), suggest that recommended RF radiation safety levels for MRI/MRS procedures may be too conservative in humans with normal thermoregulatory function for the extremities. Previously this has been discussed for whole body procedures in (20). For comparison, the metabolic rate of humans is 1.5 W/kg during sleep, 5 W/kg during moderate exercise and 15 W/kg for very heavy exercise, so the locally applied SAR values in this study (which corresponds with a maximum body average SAR of 0.15 Watt/kg) are not that extreme (10).

However care should be taken because a given SAR can result in different temperature increases depending on the type of tissue and blood flow. Especially in patients with a diminished thermoregulatory function as in diabetes, obesity or cardiovascular disease. Therefore, temperature changes seem to be a more direct indication for possible tissue damage. (20, 21, 23).

References

1. A. Heerschap, P. R. Luyten, J. I. van der Heyden, L. J. Oosterwaal, J. A. den Hollander, Broadband proton decoupled natural abundance 13C NMR spectroscopy of humans at 1.5 T. *NMR Biomed.,* **2,** 124-132, (1989).
2. N. Beckmann, In vivo 13C spectroscopy in humans, *in* "NMR basic principles and progress vol. 28", 74-99, Springer-Verlag, Berlin Heidelberg,1992.
3. P. R. Luyten, G. Bruntink, F. M. Sloff, J. W. Vermeulen, J. I. van der Heijden, J. A. den Hollander, A. Heerschap, Broadband proton decoupling in human 31P NMR spectroscopy. *NMR Biomed.,* **1,** 177-183, (1989).

4. P. A. Bottomley, C. J. Hardy, P. B. Roemer, O. M. Mueller, Proton-decoupled, Overhauser-enhanced, spatially localized carbon-13 spectroscopy in humans. *Magn. Reson. Med.,* **12,** 348-363, (1989).
5. M. J. Avison, D. L. Rothman, E. Nadel, R. G. Shulman, Detection of human muscle glycogen by natural abundance 13C NMR. *Proc. Natl. Acad. Sci. USA,* **85,** 1634-1636, (1988).
6. G. Ende, P. Bachert, Dynamic 13C-1H nuclear polarization of lipid methylene resonances applied to broadband proton-decoupled in vivo 13C MR spectroscopy of human breast and calf tissue. *Magn. Reson. Med.,* **30,** 415-423, (1993).
7. T. F. Budinger, Emerging nuclear magnetic resonance technologies. Health and safety. *Ann. N. Y. Acad. Sci.,* **649,** 1-18, (1992).
8. F. G. Shellock, E. Kanal, "Magnetic Resonance bioeffects, safety, and patient managment," Raven Press, New York, 1994.
9. F. G. Shellock, E. Kanal, Policies, guidelines, and recommendations for MR imaging safety and patient management. SMRI Safety Committee. *J. Magn. Reson. Imag.,* **1,** 97-101, (1991).
10. R. E. Gangarosa, J. E. Minnis, J. Nobbe, D. Praschan, R. W. Genberg, Operational safety issues in MRI. *Magn. Reson. Imaging,* **5,** 287-292, (1987).
11. P. A. Bottomley, R. W. Redington, W. A. Edelstein, J. F. Schenck, Estimating radiofrequency power deposition in body NMR imaging. *Magn. Reson. Med.,* **2,** 336-349, (1985).
12. P. A. Bottomley, P. B. Roemer, Homogeneous tissue model estimates of RF power deposition in human NMR studies. Local elevations predicted in surface coil decoupling. *Ann. N. Y. Acad. Sci.,* **649,** 144-159, (1992).
13. A. J. van den Bergh, S. Houtman, A. Heerschap, N. J. Rehrer, H. J. van den Boogert, B. Oeseburg, M. T. Hopman, Muscle glycogen recovery after exercise during glucose and fructose intake monitored by 13C-NMR. *J. Appl. Physiol.,* **81,** 1495-1500, (1996).
14. J. A. den Hollander, K. L. Behar, R. G. Shulman, Use of double-tuned surface coils for the application of 13C NMR to brain metabolism. *J. Magn. Reson.,, (19*92).
15. J. Mispelter, B. Tiffon, E. Quiniou, J. M. Lhoste, Optimization of 13C-{1H} double coplanar surface-coil design for the WATLZ-16 decoupling sequence. *J. Magn. Reson.,* **82,** 622-628, (1989).
16. B. Tiffon, J. Mispelter, J.-M. Lhoste, A Carbon-13 in vivo double surface-coil NMR

probe with efficient low-power proton decoupling at 400 MHz using Waltz-16 sequence. *J. Magn. Reson.,* **68,** 544-550, (1986).

17. A. J. van den Bergh, H. J. van den Boogert, A. Heerschap, Calibration of the 1H decoupling field strength and experimental evaluation of the specific RF absorption rate in 1H-decoupled human 13C- MRS. *Magn. Reson. Med.,* **39,** 642-646, (1998).
18. Guidence for Content and Review of a Magnetic Resonance Diagnostic Device 510(k) Application, US Food and Drug Administration: Rockville, MD, (1988).
19. B. J. Barber, D. J. Schaefer, C. J. Gordon, D. C. Zawieja, J. Hecker, Thermal effects of MR imaging: worst-case studies on sheep. *AJR. Am. J. Roentgenol.,* **155,** 1105-1110, (1990).
20. F. G. Shellock, D. J. Schaefer, J. V. Crues, Alterations in body and skin temperatures caused by magnetic resonance imaging: is the recommended exposure for radiofrequency radiation too conservative? *Br. J. Radiol.,* **62,** 904-909, (1989).
21. F. G. Shellock, D. J. Schaefer, E. Kanal, Physiologic responses to an MR imaging procedure performed at a specific absorption rate of 6.0 W/kg. *Radiology,* **192,** 865-868, (1994).
22. W. P. Shuman, D. R. Haynor, A. W. Guy, G. E. Wesbey, D. J. Schaefer, A. A. Moss, Superficial- and deep-tissue temperature increases in anesthetized dogs during exposure to high specific absorption rates in a 1.5-T MR imager. *Radiology,* **167,** 551-554, (1988).
23. D. Morvan, A. Leroy Willig, P. Jehenson, C. A. Cuenod, A. Syrota, Temperature changes induced in human muscle by radio-frequency H-1 decoupling: measurement with an MR imaging diffusion technique. Work in progress. *Radiology,* **185,** 871-874, (1992).
24. E. R. Adair, L. G. Berglund, Predicted thermophysiological responses of humans to MRI fields. *Ann. N. Y. Acad. Sci.,* **649,** 188-200, (1992).
25. J. Werner, M. Buse, Temperature profiles with respect to inhomogeneity and geometry of the human body. *J. Appl. Physiol.,* **65,** 1110-1118, (1988).
26. J. Werner, M. Buse, A. Foegen, Lumped versus distributed thermoregulatory control: results from a three-dimensional dynamic model. *Biol. Cybern.,* **62,** 63-73, (1989).
27. M. F. Iskander, O. Khoshdel-Milani, Numerical calculations of the temperature distribution in realistic cross sections of the human body. *Int. J. Radiat. Oncol. Biol.*

Phys., **10,** 1907-1912, (1984).

28. M. B. Ducharme, P. Tikuisis, Role of blood as heat source or sink in human limbs during local cooling and heating. *J. Appl. Physiol.,* **76,** 2084-2094, (1994).
29. A. J. Milligan, P. B. Conran, M. A. Ropar, H. A. McCulloch, R. K. Ahuja, R. R. Dobelbower, Jr., Predictions of blood flow from thermal clearance during regional hyperthermia. *Int. J. Radiat. Oncol. Biol. Phys.,* **9,** 1335-1343, (1983).
30. W. F. Taylor, J. M. Johnson, O. L. D, M. K. Park, Effect of high local temperature on reflex cutaneous vasodilation. *J. Appl. Physiol.,* **57,** 191-196, (1984).
31. M. B. Ducharme, W. P. VanHelder, M. W. Radomski, Tissue temperature profile in the human forearm during thermal stress at thermal stability. *J. Appl. Physiol.,* **71,** 1973-1978, (1991).
32. M. Buse, J. Werner, Closed loop control of human body temperature: results from a one-dimensional model. *Biol. Cybern.,* **61,** 467-475, (1989).
33. J. Werner, T. Reents, A contribution to the topography of temperature regulation in man. *Eur. J. Appl. Physiol.,* **45,** 87-94, (1980).

4 Heteronuclear cross polarization for enhanced sensitivity of in vivo ^{13}C MR spectroscopy on a clinical 1.5 T MR system

A.J. van den Bergh H.J. van den Boogert and A. Heerschap

Department of Radiology, University of Nijmegen,
The Netherlands

Abstract

The potential of heteronuclear {^{1}H-^{13}C} cross polarization was studied for optimization of the signal to noise ratio in *in vivo* ^{13}C MR spectroscopy at the clinical field strength of 1.5 T. Experiments on the human calf showed a significant chemical shift selective signal enhancement on triglyceride signals of 3.9 by heteronuclear cross polarization, compared to a standard pulse-acquire sequence. Studies on a neonatal piglet brain showed an enhancement by cross polarization of 2.2 for the detection of ^{13}C-1-glucose. This enhancement allowed a fourfold improvement in time resolution in dynamic ^{13}C MR of ^{13}C-1-glucose inflow in piglet brain. Phantom experiments demonstrated the efficiency of this technique for interleaved detection of two spectral regions. Tests with a volume coil showed the feasibility of signal enhancement by cross polarization over a large volume of interest.

This chapter is based on the publication: Heteronuclear cross polarization for enhanced sensitivity of in vivo ^{13}C MR spectroscopy on a clinical 1.5T MR system. A.J. van den Bergh, H.J. van den Boogert, A. Heerschap, *J Magn Reson,* **135**: 93-98 (1998)

Introduction

In vivo ^{13}C MR spectroscopy enables one to obtain metabolic information of humans not easily obtained by other non-invasive methods. The large chemical shift range of ^{13}C MR spectra allows the resolution of resonances of a large number of substances, and thereby the study of some metabolites of which the signals are difficult to resolve in ^{1}H MR spectroscopy.

One of the major drawbacks of ^{13}C MR spectroscopy applied to humans is its low sensitivity, that is a consequence of the low natural abundance (1.1%) and the low gyromagnetic constant γ of the carbon nucleus ($\gamma^{1}H / \gamma^{13}C \approx 4$). Furthermore, most carbons have attached protons, resulting in multiplet structures which further decrease sensitivity and complicate spectrum analyses.

Most ^{13}C MR studies performed on humans use proton decoupling to remove the multiplet-splittings, thereby enhancing sensitivity and resolution (1-5). With nuclear Overhauser enhancement (NOE) the sensitivity of ^{13}C MR spectroscopy can be further increased (6-8).

Heteronuclear polarization transfer provides another way to enhance sensitivity. This polarization transfer can be performed from the sensitive to the insensitive nucleus or vice versa (9, 10). The theoretically highest signal gain can be obtained when excitation and detection are performed at the sensitive nucleus (11-15).

This study focuses on the polarization transfer from protons to carbons to enhance sensitivity. Only a few studies have been reported in which this was applied to *in vivo* ^{13}C MR spectroscopy of humans, e.g., by the SINEPT method (16, 17) and by the DEPT method (18, 19). An alternative approach, not based on pulse-interrupted free precession, but by which transfer of magnetization is achieved by heteronuclear isotropic mixing, has recently been reported to be feasible *in vivo* at high magnetic field on a small bore NMR system (20). An adiabatic variant of this heteronuclear cross polarization has been proposed for *in vivo* applications (21). The technique of heteronuclear cross polarization has

some advantages compared to the pulse-interrupted free precession methods: (i) the resulting peaks are not in mixed phase as may occur in SINEPT which makes analyses of the signals easier; (ii) the magnetization transfer function is less critically dependent on the scalar coupling; (iii) in the DEPT sequence strong 180° refocusing pulses are used, which are often a source of artifacts in the case of inhomogeneous B_1 fields; (iv) the transfer does not depend on the multiplicity like in DEPT; (v) relaxation losses during the magnetization transfer period are limited (20); (vi) one can use decoupling without the need for a delay (which results in a further decrease in enhancement) between the polarization transfer pulses and the decoupling / acquisition period as in SINEPT (16).

The objective of this study was to explore the potential of heteronuclear {^{1}H-^{13}C} cross polarization, using a WALTZ isotropic mixing period, to enhance the sensitivity of ^{13}C MR spectroscopy on a clinical MR system at 1.5 T. The WALTZ-4 based cross polarization sequence is shown in figure 1.

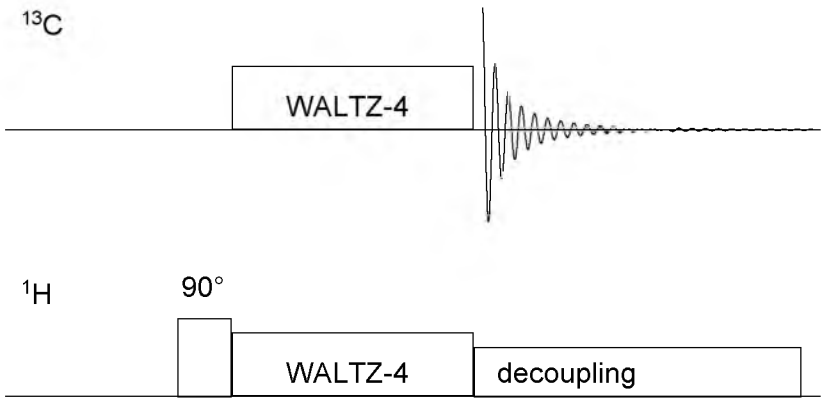

Figure 1.

The WALTZ-4 based heteronuclear cross polarization sequence. Duration of the WALTZ-4 contact pulse was 6.5 ms, which is optimal for proton-carbon coupling constants of 150 Hz.

Experimental

Measurements were performed on an 1.5 T Magnetom SP 4000 (Siemens, Erlangen, Germany) equipped with a second RF transmit channel. Two types of coil configurations were used for the different ^{13}C / ^{1}H double resonance experiments, depending on the volume of interest. The surface coil set-up consisted of an 11 cm diameter ^{13}C transmit / receive surface coil and a 17 x 23 cm ^{1}H transmit / receive butterfly coil. As a volume coil an ^{1}H linear vertically polarized birdcage constructed within the original housing of a Siemens SP head coil was used, combined with a transmit / receive ^{13}C horizontally polarized curved half volume coil (22).

Two pulse sequences were used in this study. First, a ^{13}C pulse-acquire sequence with optional proton decoupling during the acquisition period and secondly a cross polarization sequence as described in (23). The mixing period in the latter sequence consisted of one WALTZ-4 cycle with a duration of 6.5 ms, decoupling was also optional in this sequence.

For the direct detection experiments the power of the hard 260μs excitation pulse was optimized for maximal signal intensity. This optimized power level was also used for the contact pulse in polarization transfer experiments. The RF field strength of the ^{1}H coil for decoupling as well as polarization transfer was optimized for a certain volume using a localized calibration technique (24) which enables optimal settings for polarization transfer despite the use of two differently shaped coils.

Phantom studies

To demonstrate the feasibility of this sensitivity enhancement technique several phantom studies were performed. To test the surface coil set-up we used a cylindrical phantom with diameter 10 cm, containing sunflower oil, or a solution of 109 mM glycosyl units rabbit liver glycogen. Another phantom spherical in shape, with diameter 8 cm, contained a solution of glucose, lactate and glutamate. The

latter phantom was used to study interleaved cross polarization at two different frequencies.

To investigate the effect of the larger matching volume of the RF fields of the volume coil set-up we used a large spherical phantom (diameter 15 cm) filled with sunflower oil. Localized spectra were acquired using 2 dimensional chemical shift imaging (CSI); the phase encoding was applied after the polarization transfer from ^{1}H to the ^{13}C nucleus to compare the results with conventional ^{13}C 2D-CSI measurements.

In vivo studies

Postmortem decoupling and cross polarization studies were performed with the surface coil set-up on a neonatal piglet brain, containing ^{13}C-1 labeled glucose, to optimize the Hartmann-Hahn matching. *In vivo* ^{13}C MR spectroscopy was performed on the brain of an anesthetized neonatal piglet to monitor the influx of labeled ^{13}C-1-glucose. The piglet was anesthetized with pentobarbital, and catheterized in the carotid artery. Inside the magnet, anesthesia was maintained by pump-ventilating with ethrane. During spectroscopy, rectal temperature and ECG were monitored. Over a period of 15 minutes, glucose 20 % (30% enriched) (Campro Scientific, Veenendaal, The Netherlands) was infused with an infusion speed of 0.5 ml/min. In this case cross polarization was performed at one frequency region to achieve the highest time resolution possible.

Furthermore, ^{13}C MR spectra of the human calf were obtained to show that signal enhancement using cross polarization is realizable on humans *in vivo*. In this experiment, the SAR at the body surface of RF power deposition from the ^{1}H surface coil was estimated to be 2.9 Watt/kg, as calculated according to the procedure described in (24) and this is well below safety guidelines (25). This SAR value was mainly due to the decoupling part of the sequence, and not the WALTZ-4 contact period. Contribution of the ^{13}C channel was negligible because of the much lower duty cycle and its lower frequency (26).

Spectral analyses was performed using Siemens Luise software (Siemens, Erlangen, Germany). Spectra were zero-filled to 4K data-points, multiplied by a

gauss function of 64 ms, phase and baseline corrected, peaks of interest were fitted to a gaussian lineshape. Chemical shift imaging data were filtered with a hamming filter prior to fourier transformation. Spectra of individual voxels were analyzed as mentioned above.

Chemical shift scaling was performed placing the methyl signal of tetramethylsilane at 0 ppm.

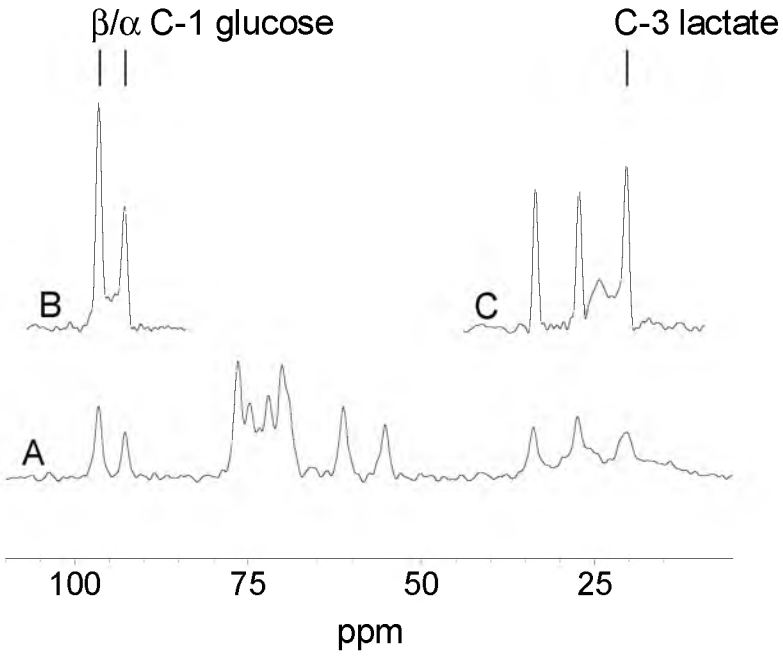

Figure 2.

^{13}C MR spectra recorded from a spherical phantom containing an aqueous solution of glucose 300 mM, lactate 250 mM and glutamate 200 mM. Shown are spectra obtained with a pulse-acquire sequence (A) compared to spectra (B, C) obtained with chemical shift selective cross polarization. Measurement parameters were as follows: 256 FIDs were accumulated for spectrum (A), for spectra (B) and (C) in an interleaved fashion: 2 times 2 blocks of 128 accumulations at each frequency, the ^{13}C frequency was placed at the C-1-glucose region (94 ppm) and at the C-3-lactate region (20 ppm) with a difference of 1200 Hz. Spectral width was 8 kHz, 512 datapoints were collected, and the repetition time was 1 s.

Results

Phantom studies

Figure 2A shows an ^{1}H decoupled ^{13}C MR pulse-acquire spectrum of a phantom filled with an aqueous solution of glucose, lactate, and glutamate, obtained with a surface coil set-up. Resonances of carbon spins from all substances are clearly visible. Spectra in figure 2B and 2C show the results of the enhancement by the use of chemical shift selective cross polarization applied in an interleaved mode for two specific spectral regions, i.e., at the C-1 resonance of glucose (94 ppm) and at the C-3 resonance of lactate (20 ppm). Enhancement factors of both resonances were 3.1 and 3.6, respectively. The present use of WALTZ-4 based cross polarization makes the experiment chemical shift selective; polarization transfer occurs in a small spectral region ($\gamma B_1/2\pi \approx 900$ Hz). Cross polarization experiments targeting a single frequency region were performed with the surface coil set-up on phantoms containing sunflower oil and a glycogen solution. On the oil phantom enhancement factors of 3.8 for the unsaturated as well as the saturated lipid carbon resonances could be achieved, which is close to the theoretical maximum enhancement of ≈ 4. The signal gain of 2.1 obtained for the C-1 signal of glycogen in solution was considerably lower.

Experiments with the volume coil and ^{13}C MR spectroscopy acquisition extended with 2D-CSI localization resulted in the data presented in figure 3. Spectral maps of the C=C spectral region at 130 ppm of the 2D-CSI data sets are shown; the spectra drawn in white were obtained with ^{1}H broadband decoupled ^{13}C 2D-CSI. Spectra drawn in red were obtained with the polarization transfer pulse sequence optimized for the C=C spectral region; broadband ^{1}H decoupling was also applied.

All voxels showed a significant signal increase, signal gains of the individual voxels ranged from 2.68 to 3.85, mean signal gain was 3.18 (SE = 0.04). The lowest signals in both experiments are in the top row voxels. These voxels are

outside the sensitive volume of the ^{13}C half volume coil which was wrapped around the bottom side of the phantom; coil wires are marked in the figure.

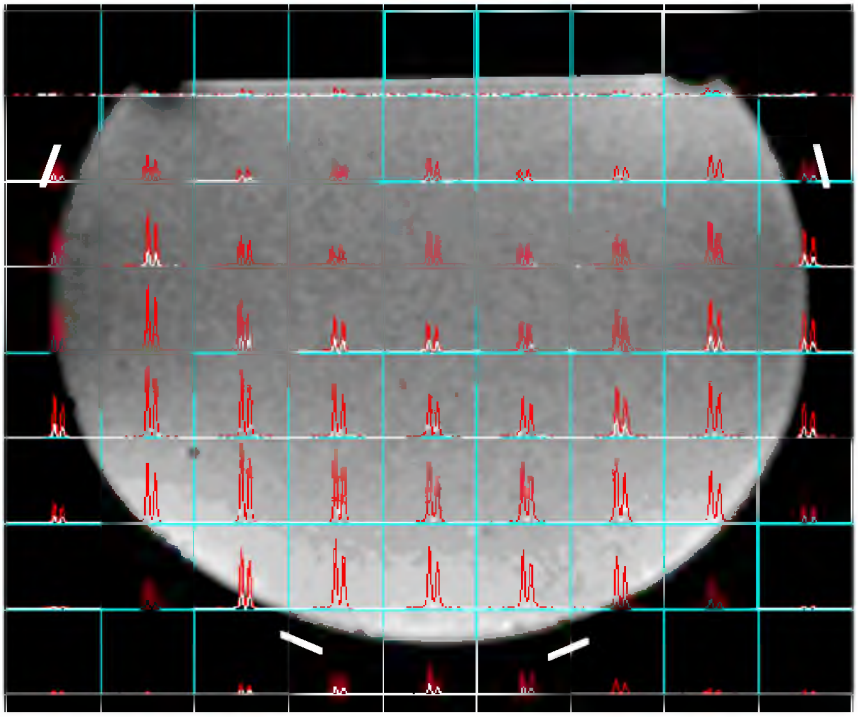

Figure 3

Spectral maps obtained from a large spherical phantom containing sunflower oil, measured using an ^{1}H / ^{13}C volume coil configuration. Spectra acquired using heteronuclear cross polarization are drawn in red, compared to the spectra obtained with a pulse-acquire technique shown in white, plotted with the same scaling. Positions of the ^{13}C half volume coil wires are indicated.
The matrix size of the CSI data was 16 x 16 x 1024, spectral width was 6 kHz, field of view of 240 mm resulting in a voxel size of 15 x 15 mm, repetition time in both puls-acquire and heteronuclear cross polarization was 1.5 s, and total measurement time of a CSI data set was 6 min. 36 s. Cross polarization was optimized for the C=C spectral region around 130 ppm.

In vivo studies

Postmortem cross polarization studies on the brain of a neonatal piglet resulted in a signal enhancement of 2.2 for the C-1 signals of ^{13}C-labeled glucose, present in the brain (figure 4A and 4B). Figure 4C shows a stack plot of spectra

recorded during infusion of ^{13}C labeled glucose using heteronuclear cross polarization applied *in vivo* to the brain of a piglet. The time resolution was 3 minutes. The first spectrum was obtained before the start of the ^{13}C-1-glucose infusion. The subsequent spectra clearly show increasing glucose signals during the infusion period and a decrease thereafter.

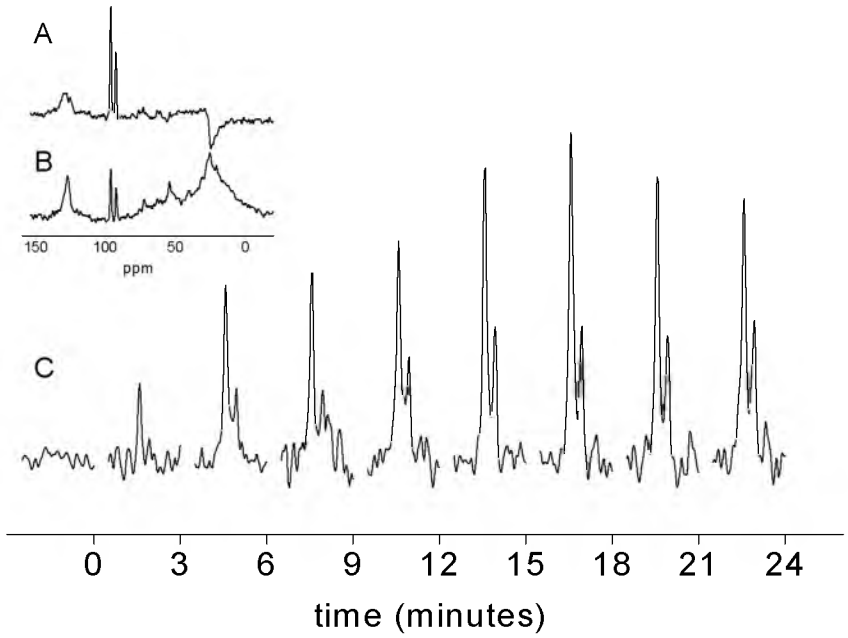

Figure 4

^{13}C MR spectra of a postmortem neonatal piglet brain containing ^{13}C-1-glucose are shown in figure 4 A and B. Spectrum A was obtained using heteronuclear cross polarization and spectrum B using direct detection and proton decoupling. *In vivo* ^{13}C MR spectra recorded from a neonatal piglet brain before, during and after administration of ^{13}C-1-glucose are shown in figure 4C. Only the C-1-glucose spectral region is shown, 80-110 ppm. Experimental parameters: 240 acquisitions, repetition time of 750 ms.

In vivo ^{13}C MR spectra of the unsaturated triglyceride carbons originating from superficial adipose tissue of the human leg are shown in figure 5. For the

spectrum in figure 5A no decoupling was used whereas for the spectrum in figure 5B, WALTZ-4 proton decoupling was applied during the signal acquisition period. Spectrum C was obtained using both cross polarization and WALTZ-4 decoupling. Enhancement factors for spectrum B and C are respectively 2.7 and 10.6 with respect to the non-decoupled spectrum. A gain larger in magnitude than 2 for decoupling can be explained by partial NOE. Cross polarization accounted for a signal gain of 3.9 in the latter experiment. Until now, no signal enhancement could be achieved *in vivo* for the C-1 signal of glycogen in human muscle compared to direct acquisition with enhancement by decoupling and NOE.

Discussion

This study shows that the sensitivity of ^{13}C MR spectroscopy at the clinical field strength of 1.5 T can be improved significantly with the use of heteronuclear cross polarization from protons to carbons. The gains obtained for triglyceride signals are close to the theoretical value, $\gamma^{1}H / \gamma^{13}C \approx 4$. The total gain achieved with cross polarization, decoupling and NOE was 10.6 for the unsaturated triglyceride carbons in *in vivo* ^{13}C MR spectra of the human calf. Polarization transfer experiments performed on the human calf with which we compare these results are from Bomsdorf et al. (16). They reported a total signal enhancement of 6 for the unsaturated fatty acid signals with the use of SINEPT and ^{1}H decoupling at 4 T.

Knüttel et al. (27) demonstrated the detection of unsaturated carbons of fatty acids by an indirect method of selecting ^{13}C attached protons. Theoretically a higher signal enhancement is possible with this method but the resulting spectrum showed some disadvantages.

Firstly, only one of the lines of the doublet is visible in the proton detected spectrum; the other line coincides with the water resonance. Secondly, at the low resolution in proton detection, one cannot discriminate between mono- and poly-

unsaturated fatty acids, as is possible in the cross polarization enhanced ^{13}C spectrum, see figure 3.

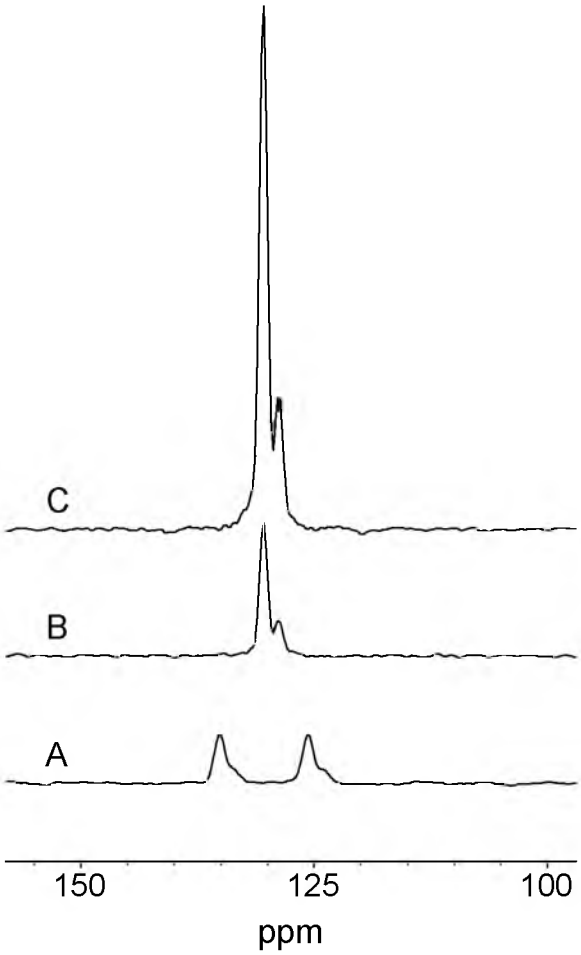

Figure 5.

Natural abundance ^{13}C MR spectra of the human calf. Spectra were obtained (A) without ^{1}H decoupling, (B) with broadband ^{1}H decoupling using WALTZ-4 and (C) with heteronuclear cross polarization optimized for the C=C spectral region (130 ppm) and broadband ^{1}H decoupling, using the surface coil setup. Spectra are plotted on the same scaling. Experimental parameters: 64 acquisitions, repetition time of 3 s, 512 data points, and spectral width 8 kHz. Subject was a 23 year old female weighing 52 kg. The study was performed after an informed consent was obtained.

In general, indirect detection of carbons in ^{1}H spectra requires good water suppression; it often results in distorted baselines and suffers a low spectral resolution (27-29). With labeled compounds often broadband ^{13}C decoupling is required during proton detection to obtain maximum signal gain and resolution.

This requires much more power than broadband ^{1}H decoupling during ^{13}C signal acquisition and is of concern regarding RF deposition safety guidelines.

In phantom studies, detection of the C-1 signal of glycogen using heteronuclear cross polarization, decoupling and partial NOE resulted in an signal gain of 2.1 compared to direct detection with decoupling and partial NOE. No signal gain was achieved *in vivo* with respect to ^{1}H decoupling and partial NOE. A significantly lower transfer efficiency for glycogen C-1 compared to lipid signals was reported for the SINEPT polarization transfer scheme (16, 17). This is likely due to a shorter (effective) T_2 of the glycogen C-1 compared to the triglyceride carbons. Knüttel et al. showed that detection of liver glycogen is possible using proton-detected ^{13}C spectroscopy (28).

The most promising application of cross polarization *in vivo* is probably the possibility to enhance the time resolution in dynamic ^{13}C-labeling studies. The increase in magnitude of the C-1 signals of glucose in the neonatal piglet brain by a factor of 2.2 improves the temporal resolution for detection of these signals by a factor over 4. An improved time resolution was also reported in a ^{13}C labeling study of RIF-1 tumors with the use of heteronuclear cross polarization (20).

Although the effective chemical shift range of the cross polarization method as applied in this study is limited, it is demonstrated that more chemical shift regions can be covered by interleaved cross polarization at different frequencies. The total measurement time, for cross polarization of two chemical shift regions, can still be shorter than the time to obtain a ^{13}C MR spectrum with the same signal to noise ratio, using the pulse-acquire method. Chemical shift selective enhancement by cross polarization at two frequencies has also been reported by Artemov et al. (20).

In the cross polarization experiments broadband ^{1}H WALTZ-4 decoupling was applied during the acquisition period to enable a comparison with the conventional ^{1}H decoupled ^{13}C MR spectroscopic pulse-acquire technique. Because of the chemical shift selective character of the present cross

polarization method broadband decoupling is not really necessary. The use of CW decoupling relaxes RF power deposition and therefore higher duty cycles can be used which further decreases measurement times.

Part of the results in this study was obtained with a double surface coil set-up, to achieve a high signal to noise ratio. However, one problem arises with surface coils and cross polarization techniques: the RF fields of both coils have to match to fulfill the Hartmann-Hahn condition. A partly mismatch may have contributed to the lack of enhancement for the C-1 signal of glycogen from the muscle as compared to an enhancement of 2.1 for this signal of glycogen in solution.

To achieve easy matching of the RF fields over a large volume of interest, we explored the use of a homogeneous ^{1}H coil in which a ^{13}C half volume coil was placed. Calibration of the necessary power to be applied to the ^{1}H coil was straightforward. For comparison of the signal gain in the individual CSI voxels the RF pulse amplitudes used on the ^{13}C half volume coil, in the pulse-acquire experiment and the cross polarization experiment were set to the same value. Signal gain was similar for all voxels in the sensitive area of the ^{13}C coil, showing good Hartmann-Hahn matching of the RF fields over the large volume of the phantom.

In this study both non-localized spectra and CSI localized spectra were measured. Improvements in localization can be made by using a slice selective proton excitation pulse or other means of volume selection like ISIS (8, 9, 18, 19, 30) which can be placed before the polarization transfer element in the sequence.

Acknowledgement

The authors thank Theo Arts for animal preparation.

References

1. M. J. Avison, D. L. Rothman, E. Nadel, R. G. Shulman, Detection of human muscle glycogen by natural abundance 13C NMR. *Proc. Natl. Acad. Sci. USA,* **85,** 1634-1636, (1988).
2. C. T. Moonen, R. J. Dimand, K. L. Cox, The noninvasive determination of linoleic acid content of human adipose tissue by natural abundance carbon-13 nuclear magnetic resonance. *Magn. Reson. Med.,* **6,** 140-157, (1988).
3. A. Heerschap, P. R. Luyten, J. I. van der Heyden, L. J. Oosterwaal, J. A. den Hollander, Broadband proton decoupled natural abundance 13C NMR spectroscopy of humans at 1.5 T. *NMR Biomed.,* **2,** 124-132, (1989).
4. N. Beckmann, In vivo 13C spectroscopy in humans, *in* "NMR basic principles and progress vol. 28", 74-99, Springer-Verlag, Berlin Heidelberg,1992.
5. A. J. van den Bergh, S. Houtman, A. Heerschap, N. J. Rehrer, H. J. van den Boogert, B. Oeseburg, M. T. Hopman, Muscle glycogen recovery after exercise during glucose and fructose intake monitored by 13C-NMR. *J. Appl. Physiol.,* **81,** 1495-1500, (1996).
6. G. Ende, P. Bachert, Dynamic 13C-1H nuclear polarization of lipid methylene resonances applied to broadband proton-decoupled in vivo 13C MR spectroscopy of human breast and calf tissue. *Magn. Reson. Med.,* **30,** 415-423, (1993).
7. P. A. Bottomley, C. J. Hardy, P. B. Roemer, O. M. Mueller, Proton-decoupled, Overhauser-enhanced, spatially localized carbon-13 spectroscopy in humans. *Magn. Reson. Med.,* **12,** 348-363, (1989).
8. R. Gruetter, D. L. Rothman, E. J. Novotny, R. G. Shulman, Localized 13C NMR spectroscopy of myo-inositol in the human brain in vivo. *Magn. Reson. Med.,* **25,** 204-210, (1992).
9. W. P. Aue, S. Muller, J. Seelig, Localized 13C NMR spectra with enhanced sensitivity obtained by volume-selective excitation. *J. Magn. Reson.,* **61,** 392-395, (1985).
10. M. G. Irving, S. J. Simpson, W. M. Brooks, R. S. Holmes, D. M. Doddrell, Application of the reverse dept polarization-transfer pulse sequence to monitor in vitro and in vivo metabolism of 13C- ethanol by 1H-NMR spectroscopy. *Int. J. Biochem.,* **17,** 471-478, (1985).

11. S. M. Fitzpatrick, H. P. Hetherington, K. L. Behar, R. G. Shulman, The flux from glucose to glutamate in the rat brain in vivo as determined by 1H-observed, 13C-edited NMR spectroscopy. *J. Cereb. Blood. Flow. Metab.,* **10,** 170-179, (1990).
12. C. Kunze, R. Kimmich, Motion-insensitive localized 13C spectroscopy using cyclic and slice-selective J cross polarization. *J. Magn. Reson.,* **series B 105,** 38-44, (1994).
13. P. C. van Zijl, A. S. Chesnick, D. DesPres, C. T. Moonen, J. Ruiz Cabello, P. van Gelderen, In vivo proton spectroscopy and spectroscopic imaging of [1-13C]-glucose and its metabolic products. *Magn. Reson. Med.,* **30,** 544-551, (1993).
14. E. J. Novotny, Jr., T. Ogino, D. L. Rothman, O. A. Petroff, J. W. Prichard, R. G. Shulman, Direct carbon versus proton heteronuclear editing of 2-13C ethanol in rabbit brain in vivo: a sensitivity comparison. *Magn. Reson. Med.,* **16,** 431-443, (1990).
15. D. L. Rothman, K. L. Behar, H. P. Hetherington, J. A. den Hollander, M. R. Bendall, O. A. Petroff, R. G. Shulman, 1H-Observe/13C-decouple spectroscopic measurements of lactate and glutamate in the rat brain in vivo. *Proc. Natl. Acad. Sci. USA,* **82,** 1633-1637, (1985).
16. H. Bomsdorf, P. Roschmann, J. Wieland, Sensitivity enhancement in whole-body natural abundance 13C spectroscopy using 13C/1H double-resonance techniques at 4 Tesla. *Magn. Reson. Med.,* **22,** 10-22, (1991).
17. M. Saner, G. McKinnon, P. Boesiger, Glycogen detection by in vivo 13C NMR: A comparison of proton decoupling and polarization transfer. *Magn. Reson. Med.,* **28,** 65-73, (1992).
18. N. Beckmann, S. Muller, Analysis of localized polarization transfer for 13C volume-selective spectroscopy with surface coils. *J. Magn. Reson.,* **93,** 299-318, (1991).
19. R. Gruetter, G. Adriany, H. Merkle, P. M. Andersen, Broadband decoupled, 1H-localized 13C MRS of the human brain at 4 Tesla. *Magn. Reson. Med.,* **36,** 659-664, (1996).
20. D. Artemov, Z. M. Bhujwalla, J. D. Glickson, In vivo selective measurement of (1-13C)-glucose metabolism in tumors by heteronuclear cross polarization. *Magn. Reson. Med.,* **33,** 151-155, (1995).

21. H. Kostler, R. Kimmich, Adiabatic J cross polarization for localized direct and proton-detected 13C spectroscopy. *J. Magn. Reson.,* **Series B 102,** 285-292, (1993).
22. H. J. van den Boogert, A. J. van den Bergh, A. Heerschap. A multipurpose coil configuration for 1H decoupled 31P or 13C MRS, *in* "ISMRM 4th Annual Meeting, New York, 1996," p. 1423
23. D. Y. Artemov, WALTZ-16-Based heteronuclear cross polrization. *J. Magn. Reson.,* **91,** 405-407, (1991).
24. A. J. van den Bergh, H. J. van den Boogert, A. Heerschap, Calibration of the 1H decoupling field strength and experimental evaluation of the specific RF absorption rate in 1H decoupled human 13C-MRS. *Magn. Reson. Med.,* **39,** 642-646, (1998).
25. F. G. Shellock, E. Kanal, Policies, guidelines, and recommendations for MR imaging safety and patient management. SMRI Safety Committee. *J. Magn. Reson. Imag.,* **1,** 97-101, (1991).
26. M. Grandolfo, A. Polichetti, P. Vecchia, O. P. Gandhi, Spatial distribution of RF power in critical organs during magnetic resonance imaging. *Ann. N. Y. Acad. Sci.,* **649,** 176-187, (1992).
27. A. Knuttel, R. Kimmich, K.-H. Spohn, Indirect 13C tomography and volume-selective spectroscopy via proton NMR. I Spectroscopic Techniques. *J. Magn. Reson.,* **86,** 526-541, (1990).
28. A. Knuttel, R. Kimmich, K. H. Spohn, Motion-insensitive volume-selective pulse sequences for direct and proton-detected 13C spectroscopy: detection of glycogen in the human liver in vivo. *Magn. Reson. Med.,* **17,** 470-482, (1991).
29. D. L. Rothman, A. M. Howseman, G. D. Graham, O. A. Petroff, G. Lantos, P. B. Fayad, L. M. Brass, G. I. Shulman, R. G. Shulman, J. W. Prichard, Localized proton NMR observation of [3-13C]lactate in stroke after [1-13C]glucose infusion. *Magn. Reson. Med.,* **21,** 302-307, (1991).
30. R. J. Ordidge, A. Connelly, J. A. B. Lohman, Image-selected in vivo spectroscopy (ISIS). A New technique for spatially selective NMR spectroscopy. *J. Magn. Reson.,* **66,** 283-294, (1986).

5 Muscle glycogen recovery after exercise during glucose and fructose intake monitored by ^{13}C-NMR

A.J. van den Bergh[1], S. Houtman[2], A. Heerschap[1], N. J. Rehrer[3], H. J. van den Boogert[1], B. Oeseburg[2], M. T.E. Hopman[2]

[1])Department of Radiology, University of Nijmegen, The Netherlands
[2])Department of Physiology, University of Nijmegen, The Netherlands
[3])School of Physical Education, Otago University, Dunedin, New Zealand

Abstract

The purpose of this study was to examine muscle glycogen recovery with glucose feeding (GF) in comparison to fructose feeding (FF) during the first eight hours after partial glycogen depletion using ^{13}C Nuclear Magnetic Resonance (^{13}C-NMR) on a clinical 1.5 T MR system. After measuring the glycogen concentration of the vastus lateralis (VL) muscle, glycogen stores of the VL were depleted by bicycle exercise in seven male subjects. During eight hours following completion of exercise, subjects were orally given either GF or FF, while the glycogen content of the VL was monitored by ^{13}C-NMR spectroscopy every second hour. The muscular glycogen concentration was expressed as a percentage of the glycogen concentration measured before exercise. The glycogen recovery rate during GF (4.2±0.2 %/h) was significantly higher ($p < 0.05$) compared to FF (2.2 ± 0.3 %/h). This study shows: 1) muscle glycogen levels are perceptible by ^{13}C-NMR spectroscopy at 1.5 T, 2) the glycogen restoration rate is higher following GF compared to FF.

This chapter is based on the publication: Muscle glycogen recovery after exercise during glucose and fructose intake monitored by ^{13}C-NMR. A.J. van den Bergh, S. Houtman, A. Heerschap, N.J. Rehrer, H.J. van den Boogert, B. Oeseburg, M.T.E. Hopman, *J Appl Physiol*, **81**:1495-1500 (1996)

Introduction

One of the most important limiting factors in long term muscular performance is the depletion of glycogen in the working muscle (1-3). It has been suggested that some of the feelings of tiredness associated with overtraining are related to lowered glycogen reserves. The resynthesis of muscle glycogen during the recovery period is therefore an important metabolic process. Muscle glycogen repletion is highly dependent on adequate carbohydrate (CHO) intake (4, 5). Biopsy studies of the vastus lateralis (VL) muscle have shown that glucose feeding (GF) results in a faster recovery of muscle glycogen levels than fructose feeding (FF) (6).

However, the performance of biopsies is difficult at short time intervals from the same muscle and it may affect metabolic processes. ^{13}C Nuclear Magnetic Resonance (^{13}C-NMR) spectroscopy has emerged as an appropriate non-invasive alternative for the assessment of muscle glycogen metabolism. Taylor et al. (7) showed that the C-1 resonance from glycogen, which is well resolved from other spectral components, can be used to quantify muscle glycogen levels. Price et al. (8, 9) studied muscle glycogen resynthesis employing ^{13}C-NMR spectroscopy. After depletion up to 25% of its original amount, glycogen repletion was fast in the first hour and slower in the following hours without any feeding. Recently Moriarty et al. (10) also used ^{13}C-NMR spectroscopy to study glycogen utilization and restoration in liver and skeletal muscle. In their study, the effect of the consumption of glucose and sucrose drinks on glycogen repletion was compared. No difference was detected between glycogen recovery rates (GRRs) as a result of glucose and sucrose intake. These two studies (9, 10) were performed at magnet field strengths of 4.7 and 3.0 T. It has been demonstrated that glycogen depletion and recovery can also be observed at the more commonly available field strength of 1.5 T (11, 12).

So far no ^{13}C-NMR data is available comparing glycogen restoration during GF and during FF after glycogen depletion. In the present study muscle glycogen

recovery was examined the first 8 hours after depletion during GF and FF with ^{13}C-NMR spectroscopy at 1.5 T.

Methods

Subjects. Seven healthy, well trained, male subjects participated in this study after an informed consent was obtained. Mean age of the subjects was 24 yr (range: 23-27 yr), body mass 78 kg (71-90 kg), height 1.87 m (1.79-1.93 m), and fat percentage 10 % (7.0-12.0 %). The Medical Faculty Ethics Committee approved this study.

Preparation protocol. At least 1 week before the actual experiments were performed, the individual maximum power output (Wmax) was determined on an electromagnetically braked bicycle-ergometer (LODE, The Netherlands), using a continuous incremental exercise test. The exercise started at 20 Watt (W) and increased with 20 W/min. The subjects had to maintain the revolution rate between 60-80 revolutions/min (rpm). The individual Wmax was equal to the last power output completed for 1 minute with a pedalling rate above 60 rpm.

All subjects performed two glycogen 'depletion-restoration' experiments with at least five days in between. Subjects were asked not to participate in exhaustive exercise two days in advance of both experiments and to fast (except for water) 10 hours before the start of the experiments. The actual experiment started with the determination of the glycogen content of the VL muscle using ^{13}C-NMR spectroscopy.

Glycogen depletion protocol. All subjects performed bicycle exercise according to a protocol described by Kuipers et al. (13), in order to deplete the VL of glycogen. Bicycle exercise was performed on an electro-magnetically braked bicycle-ergometer. The glycogen depletion protocol consisted of alternating 2 minute intervals of 90 % Wmax and 50 % Wmax. When the subject was unable to perform at 90 % Wmax, the workload was lowered to subsequently 80 %, 70 % and 60 % Wmax. When 60 % Wmax could not be maintained the exercise

was stopped and the glycogen content of the VL was determined again by ^{13}C-NMR spectroscopy to measure the extent of the glycogen depletion. The exercise was performed at ± 18 °C, and subjects were free to drink water.

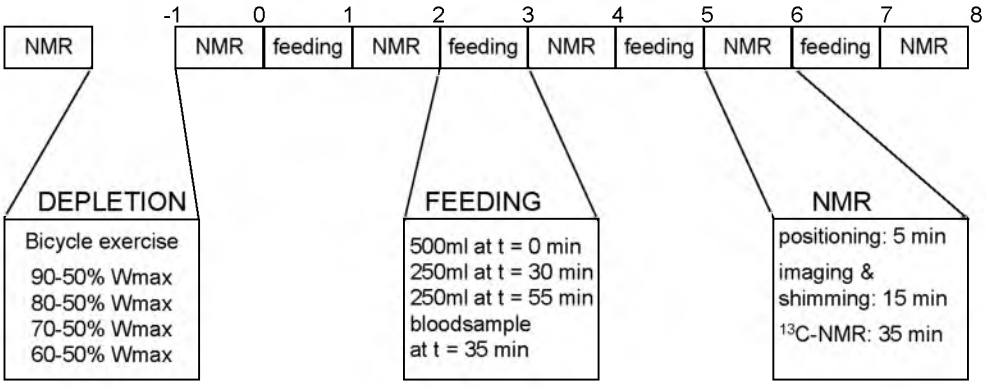

Figure 1

Schematic presentation of experiment 1 and 2. During 8 hours following glycogen depletion ^{13}C-NMR measurements and feeding hours were alternated. The feeding and NMR hours were structured as shown in the enlarged sections.

CHO-feeding protocol. During 8 hours after the depletion exercise and the second NMR measurement, CHO-ingestion was alternated with glycogen measurements every hour, according to figure 1.

During the CHO-feeding hours, subjects drank 500 ml of a CHO solution at 0 minutes, 250 ml at 30 minutes and 250 ml at 60 minutes. CHO feeding was given in counter balanced order: in one experiment GF, in the other experiment FF. CHO solutions consisted of 80 g CHO (AMYLUM NV, Belgium) and 1.15 g NaCl (MERCK, Germany) dissolved in 950 ml tap-water. The CHO solutions were stored at ± 6 °C, for an optimal fast resorption.

Blood- and urine samples were obtained to verify possible loss of glucose. Blood glucose was determined in a capillary blood sample from the finger using a photometer apparatus (HEMOCUE AB, Sweden). Urine was checked for glucose using glucosticks (BAYER, Germany).

During CHO intake the actual ^{13}C-NMR measurement started always exactly 2 hours after the start of the previous ^{13}C-NMR measurement.

^{13}C-NMR spectroscopy. VL glycogen levels were monitored by natural abundance ^{13}C-NMR spectroscopy at 1.5 T on a Siemens Magnetom SP63/84 (SIEMENS, Germany), equipped with a second radio frequency channel. The radio frequency probe consisted of two surface coils; a butterfly shaped (0.11 x 0.24 m) ^{1}H-coil and a circular ^{13}C-coil (0.10 m diameter). The proton coil was used for shimming, imaging and decoupling. The line width at half height of the water resonance was shimmed below 30 Hz.

The pulse sequence for acquisition of ^{13}C-NMR spectra consisted of an adiabatic excitation pulse of 2.56 ms length preceded by a low angle hard pulse and a dephasing gradient to reduce signals from superficial fat. During the first 65 ms of the acquisition period broadband WALTZ-4 proton decoupling was used. A chemical shift imaging (CSI) based calibration program was used to compute an optimum for repetition time and decoupling power within the guidelines for specific absorption rate (SAR) recommended by the FDA (14). Average power dissipated at the body surface was 7.5 W/kg and 0.9 W/kg averaged over the tissue sampled by the coil, calculated according to Heerschap et al. (12). The repetition time was 0.7 s, the sample width 8000 Hz and the number of data points was 1024. Each ^{13}C-NMR measurement consisted of 3000 acquisitions, which equals to 35 minutes of acquisition time. The total measurement time was 50 minutes including imaging and shimming. Possible Nuclear Overhauser enhancement (NOE) and saturation of the creatine C-3 resonance under the present measurement conditions were determined for 3 volunteers by acquiring spectra without decoupling and at a repetition time of 1.4 s. Possible NOE and saturation of the glycogen C-1 resonance were determined in a 110 mM (glucose units) glycogen solution.

Positioning. The anterolateral part of the right leg was placed on the ^{13}C-surface coil with the center of the coil at 65 % of the distance from the spina iliaca anterior superior to the medial femoral epicondyle. By means of an NMR image

the position of the VL was checked. Once the first glycogen measurement was done at a certain position this position was reproduced as closely as possible for the subsequent measurements.

Spectroscopic analysis. The spectroscopic data was analyzed using the software package Luise (SIEMENS, Germany). Free induction decays (FIDs) were zerofilled to 4 K, multiplied by a 10 Hz gauss filter, Fourier transformed and phase and baseline corrected. The C-1 resonance of glycogen and the C-3 resonance of creatine were fitted to a gaussian line shape. The natural line width at one-half maximum of the C-1 resonance of glycogen before exercise ranged from 55-89 Hz. The fit program was allowed to vary the line width between 50-100 Hz in all evaluations. These line width limits for the glycogen C-1 resonance were the only prior knowledge constraints used in the fitting procedure. Integrated areas of the fits were taken for further evaluation. Signal to noise ratios (SNRs) were calculated by the formula: 2.5 x signal heigt/peaknoise.

Glycogen restoration data are presented as relative glycogen content (RGC), with RGC at time t = (peak integral at t/peak integral before depletion) x 100.

Statistical analysis. Least-squares linear regression lines were fitted through the averaged RGC values (N= 7) of each time point. Slopes and intercepts of both monosaccharides were tested by analysis of variance for significant differences. All statistical analysis were two-sided, with p-values < 0.05 considered being statistically significant.

Results

The mean exercise time of the glycogen depletion protocol was 96 minutes (range 54-130 minutes). The mean absolute difference within subjects between the first and second glycogen depletion was 7 minutes in duration, which was not statistically significant.

Blood glucose during GF (mean ± standard deviation: 6.3 ± 1.4 mM) was significantly different ($p < 0.05$) from blood glucose during FF (4.6 ± 0.6 mM).

The blood glucose level remained between 3.1 and 10.0 mM throughout both feeding periods. Glucosuria was not detected in any subject (loss < 5.5 mM).

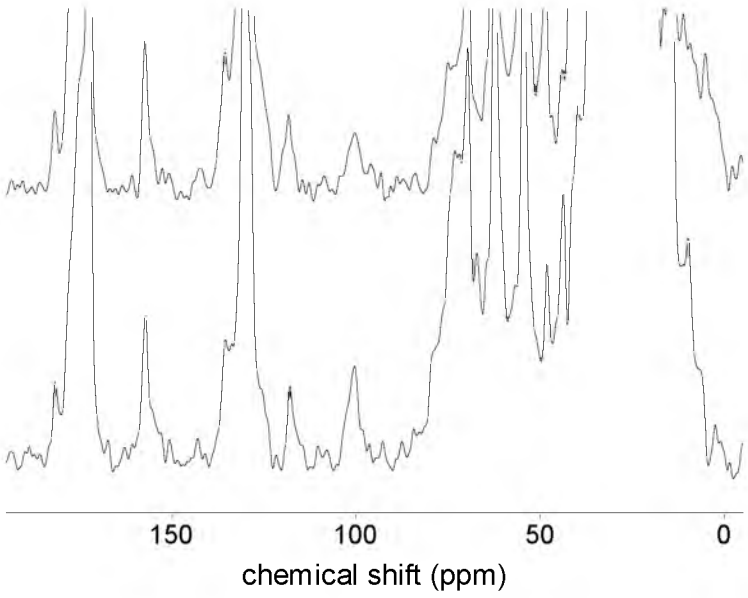

Figure 2.

^{13}C-NMR spectra recorded pre-exercise (bottom) and post-exercise (top) of the vastus lateralis muscle of a volunteer obtained during one experiment with glucose intake. The muscle was depleted up to 62 % of the initial glycogen content.

^{13}C-NMR spectroscopy. Figure 2 shows two ^{13}C-NMR spectra obtained at 1.5 T from the VL muscle of a volunteer during a depletion-repletion experiment with GF. The bottom spectrum was recorded pre-exercise. Glycogen signals can be observed at 100.5 ppm (C-1) and also at 70-74 ppm (C-2 - C-5) close to the glycerol backbone C-2 resonance. The top spectrum was obtained shortly after exercise. Depletion of muscle glycogen is clearly visible in the top spectrum, for the resonance at 100.5 ppm and also in the region 70-74 ppm despite the overlapping signals from the glycerol backbone. Notice the good reproducibility

of the spectra for signals of other muscle compounds, for instance creatine at 157 ppm. The reproducibility, concerning positioning and instrument performance, of the ^{13}C-NMR experiment was examined in 3 volunteers. Glycogen signal levels were measured in the non-depleted state under the same conditions during two successive examinations. The mean coefficient of variation was 5.0 ± 4.0 %. The SNR of the glycogen C-1 resonance in the resting state was found to vary between 4 and 13 with an average of 8 ± 1 (± SE). A paired t-test of the SNR values before GF and FF revealed an effective pairing (one tailed P-value: 0.039) and a non-significant difference between these groups (two tailed P-value: 0.99).From each control spectrum, obtained at rest before the start of a GF or FF experiment, the glycogen/creatine signal integral ratio was determined. This ratio showed, as with the SNR values, a quite large intersubject variability: i.e. it ranged from 0.6 to 2.2 with an average of 1.36 ± 0.13 (± SE). However, for all individuals this ratio was almost the same in both experiments. A paired t-test of the data sets revealed a non-significant difference (two-tailed P-value: 0.394), the pairing in this test was very effective (one tailed P-value: 0.0019).

			Post-exercise				
Feeding	n	Pre-exercise	0 h	2 h	4 h	6 h	8 h
Glucose	7	100	48±4	58±7	64±7	72±5	82±5
Fructose	7	100	43±4	52±7	54±6	56±7	63±5

Table 1.

Mean relative glycogen content pre-exercise and post-exercise. Post-exercise values are mean relative glycogen content ± SE in %; n= no. subjects.

In order to estimate average muscular glycogen content in the VL from the glycogen-to-creatine signal integral ratios, any NOE and saturation of the C-1 glycogen and C-3 creatine resonances imposed by the present experimental conditions (decoupling and scan repetition time) were evaluated. For the C-1 resonance of glycogen in solution, no NOE and signal saturation were detected; this is also expected to be so *in vivo* (15). For the C-3 resonance of creatine, signal saturation was not significant, but an enhancement factor of 1.6 ± 0.17 (SE) was observed. If we assume the muscular creatine content to be 42.7 mM (16) and take a correction factor of 1.6 into account, the average glycogen content in the nondepleted state in our volunteers is estimated to be 93 ± 8.8 mM (±SE).

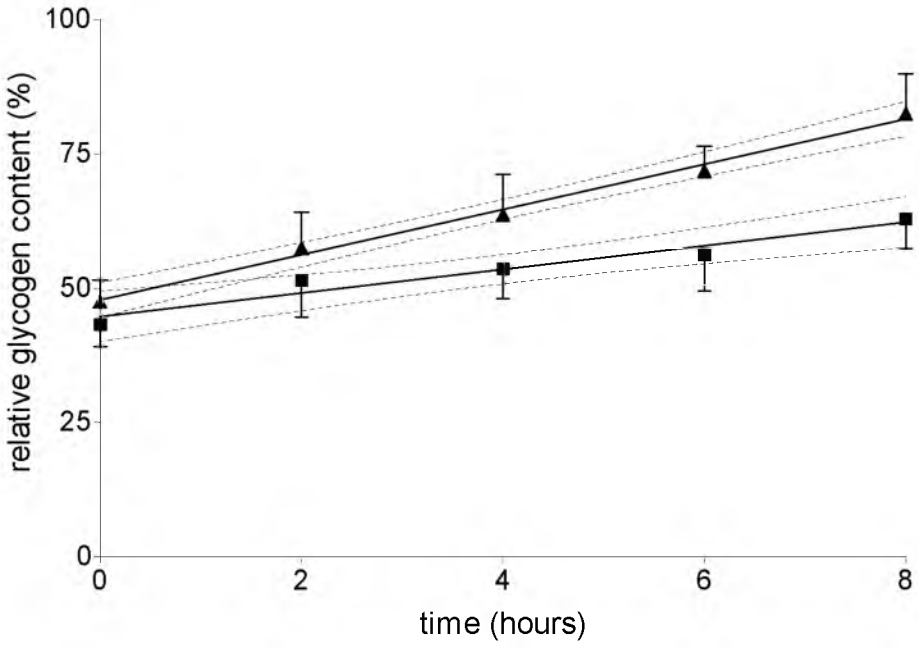

Figure 3.

Muscular glycogen levels during fructose (■) and glucose (▲) feeding (mean and SEM). Linear regression curves are shown with 95 % confidence intervals.

Glycogen restoration. Table 1 shows the mean RGC values for each point in time during GF and FF. During the time course of the CHO intake a linear relationship between glycogen content and time was assumed. Figure 3 shows the linear regression lines for the glucose (r^2 = 0.993) and fructose (r^2 = 0.946) experiments, lines are drawn with their 95 % confidence intervals.

The intercept, representing the glycogen left after depletion, were 48 ± 1.0 (SE) and 45 ± 1.5 % of the initial glycogen content for GF and FF, respectively, which is not significantly different. The slope, representing GRR, was significantly higher ($p < 0.05$) during GF (4.2 ± 0.2 %/h) than during FF (2.2 ± 0.3 %/h).

Discussion

Although biopsy studies have shown a faster glycogen restoration rate after 10 or more hours with GF compared with FF, only a few studies have focused on GRR in humans during the first hours following depletion.

Taylor et al. (7) demonstrated that *in vivo* ^{13}C-NMR measurements of muscular glycogen levels can be performed accurately and with a higher precision than in biopsy assessment. For the set-up in the present study the precision to measure glycogen in the non-depleted state appears to be comparable. Employing creatine C-3 signal as an internal reference the estimated average glycogen content in the VL of the volunteers is 93 mM, which is similar to the average glycogen content measured in the human gastrocnemius by ^{13}C-NMR employing external standardization.

All subjects refrained from exercise 48 hours prior to the experiments and performed both experiments at the same time of the day. It is therefore reasonable to assume that the initial glycogen content in individuals before exercise was the same in both carbohydrate intake experiments and the GRR could be compared based on RGC values. This assumption is supported by the non-significant difference and the effective pairing between control spectra

before GF and FF for the glycogen/creatine signal ratios as well as the SNR of the C-1 resonance of glycogen.

Because the number of intervals and the total exercise time within subjects was about equal in both experiments, it is likely that glycogen was depleted to the same level in both experiments. This is confirmed by the intercepts of the restoration curves being not significantly different between the two sets of experiments.

In this study, the first RGC value measured is high compared to values of approximately 20% reported in other studies (2, 6). This can partly be explained by the glycogen restoration that occurs during the ± 40 minutes between cessation of cycling and the actual ^{13}C-NMR measurement.

The amount of monosaccharides administered in this study (i.e. 80 g every 2 h) should be sufficient to achieve a maximal glycogen resynthesis rate with GF or FF (3, 17).

Significant loss of glucose or fructose in the urine or faeces could lead to an underestimation of the GRR. If CHO was not absorbed in the bowel, this would lead to osmotic diarrhea, which was not observed in this study. Because glucose was not detected in the urine of any subject and because fructose in the urine is very rare, loss of glucose or fructose may considered to be minimal.

Price et al. (9) found a linear and single-phased relationship between glycogen concentration and time after glycogen depletion to 50 %. Therefore, linear regression lines were fitted to RGC versus time, to obtain GRR. The finding that glucose results in a faster muscle glycogen recovery confirms earlier biopsy studies by Blom et al. (6); however, the recovery rates we found were lower: i.e., 2.2 %/h versus 3.0 %/h for fructose and 4.2 %/h versus 5.8 %/h for glucose. A possible explanation for this difference is that glycogen depletion at the start of our recovery experiments was less than in the experiments performed by Blom et al. At depletion levels down to 20 %, the glycogen recovery has been reported to be biphasic (9). A stage of fast recovery followed by a much slower recovery rate when a level of 30 mM is reached. Another explanation for the slower

recovery rate is the 1 hour interval between cessation of exercise and the start of the CHO intake. The GRR is reported to be lower if CHO ingestion after exercise is delayed (18, 19).

To our knowledge, there have been no comparable ^{13}C-NMR studies on glycogen restoration with GF or FF with which to compare the results of this study. However, it has generally been found in biopsy studies that GRR is higher after GF compared to FF (2, 6, 16). Although fructose probably can be transformed into glycogen in the skeletal muscle cell (17), several factors may contribute to a slower muscle glycogen restoration with FF compared with GF. It may be because of a slower absorption of fructose from the intestine. Because the blood glucose level during GF is significantly higher than during FF, a higher plasma insulin level is expected to be present and thus an increased glucose uptake will occur (20). In addition, fructose gives rise to more liver glycogen than glucose (4, 21, 22), thus leaving less CHO directly available for muscle glycogen resynthesis.

Conclusion. This study demonstrates that GF restores muscle glycogen faster than FF during the first 8 hours after depletion to a level of ±40% of the initial glycogen content. In general, it appears that ^{13}C-NMR spectroscopy at 1.5 T is suitable to monitor physiological changes in muscle glycogen levels.

Acknowledgements

The authors thank B. Ringnalda and A.C.A. Visser for valuable advises and gratefully acknowledge the participation of the subjects, who were extremely cooperative. AMYLUM (Belgium) kindly granted the glucose and fructose needed for this study.

References

1. J. Bergstrom, E. Hultman, A study of the glycogen metabolism during exercise in man. *Scand. J. Clin. Lab. Invest.,* **19,** 218-228, (1967).

2. R. K. Conlee, Muscle glycogen and exercise endurance: a twenty-year perspective. *Exerc. Sport. Sci. Rev.,* **15,** 1-28, (1987).
3. E. Hultman, Studies on muscle metabolism of glycogen and active phosphate in man with special reference to exercise and diet. *Scand. J. Clin. Lab. Invest. Suppl.,* **94,** 1-63, (1967).
4. D. L. Costill, M. Hargreaves, Carbohydrate nutrition and fatigue. *Sports. Med.,* **13,** 86-92, (1992).
5. J. O. Holloszy, F. W. Booth, Biochemical adaptations to endurance exercise in muscle. *Annu. Rev. Physiol.,* **38,** 273-291, (1976).
6. P. C. Blom, A. T. Hostmark, O. Vaage, K. R. Kardel, S. Maehlum, Effect of different post-exercise sugar diets on the rate of muscle glycogen synthesis. *Med. Sci. Sports. Exerc.,* **19,** 491-496, (1987).
7. R. Taylor, T. B. Price, D. L. Rothman, R. G. Shulman, G. I. Shulman, Validation of 13C NMR measurement of human skeletal muscle glycogen by direct biochemical assay of needle biopsy samples. *Magn. Reson. Med.,* **27,** 13-20, (1992).
8. T. B. Price, D. L. Rothman, M. J. Avison, P. Buonamico, R. G. Shulman, 13C-NMR measurements of muscle glycogen during low-intensity exercise. *J. Appl. Physiol.,* **70,** 1836-1844, (1991).
9. T. B. Price, D. L. Rothman, R. Taylor, M. J. Avison, G. I. Shulman, R. G. Shulman, Human muscle glycogen resynthesis after exercise: insulin- dependent and -independent phases. *J. Appl. Physiol.,* **76,** 104-111, (1994).
10. K. T. Moriarty, D. G. O. McIntryre, K. Bingham, R. Coxon, P. M. Glover, P. L. Greenhaff, I. A. Macdonald, H. S. Bachelard, P. G. Morris, Glycogen resynthesis in liver and muscle after exercise: measurement of the rate of resynthesis by 13C magnetic resonance spectroscopy. *Magma,* **2,** 429-432, (1994).
11. N. Beckmann, J. Seelig, H. Wick, Analysis of glycogen storage disease by in vivo 13C NMR: comparison of normal volunteers with a patient. *Magn. Reson. Med.,* **16,** 150-160, (1990).
12. A. Heerschap, P. R. Luyten, J. I. van der Heyden, L. J. Oosterwaal, J. A. den Hollander, Broadband proton decoupled natural abundance 13C NMR spectroscopy of humans at 1.5 T. *NMR Biomed.,* **2,** 124-132, (1989).
13. H. Kuipers, H. A. Keizer, F. Brouns, W. H. Saris, Carbohydrate feeding and glycogen synthesis during exercise in man. *Pflugers Arch.,* **410,** 652-656, (1987).

14. A. J. van den Bergh, H. J. van den Boogert, H. Heerschap. Spatially localized calibration of the decoupler radio frequency field strength, *in* "SMR 2nd Meeting, San Francisco, 1994," p. 760
15. L. H. Zang, M. R. Laughlin, D. L. Rothman, R. G. Shulman, 13C NMR relaxation times of hepatic glycogen in vitro and in vivo. *Biochemistry,* **29,** 6815-6820, (1990).
16. R. C. Harris, E. Hultman, L. O. Nordesjo, Glycogen, glycolytic intermediates and high-energy phosphates determined in biopsy samples of musculus quadriceps femoris of man at rest. Methods and variance of values. *Scand. J. Clin. Lab. Invest.,* **33,** 109-120, (1974).
17. J. Bergstrom, E. Hultman, Synthesis of muscle glycogen in man after glucose and fructose infusion. *Acta. Med. Scand.,* **182,** 93-107, (1967).
18. J. L. Ivy, M. C. Lee, J. T. Brozinick, Jr., M. J. Reed, Muscle glycogen storage after different amounts of carbohydrate ingestion. *J. Appl. Physiol.,* **65,** 2018-2023, (1988).
19. J. L. Ivy, A. L. Katz, C. L. Cutler, W. M. Sherman, E. F. Coyle, Muscle glycogen synthesis after exercise: effect of time of carbohydrate ingestion. *J. Appl. Physiol.,* **64,** 1480-1485, (1988).
20. P. Vollenweider, L. Tappy, D. Randin, P. Schneiter, E. Jequier, P. Nicod, U. Scherrer, Differential effects of hyperinsulinemia and carbohydrate metabolism on sympathetic nerve activity and muscle blood flow in humans. *J. Clin. Invest.,* **92,** 147-154, (1993).
21. C. F. Cori, The fate of sugar in the animal body. III. The rate of glycogen formation in the liver of normal and insulinized rats during the absorption of glucose, fructose, and galactose. *J. Biol. Chem.,* **70,** 577-585, (1926).
22. L. H. Nilsson, E. Hultman, Liver and muscle glycogen in man after glucose and fructose infusion. *Scand. J. Clin. Lab. Invest.,* **33,** 5-10, (1974).

6 Assessment of human muscle glycogen synthesis and total glucose content by *in vivo* ^{13}C MR spectroscopy under euglycemic clamp conditions

A.J. van den Bergh[1], C.J.J. Tack[2], H.J. van den Boogert[1], G. Vervoort[2], P. Smits[3], A. Heerschap[1]

Department of Radiology[1], Department of Internal Medicine[2], Department of Pharmacology[3], University Hospital Nijmegen, The Netherlands

Abstract

Obesity is often accompanied by a decreased ability of insulin to stimulate glucose uptake and glycogenesis in skeletal muscle. The aim of this study was to investigate the rate of glycogen formation and of muscular glucose content in relation to insulin sensitivity under euglycemic conditions. We applied a hyperinsulinemic (430 $pmol \cdot m^{-2} \cdot min^{-1}$) euglycemic clamp with infusion of 20% glucose (30 % enriched with ^{13}C-1-glucose) to 8 subjects with a wide range of insulin sensitivities. Glycogen and glucose levels were monitored simultaneously by ^{13}C MR spectroscopy of the calf muscle on a clinical MR system at 1.5T field strength.

Glycogen synthesis rate showed a strong correlation with whole body glucose uptake during the clamp ($r=0.93$, $P<0.01$). With the use of ^{13}C MR spectroscopy, total muscular glucose content could be determined *in vivo*, and showed a positive, linear correlation with glycogen synthesis rate ($r=0.85$, $P<0.01$). Preliminary results indicate that the glycogen synthesis rate improves after treatment with troglitazone.

This chapter is based on a paper submitted to European Journal of Clinical Investigations

Introduction

Insulin resistance is a feature of several related disorders like non-insulin dependent diabetes mellitus (NIDDM), hypertension, obesity and dyslipidemia (1-4). In healthy subjects most of the insulin-induced glucose uptake in muscle is metabolized to glycogen (5, 6). The principal defect in insulin resistance appears to be a decreased insulin-induced glucose uptake in skeletal muscle, which is reflected in a decreased glycogen synthesis (6).

The rate of glycogen formation in response to insulin, however is difficult to assess in humans *in vivo*, and requires sequential muscle biopsies. Furthermore, the changes in glycogen concentrations maybe so small that they cannot be detected with accuracy by current biopsy techniques. *In vivo* ^{13}C MR spectroscopy of muscle, pioneered by R. Shulman and colleagues (7, 8), offers an attractive alternative permitting non-invasive and continuous measurement of muscle glycogen levels (9-13). Moreover, with the use of ^{13}C-enriched glucose infusion, the sensitivity of the measurement can be further increased and both the monitoring of glycogen synthesis and of total glucose content in muscle has become possible (14-17).

By combining ^{13}C MR spectroscopy with a hyperglycemic-hyperinsulinemic clamp, it was demonstrated that muscle glycogen synthesis rate is decreased in subjects with NIDDM as compared to normal subjects (18). Similar findings were obtained in obese subjects (19). Up to now, most ^{13}C MR spectroscopic studies have used hyperglycemic conditions to measure ^{13}C-1-glucose and ^{13}C-1-glycogen formation (14, 15, 18). Application of hyperglycemia in nondiabetic subjects has some specific disadvantages such as the nonphysiologic glucose concentrations, the necessity to use somatostatin to suppress endogenous insulin secretion and the high volume load, which all may influence the outcome of a study. Only a limited number of studies have been performed on healthy non insulin resistant subjects under euglycemic clamp conditions (17, 20, 21), but not yet as a function of insulin resistance. In addition, previous measurements were

performed at high magnetic fields (> 2T), not widely available in the clinical situation.

The first aim of the present study therefore was to demonstrate that muscle glycogen formation and muscle glucose content can be monitored simultaneously by *in vivo* ^{13}C MR spectroscopy at the commonly available field strength of 1.5T, under euglycemic clamp conditions. Secondly, we addressed the question how these non-invasively measured parameters correlate with insulin sensitivity, in a group of non-diabetic volunteers with a wide range of insulin sensitivities.

In addition we tested if the above described measurement conditions could detect changes in insulin sensitivity within a subject. In order to perform this examination, three insulin resistant obese subjects (BMI > 30) were also studied after 8 weeks of treatment with troglitazone. Troglitazone, a member of the class of thiazolidine-diones, is capable of improving insulin sensitivity in patients with diabetes and in obese subjects (22-26). *In vitro* studies have shown a beneficial effect on glycogen synthesis in human skeletal muscle cultures obtained from insulin resistant obese subjects (27). Troglitazone may thus improve glycogen synthesis *in vivo* in humans.

Subjects, materials and methods

Eight healthy male volunteers were studied. Inclusion criteria were: age between 20-50 years, non-smoking, absence of hypertension and a normal fasting plasma glucose concentration. Subjects varied from lean to obese. Three obese subjects with BMI > 30 kg/m^2 were studied twice. Subjects received either troglitazone 400 mg daily, or placebo for a period of eight weeks in a randomized, double-blind, cross over design. These subjects were selected from a larger randomized trial (26). All subjects gave written informed consent. The protocol was approved by the hospital ethics committee.

^{13}C MR spectroscopy of the calf muscle, combined with hyperinsulinemic (430 pmol•m^{-2}•min^{-1}) euglycemic clamps were performed after an overnight fast. A

catheter (Venflon®, 20G, 32mm) was inserted into a large forearm vein for the infusion of insulin and glucose 20% solution (30 % enriched with ^{13}C-1-glucose)(Campro Scientific, Veenendaal, The Netherlands). Blood was sampled from the collateral side with 7.5 minute intervals. Plasma glucose levels were measured by the glucose oxidation method (Beckman Glucose Analyzer 2, Beckman Instruments Inc, Fullerton, CA, USA). Whole body glucose uptake, derived from glucose infusion rate, was calculated during the last hour of the clamp and expressed in $\mu mol \cdot kg^{-1} \cdot min^{-1}$.

Blood samples for insulin measurements were taken before and at the end of the euglycemic hyperinsulinemic clamp. Plasma insulin was measured with a double antibody radioimmunoassay (interassay coefficient of variation 6.2%).

^{13}C MR spectroscopy was performed at 1.5 T using a whole body MR system (Magnetom SP, Siemens, Erlangen, Germany). Subjects were placed in a supine position with the calf muscle positioned on a double surface coil. The coil configuration consisted of an 11 cm circular ^{13}C surface coil and a 17 x 23 cm ^{1}H butterfly coil.

The proton coil was used for MR imaging, magnet field shimming and ^{1}H decoupling. The line width at one-half the height of the water resonance was shimmed to below 25 Hz.

Proton decoupled ^{13}C MR spectra were collected with a time resolution of 15 minutes. Data acquisition conditions were as follows: 2.56 ms sincos excitation pulse, pulse repetition time of 180 ms, 1024 datapoints were collected, spectral bandwidth of 6 kHz, the number of averages was 5000. Continuous wave proton decoupling was applied at the ^{1}H frequency of the glycogen C-1 proton during the first 50 ms of the acquisition period. Continuous wave decoupling was sufficient for decoupling of the glycogen C-1 and glucose C-1 signal regions. The specific absorption rate (SAR) at the body surface was kept below FDA guidelines (28) using an empirical procedure to predict the local SAR (29).

Spectral analysis was performed using Luise software (Siemens, Erlangen Germany). Spectra were zerofilled, multiplied by a 10 Hz gaussian filter, phase

and baseline corrected. Signals of creatine C-3, glycogen C-1 and glucose C-1α and C-1β were fitted to a gaussian line shape for further analysis.

Basal glycogen concentrations (glycosyl units) were calculated using creatine as an internal concentration standard (10, 30-32). Pulse saturation effects and nuclear Overhauser enhancement (NOE) were measured for the glycogen and creatine signals in separate experiments, from this a total multiplication factor of 1.17 was derived for the calculation of the basal glycogen concentration. To obtain glycogen and glucose concentrations from the *in vivo* ^{13}C infusion experiments, a correction was made for the ^{13}C fractional enrichment determined from plasma samples obtained at corresponding MR measurement times.

Blood plasma glucose enrichment levels were measured using high resolution proton NMR. Preparation of plasma samples prior to NMR consisted of deproteinization by centrifugation for 1 hour at 3000 G over a 10 kD filter (Sartorius, Göttingen, Germany) (33). From the filtrate 500 µl was taken and 20 µl of D_2O with 2,2,3,3-tetradeuteropropionic acid as internal standard was added. Proton spectra were recorded on an AMX-600 spectrometer (Bruker, Karlsruhe, Germany). The number of averages was 64, a repetition time of 5 seconds was used. Spectra were analyzed using WIN-NMR software (Bruker, Karlsruhe, Germany). Fractional enrichment was calculated from the ratios of the Lorentzian fitted signals of the proton attached to the ^{12}C / ^{13}C α-C1-glucose.

Glycogen synthesis rate was obtained by fitting MR data of glycogen increase over a period of 75 minutes with linear regression.

Total muscle glucose levels were determined from the *in vivo* ^{13}C MR spectra at the end of the infusion when glucose levels were in steady state. Saturation effects and NOE are unknown for the glucose C-1 signals with respect to the C-3 creatine signal so glucose levels are expressed in arbitrary units with respect to the creatine signal.

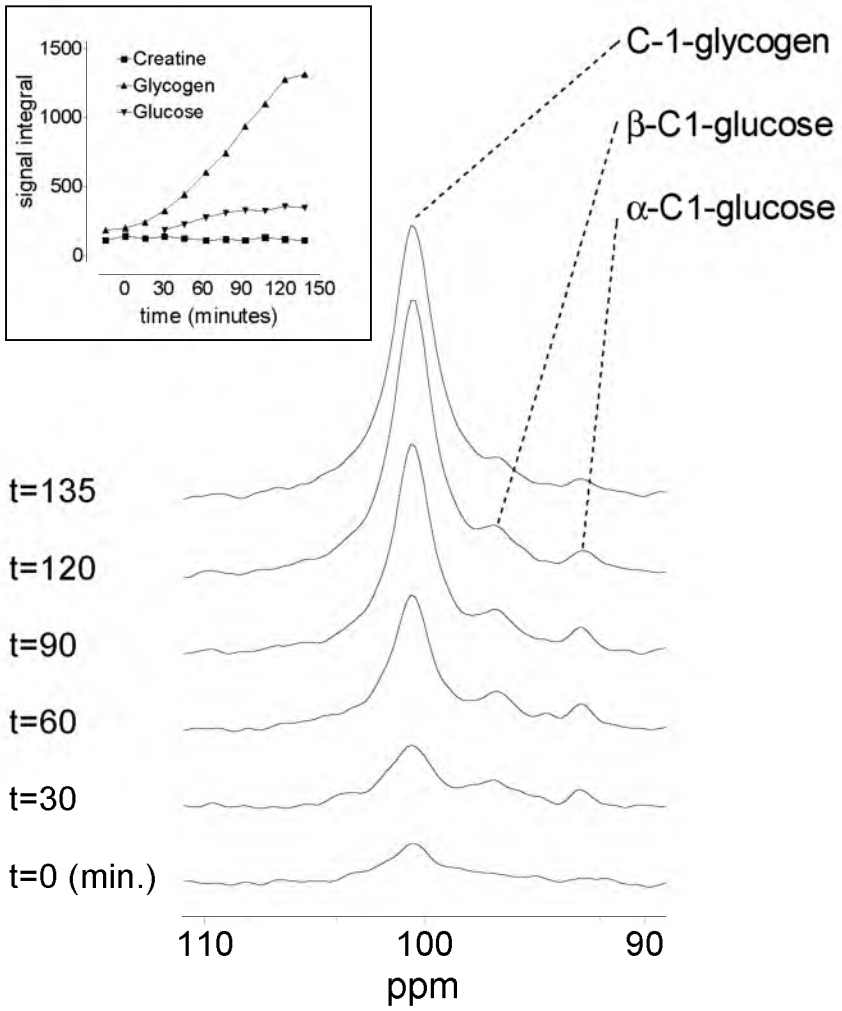

Figure 1

In vivo ^{13}C MR spectra recorded of the human calf muscle at 1.5T under euglycemic hyperinsulinemic conditions. The first spectrum at the bottom shows the natural abundance C-1 signal of glycogen. During the clamp signals from both glucose anomers are clearly visible. The strong increasing intensity for the C-1 signal of glycogen shows the incorporation of labeled glucose. The insert show the integral values of the fitted signals from creatine, glycogen and glucose.

Results

Insulin infusion increased plasma insulin concentrations from 66 ± 12 to 648 ± 47 pmol/l. Plasma glucose concentrations during the euglycemic (≈5mM) clamp were stable in all subjects (mean coefficient of variation 5.94%).

Figure 1 shows a stack plot of spectra recorded during an euglycemic hyperinsulinemic clamp of ^{13}C-1-glucose infusion (enrichment 30%), obtained from a healthy lean subject; only the region around the C-1 signal of glycogen is presented (89-111ppm). The total ^{13}C MR spectrum shows resonances for superficial lipid as well as signals for muscle creatine and other glycogen carbons. In the first spectrum the natural abundance glycogen signal is clearly visible, the subsequent spectra not only show an increasing signal intensity for glycogen but also the appearance of ^{13}C-1 signals for both the α and β glucose anomers. These signals represent the total muscular glucose pool: glucose-6-phosphate (G6P), intracellular and extracellular glucose. After approximately 90 minutes of infusion, the signals representing glucose reach a plateau. The insert in figure 1 shows the integral values of the analyzed signals from creatine, glycogen and glucose against time. This graph demonstrates that the creatine signals were stable during the clamp, indicating a good reproducibility of the ^{13}C MR spectra.

Results of the measurements of the individual subjects are summarized in table 1. The insulin resistant subjects 6, 7 and 8 were measured twice; the suffix -2 indicates the measurement after troglitazone treatment. As can be derived from the table, there was a tendency for a higher basal muscle glycogen content measured with *in vivo* ^{13}C MR spectroscopy in subjects with a high insulin sensitivity expressed as whole body glucose uptake ($r = 0.68$, $p < 0.05$). In addition, glycogen synthesis rate showed a strong correlation ($r = 0.93$, $p < 0.01$) with whole body glucose uptake as derived from the clamp (see figure 2). Furthermore, a positive linear correlation ($r = 0.85$, $p < 0.01$) was found between the glycogen synthesis rate and the steady state total muscular glucose content measured *in vivo* by ^{13}C MR spectroscopy.

Subject	age	BMI	WBGU	[INSULIN]		[glycogen]	synthesis	glucose
				before	end	at t=0	rate	content
	(years)	($kg \cdot m^{-2}$)	$\mu mol \cdot kg^{-1} \cdot min^{-1}$	pmol/l	pmol/l	(mM)	(mM/h)	(a.u.)
1	28	22	90.4	29	502	77.4	18.6	6.3
2	22	24	76.2	29	402	79.8	11.1	5.5
3	23	21	60.7	43	473	92.7	11.7	4.9
4	47	27	41.9	29	796	76.1	5.3	4.5
5	45	29	43.7	*	652	52.7	6.9	4.3
6-1	28	31	35.2	72	724	64.6	6.8	3.9
6-2	28	31	56.9	79	774	62.9	9.4	5.3
7-1	40	34	29.6	108	731	52.7	4.8	4.1
7-2	40	34	30.7	108	832	45.3	6.5	4.8
8-1	32	33	31.4	*	*	51.9	5.2	3.6
8-2	32	33	43.0	100	595	44.1	8.6	4.1

Table 1.

Summarized results from the individual subjects. The suffix -2 indicates the measurement after troglitazone treatment of these individuals. Insulin concentrations marked by an * were not determined. Insulin concentrations were measured before and at the end of the clamp. Glucose content is expressed in arbitrary units.

Discussion

In this study, we demonstrate the feasibility of measuring not only muscular glycogen synthesis rate but also total muscular glucose content using hyperinsulinemic euglycemic clamp conditions in combination with *in vivo* ^{13}C MR spectroscopy at the clinical field strength of 1.5 T.

^{13}C MR spectroscopy, combined with hyperinsulinemia and ^{13}C-enriched glucose infusion, is uniquely suited for detection of glycogen signals in human tissue like muscle and liver, and allows non-invasive and sequential measuring of glycogen synthesis rates (7). To date, most studies are performed at high magnetic field strengths using hyperglycemic clamp conditions (applying enriched ^{13}C-1-

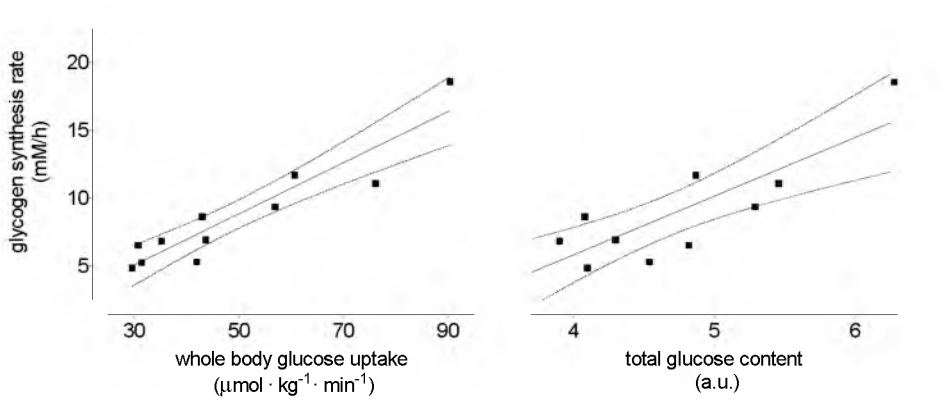

Figure 2

Figure 2A shows the correlation between glycogen synthesis and the whole body glucose uptake, reflecting insulin sensitivity. Figure 2B shows the glycogen synthesis rate as a function of the total muscle glucose content measured by *in vivo* ^{13}C MR spectroscopy.

glucose), for optimal sensitivity in *in vivo* ^{13}C MR spectroscopy. Only a few report on euglycemic clamp conditions in healthy non insulin resistant subjects (17, 20, 21, 34). In this study, we measured muscle glycogen synthesis rates *in vivo* by ^{13}C MR spectroscopy at 1.5T using hyperinsulinemia in combination with euglycemia in insulin sensitive subjects and also in insulin resistant obese subjects. The use of normal plasma glucose levels may have advantages, especially in the study of insulin sensitivity in nondiabetic subjects.

The tendency of a lower basal muscular glycogen concentration in obese insulin resistant subjects is in good agreement with Shulman *et al.* and Petersen *et al.* (18, 19) who report on a lower basal muscular glycogen concentration in obesity, and an even lower concentration in NIDDM.

The range of glycogen synthesis rates measured in this study are comparable to the synthesis rates reported earlier during hyperglycemic clamping in normal and obese subjects (18, 19). The higher insulin level in our study can explain the

similarity of the glycogen synthesis rates between hyperglycemic and euglycemic clamping. Earlier findings (14, 17, 18) that glucose disposal during the clamp is mainly accounted for by glycogen synthesis, is reflected in the strong correlation between glucose infusion rate and glycogen synthesis rate. Data as presented in figure 2a are in good agreement with data obtained by Roussel *et al.* at different glycemic clamp levels (17).

An exciting finding in this study is that the current set-up allows for the non-invasive determination in muscle of total glucose content simultaneously with the content of glycogen. The relation between the steady state muscle glucose content and the glycogen synthesis rate appears to be linear. The glucose C-1 signals arise from extracellular glucose, but intracellular glucose and G6P can also contribute. As the C-1 signals of glucose and G6P have similar chemical shift positions in the spectra, they can not be discriminated by ^{13}C MR spectroscopy (15). It has repeatedly been reported that under euglycemic conditions no accumulation of intracellular glucose occurs (15, 17, 35). Thus a reduced total glucose pool as found in insulin resistant subjects can only be explained by either a lower intracellular G6P concentration or by a reduced extracellular glucose pool compared with insulin sensitive subjects. The respective contributions of extracellular glucose and intracellular G6P to the glucose signals can be estimated. Assuming 70 ml of extracellular water/kg, and using plasma glucose concentrations we can calculate the extracellular glucose content during the euglycemic clamp conditions. These conditions were similar for the insulin resistant and insulin sensitive subjects in our study (36). Using reported values for G6P content obtained during hyperglycemic hyperinsulinemic clamp conditions in healthy and insulin resistant obese subjects (19), the expected signal change due to G6P can be estimated to be 1.16. The change in total glucose content presented here is much larger than can be attributed to a change in G6P. A possible explanation is that insulin-mediated muscle specific tissue recruitment as suggested by Bonadonna *et al.* (37), may contribute to an increased total muscular glucose content. This is supported by the fact that

several studies have suggested an important role for insulin-induced vasodilatation (38-41).

A decreased glycogen synthesis rate in insulin resistant obese subjects may thus be due to a reduced glucose metabolic rate but also due to a defect in glucose supply to the cell. Thus the total glucose content measured by *in vivo* ^{13}C MR spectroscopy reflecting both defects is an important parameter representing insulin sensitivity.

Troglitazone, a member of the thiazolidine-diones, a new class of hypoglycemic drugs, has been shown to improve insulin sensitivity, in NIDDM as well as in obesity (22, 42). Troglitazone presumably improves insulin action at the level of the skeletal muscle, but the mechanism of action is complex and only partly revealed. In this study we were able to detect changes in glycogen formation in 3 subjects induced by troglitazone. This action of troglitazone, has only recently been reported in muscle cultures (27). Because we studied obese, insulin resistant, but nondiabetic subjects, the effect of troglitazone on glycogen formation cannot be explained by changes in blood glucose concentration ("glucose toxicity"), and probably represents a direct action of the drug on skeletal muscle.

In summary, we demonstrated the feasibility of *in vivo* ^{13}C MR spectroscopy at 1.5T in combination with an euglycemic (^{13}C-1 enriched glucose) hyperinsulinemic clamp for the measurement of not only glycogen synthesis but also total muscular glucose content. Baseline muscle glycogen content tended to be lower in insulin resistant subjects, whereas glycogen synthesis rate and total muscle glucose content tended to increased in insulin sensitive subjects.

Acknowledgements

The authors thank Arnoud Jansen-van Rosendaal for technical assistance during clamping experiments. We thank U. Engelke and R. Wevers for their assistance in analyzing the plasma samples with high resolution proton NMR spectroscopy.

^{1}H - NMR spectra were recorded at the Dutch hf-NMR facility at the department of Biophysical Chemistry (head, Prof. Dr. C.W. Hilbers). We also thank J. Joordens for invaluable help and assistance.
We thank GlaxoWellcome for financial support and for providing Troglitazone.

References

1. E. Ferrannini, G. Buzzigoli, R. Bonadonna, M. A. Giorico, M. Oleggini, L. Graziadei, R. Pedrinelli, L. Brandi, S. Bevilacqua, Insulin resistance in essential hypertension. *N. Engl. J. Med.,* **317,** 350-357, (1987).
2. G. M. Reaven, H. Lithell, L. Landsberg, Hypertension and associated metabolic abnormalities--the role of insulin resistance and the sympathoadrenal system. *N. Engl. J. Med.,* **334,** 374-381, (1996).
3. B. C. Martin, J. H. Warram, A. S. Krolewski, R. N. Bergman, J. S. Soeldner, C. R. Kahn, Role of glucose and insulin resistance in development of type 2 diabetes mellitus: results of a 25-year follow-up study. *Lancet,* **340,** 925-929, (1992).
4. A. Fontbonne, Insulin-resistance syndrome and cardiovascular complications of non-insulin-dependent diabetes mellitus. *Diabetes, Metab* **22,** 305-313, (1996).
5. R. A. DeFronzo, E. Jacot, E. Jequier, E. Maeder, J. Wahren, J. P. Felber, The effect of insulin on the disposal of intravenous glucose. Results from indirect calorimetry and hepatic and femoral venous catheterization. *Diabetes,* **30,** 1000-1007, (1981).
6. R. A. DeFronzo, Lilly lecture 1987. The triumvirate: beta-cell, muscle, liver. A collusion responsible for NIDDM. *Diabetes,* **37,** 667-687, (1988).
7. R. G. Shulman, D. L. Rothman, T. B. Price, Nuclear magnetic resonance studies of muscle and applications to exercise and diabetes. *Diabetes,* **45 Suppl 1,** S93-98, (1996).

8. R. G. Shulman, G. Bloch, D. L. Rothman, In vivo regulation of muscle glycogen synthase and the control of glycogen synthesis. *Proc. Natl. Acad. Sci. USA,* **92,** 8535-8542, (1995).
9. T. B. Price, D. L. Rothman, R. Taylor, M. J. Avison, G. I. Shulman, R. G. Shulman, Human muscle glycogen resynthesis after exercise: insulin-dependent and -independent phases. *J. Appl. Physiol.,* **76,** 104-111, (1994).
10. A. J. van den Bergh, S. Houtman, A. Heerschap, N. J. Rehrer, H. J. van den Boogert, B. Oeseburg, M. T. Hopman, Muscle glycogen recovery after exercise during glucose and fructose intake monitored by 13C-NMR. *J. Appl. Physiol.,* **81,** 1495-1500, (1996).
11. P. Jehenson, D. Duboc, G. Bloch, M. Fardeau, A. Syrota, Diagnosis of muscular glycogenosis by in vivo natural abundance 13C NMR spectroscopy. *Neuromuscul. Disord.,* **1,** 99-101, (1991).
12. N. Beckmann, J. Seelig, H. Wick, Analysis of glycogen storage disease by in vivo 13C NMR: comparison of normal volunteers with a patient. *Magn. Reson. Med.,* **16,** 150-160, (1990).
13. R. Taylor, T. B. Price, D. L. Rothman, R. G. Shulman, G. I. Shulman, Validation of 13C NMR measurement of human skeletal muscle glycogen by direct biochemical assay of needle biopsy samples. *Magn. Reson. Med.,* **27,** 13-20, (1992).
14. T. Jue, D. L. Rothman, G. I. Shulman, B. A. Tavitian, R. A. DeFronzo, R. G. Shulman, Direct observation of glycogen synthesis in human muscle with 13C NMR. *Proc. Natl. Acad. Sci. USA,* **86,** 4489-4491, (1989).
15. R. Roussel, G. Velho, P. G. Carlier, L. Jouvensal, G. Bloch, In vivo NMR evidence for moderate glucose accumulation in human skeletal muscle during hyperglycemia. *Am. J. Physiol.,* **271,** E434-438, (1996).
16. R. Roussel, P. G. Carlier, C. Wary, G. Velho, G. Bloch, Evidence for 100% 13C NMR visibility of glucose in human skeletal muscle. *Magn. Reson. Med.,* **37,** 821-824, (1997).
17. R. Roussel, P. G. Carlier, J. J. Robert, G. Velho, G. Bloch, 13C/31P NMR

studies of glucose transport in human skeletal muscle. *Proc. Natl. Acad. Sci. USA,* **95,** 1313-1318, (1998).

18. G. I. Shulman, D. L. Rothman, T. Jue, P. Stein, R. A. DeFronzo, R. G. Shulman, Quantitation of muscle glycogen synthesis in normal subjects and subjects with non-insulin-dependent diabetes by 13C nuclear magnetic resonance spectroscopy. *N. Engl. J. Med.,* **322,** 223-228, (1990).
19. K. F. Petersen, R. Hendler, T. Price, G. Perseghin, D. L. Rothman, N. Held, J. M. Amatruda, G. I. Shulman, 13C/31P NMR studies on the mechanism of insulin resistance in obesity. *Diabetes,* **47,** 381-386, (1998).
20. D. Laurent, K. F. Petersen, R. R. Russell, G. W. Cline, G. I. Shulman, Effect of epinephrine on muscle glycogenolysis and insulin-stimulated muscle glycogen synthesis in humans. *Am. J. Physiol.,* **274,** E130-138, (1998).
21. M. Roden, T. B. Price, G. Perseghin, K. F. Petersen, D. L. Rothman, G. W. Cline, G. I. Shulman, Mechanism of free fatty acid-induced insulin resistance in humans. *J. Clin. Invest.,* **97,** 2859-2865, (1996).
22. J. J. Nolan, B. Ludvik, P. Beerdsen, M. Joyce, J. Olefsky, Improvement in glucose tolerance and insulin resistance in obese subjects treated with troglitazone. *N. Engl. J. Med.,* **331,** 1188-1193, (1994).
23. S. L. Suter, J. J. Nolan, P. Wallace, B. Gumbiner, J. M. Olefsky, Metabolic effects of new oral hypoglycemic agent CS-045 in NIDDM subjects. *Diabetes Care,* **15,** 193-203, (1992).
24. B. H. Wolffenbuttel, M. B. Graal, New treatments for patients with type 2 diabetes mellitus. *Postgrad. Med. J.,* **72,** 657-662, (1996).
25. M. N. Ghazzi, J. E. Perez, T. K. Antonucci, J. H. Driscoll, S. M. Huang, B. W. Faja, R. W. Whitcomb, Cardiac and glycemic benefits of troglitazone treatment in NIDDM. The Troglitazone Study Group. *Diabetes,* **46,** 433-439, (1997).
26. C. J. J. Tack, M. K. E. Ong, J. A. Lutterman, P. Smits, Insulin-induced vasodilatation and endothelial function in obesity/insulin resistance. Effects of troglitazone. *Diabetologia,* **41,** 569-576, (1998).

27. K. S. Park, T. P. Ciaraldi, L. Abrams-Carter, S. Mudaliar, S. E. Nikoulina, R. R. Henry, Troglitazone regulation of glucose metabolism in human skeletal muscle cultures from obese type II diabetic subjects. *J. Clin. Endocrinol. Metab.,* **83,** 1636-1643, (1998).
28. F. G. Shellock, E. Kanal, "Magnetic Resonance bioeffects, safety, and patient managment.," Raven Press, New York, 1994.
29. A. J. van den Bergh, H. J. van den Boogert, A. Heerschap, Calibration of the 1H decoupling field strength and experimental evaluation of the specific RF absorption rate in 1H decoupled human 13C-MRS. *Magn. Reson. Med.,* **39,** 642-646, (1998).
30. A. Katz, A. D. Lee, G-1,6-P2 in human skeletal muscle after isometric contraction. *Am. J. Physiol.,* **255,** C145-148, (1988).
31. A. Katz, G-1,6-P2, glycolysis, and energy metabolism during circulatory occlusion in human skeletal muscle. *Am. J. Physiol.,* **255,** C140-144, (1988).
32. S. Rotman, J. Slotboom, C. Boesch, E. Jequier. Muscle glycogen recovery after exercise measured by 13C-NMR in humans: Effect of nutritional solutions, *in* "ESMRMB, Geneva, 1998," p. 562
33. R. A. Wevers, U. Engelke, A. Heerschap, High-resolution 1H-NMR spectroscopy of blood plasma for metabolic studies. *Clin. Chem.,* **40,** 1245-1250, (1994).
34. D. L. Rothman, I. Magnusson, G. Cline, D. Gerard, C. R. Kahn, R. G. Shulman, G. I. Shulman, Decreased muscle glucose transport/phosphorylation is an early defect in the pathogenesis of non-insulin-dependent diabetes mellitus. *Proc. Natl. Acad. Sci. USA,* **92,** 983-987, (1995).
35. A. Katz, B. L. Nyomba, C. Bogardus, No accumulation of glucose in human skeletal muscle during euglycemic hyperinsulinemia. *Am. J. Physiol.,* **255,** E942-945, (1988).
36. G. Sjogaard, B. Saltin, Extra- and intracellular water spaces in muscles of

man at rest and with dynamic exercise. *Am. J. Physiol.,* **243,** R271-280, (1982).

37. R. C. Bonadonna, M. P. Saccomani, S. Del Prato, E. Bonora, R. A. DeFronzo, C. Cobelli, Role of tissue-specific blood flow and tissue recruitment in insulin- mediated glucose uptake of human skeletal muscle. *Circulation,* **98,** 234-241, (1998).
38. E. A. Anderson, R. P. Hoffman, T. W. Balon, C. A. Sinkey, A. L. Mark, Hyperinsulinemia produces both sympathetic neural activation and vasodilation in normal humans. *J. Clin. Invest.,* **87,** 2246-2252, (1991).
39. M. Laakso, S. V. Edelman, G. Brechtel, A. D. Baron, Decreased effect of insulin to stimulate skeletal muscle blood flow in obese man. A novel mechanism for insulin resistance. *J. Clin. Invest.,* **85,** 1844-1852, (1990).
40. C. J. Tack, A. E. Schefman, J. L. Willems, T. Thien, J. A. Lutterman, P. Smits, Direct vasodilator effects of physiological hyperinsulin-aemia in human skeletal muscle. *Eur. J. Clin. Invest.,* **26,** 772-778, (1996).
41. M. Raitakari, P. Nuutila, J. Knuuti, O. T. Raitakari, H. Laine, U. Ruotsalainen, O. Kirvela, T. O. Takala, H. Iida, H. Yki-Jarvinen, Effects of insulin on blood flow and volume in skeletal muscle of patients with IDDM: studies using [15O]H2O, [15O]CO, and positron emission tomography. *Diabetes,* **46,** 2017-2021, (1997).
42. D. G. Maggs, T. A. Buchanan, C. F. Burant, G. Cline, B. Gumbiner, W. A. Hsueh, S. Inzucchi, D. Kelley, J. Nolan, J. M. Olefsky, K. S. Polonsky, D. Silver, T. R. Valiquett, G. I. Shulman, Metabolic effects of troglitazone monotherapy in type 2 diabetes mellitus. A randomized, double-blind, placebo-controlled trial. *Ann. Intern. Med.,* **128,** 176-185, (1998).

In the recent decades, Magnetic Resonance Imaging (MRI) has evolved to a routinely used technique to obtain high quality anatomical information. Magnetic Resonance Spectroscopy (MRS) does not provide anatomical information but chemical information of the tissue studied, in the form of a spectrum. The non invasiveness of MRS makes it an attractive alternative for biopsy methods.

In chapter 1 the current status of human *in vivo* ^{13}C MR spectroscopy is reviewed. Normal and pathological metabolism that can be studied using natural abundance or labeling in *in vivo* ^{13}C MR spectroscopy is described. The application of double resonance techniques such as decoupling and polarization transfer are discussed, with the required coil configurations for such experiments. Finally, current localization and quantification methods are described.

In chapter 2 and 3 safety issues regarding RF deposition which may lead to tissue heating are discussed. In chapter 2, an empirical procedure is described to estimate the minimal power required to obtain adequately decoupled spectra. This procedure also enables one to calculate the RF energy deposited in the body during ^{1}H decoupled ^{13}C MR spectroscopy. It was shown that for the human head, liver, muscle gastrocnemius and muscle vastus lateralis decoupling could be performed within RF deposition safety guidelines.

In chapter 3 the thermoregulatory response of the skin was investigated during prolonged exposure to several levels of RF radiation by a surface coil. Temperature changes induced by RF radiation were measured at the skin of the calf muscle by a fluoroptic probe. Although the temperature increase was higher at higher applied RF levels, these values did not exceed the recommended temperature limit for the extremities. This implies that there is a contradiction between the current guidelines for safe MR operation regarding RF specific absorption rate and temperature limits for the extremities. The guidelines for specific absorption rate may be too conservative for humans with normal thermoregulatory function.

In chapter 4 the potential of heteronuclear {^{1}H-^{13}C} cross polarization was studied for optimization of the signal to noise ratio in *in vivo* ^{13}C MR spectroscopy. Experiments on the human calf showed a signal gain over tenfold by combined application of polarization transfer NOE and decoupling. Heteronuclear polarization transfer seems most promising for the study of dynamic processes, especially when specific ^{13}C labeled compounds are introduced. A dynamic study of inflow of ^{13}C-1-glucose in the neonatal piglet brain was perfumed.

In chapter 5 the muscle glycogen recovery was examined with glucose feeding in comparison to fructose feeding during the first eight hours after partial glycogen depletion using ^{13}C MR spectroscopy. After measuring the glycogen concentration of the vastus lateralis (VL) muscle, glycogen stores of the VL were depleted by bicycle exercise. During eight hours following completion of exercise, subjects were orally given either glucose or fructose, while the glycogen content of the VL was monitored by ^{13}C-NMR spectroscopy. The glycogen recovery rate during glucose feeding was significantly higher compared to fructose feeding.

The uptake of glucose in muscle and its metabolism to glycogen in response to insulin is reduced in diabetes. To investigate these processes *in vivo* ^{13}C MR spectroscopy was applied in combination with the infusion of labelled ^{13}C glucose. Furthermore, the effect of troglitazone on insulin sensitivity was assessed. The results, as described in chapter 6, showed a correlation between the glycogen synthesis rate and the whole body glucose uptake. With the use of ^{13}C MR spectroscopy, *in vivo* muscular glucose levels could be detected, and showed a positive, linear correlation with glycogen synthesis rate. The improved glycogen synthesis rate after treatment with Troglitazone is a good indication for a positive effect of this drug on insulin resistance.

Magnetische Resonantie Imaging (MRI) wordt tegenwoordig routinematig toegepast voor het verkrijgen van anatomische afbeeldingen. Magnetische Resonantie Spectroscopie (MRS) levert een spectrum op in plaats van een anatomische afbeelding. Het spectrum bevat informatie over de chemische samenstelling van het onderzochte weefsel. Daar MRS een noninvasieve techniek is, is het een aantrekkelijk alternatief voor invasieve biopsiemethoden.

In hoofdstuk 1 worden de huidige ontwikkelingen in *in vivo* ^{13}C-MRS gericht op humane fysiologie en pathologie beschreven. De toepassing en voordelen van dubbelresonantie technieken zoals protonontkoppeling en polarisatietransfer worden beschreven samen met de daarvoor benodigde speciale Radio Frequente (RF) spoelontwerpen. Tenslotte wordt er een overzicht gegeven van lokalisatietechnieken en quantificatiemethoden.

In de hoofdstukken 2 en 3 wordt er aandacht besteed aan de veiligheid van MRS. Met name de absorptie van RF-energie, die kan leiden tot lokale opwarming van het weefsel, komt hier aan de orde. In hoofdstuk 2 wordt een methode beschreven, die het mogelijk maakt de minimaal benodigde energie te bepalen waarbij adequaat ontkoppelde spectra kunnen worden verkregen. Deze methode kan bovendien gebruikt worden om te bepalen aan welke hoeveelheid RF-straling het lichaam wordt blootgesteld. Met behulp van deze methode is aangetoond, dat protonontkoppeling tijdens ^{13}C-MR spectroscopie van het hoofd, lever of beenspieren toegepast kan worden binnen veiligheidsrichtlijnen.

In hoofdstuk 3 wordt de temperatuurstijging van de huid onderzocht als gevolg van langdurige blootstelling aan verschillende niveaus van RF-straling. Ofschoon er een relatie is tussen het RF-stralingsniveau en de bereikte temperatuur wordt bij vermogens boven de richtlijnen de temperatuurlimiet, opgesteld voor de extremiteiten, niet overschreden. De resultaten suggereren dat er een tegenstrijdigheid is tussen de temperatuur- en vermogenslimieten voor de extremiteiten.

De mogelijkheden van heteronucleaire (^{1}H-^{13}C) polarisatie transfer technieken ter verbetering van de gevoeligheid worden onderzocht in hoofdstuk 4. Meer dan een tienvoudige verbetering was haalbaar voor onderhuids vetweefsel door toepassing van zowel polarisatietransfer, "NOE" en protonontkoppeling. Deze techniek is het meest waardevol voor de bestudering van dynamische processen met specifiek ^{13}C gelabelde verbindingen zoals glucose. De toepasbaarheid hiervan is succesvol getoetst op de hersenen van een biggetje.

In hoofdstuk 5 wordt met behulp van *in vivo* ^{13}C MRS het herstel van spierglycogeen onderzocht tijdens voeding met glucose in vergelijking tot voeding met fructose. Na het meten van de basale spierglycogeenconcentraties met ^{13}C MRS, werd de spier uitgeput door uitvoering van een fietsprotocol. Gedurende de eerste 8 uur in de herstelfase werden ^{13}C MRS metingen afgewisseld met suikeropname (glucose of fructose). Glucosevoeding resulteerde in een significant sneller spierglycogeenherstel dan fructosevoeding.

De opname in de spier van glucose en de omzetting daarvan in glycogeen onder invloed van insuline spelen een belangrijke rol in de pathologie van diabetes. Om deze processen te kunnen meten werd ^{13}C MRS toegepast in combinatie met infusie van specifiek gelabeld ^{13}C-1-glucose. Daarnaast werd het effect van het medicijn Troglitazone op insulineresistentie onderzocht. De resultaten van dit onderzoek zoals beschreven in hoofdstuk 6, lieten een correlatie zien tussen de insulinegevoeligheid en de glycogeensynthese-snelheid. Daarnaast was er ook een positieve lineaire correlatie tussen het totale spierglucosegehalte en de glycogeensynthese. De verhoging van de glycogeensynthese als gevolg van behandeling met het middel Troglitazone in insuline resistente personen is een goede indicatie voor de positieve werking van het medicijn.

De totstandkoming van dit proefschrift was geen sinecure voor de betrokken promovendus. Zonder de invloed en betrokkenheid van vele mensen zou dit resultaat niet voor u liggen. Het is mij dan ook een groot genoegen om iedereen die heeft bijgedragen te kunnen bedanken. Een aantal van hen zal ik noemen, in de hoop niemand te kort te doen.

Bedankt:

- Prof. dr. A. Heerschap, kortweg Arend, jij zal wel verheugd zijn dat het eerste 'klinische' MR spectroscopische boekje voltooid is. Je hebt richting gegeven aan het onderzoek zonder mij in mijn wetenschappelijke vrijheid te beperken.
- Erik van den Boogert voor je praktische blik op 'alles' en je handigheid met de soldeerbout. Voor die ene keer het lenen van je ATB.
- Ad de Koster voor je introductie in de MR spectroscopie.
- Mijn kamergenoten Marinette van der Graaf, Boudewijn van der Sanden en René in 't Zandt voor de vele discussies die soms ook wetenschappelijk waren. Marinette dank ik in het bijzonder voor het 'moederen' tijdens de congresbezoeken.
- Mark Rijpkema.
- Alle laboranten MR voor de vele gezellige uren en voor al die keren dat ik snel even tussendoor mocht experimenteren. In het bijzonder dank ik Kevin Pouwel, Jolanda van Nieuwkerk, Denise Janssen-Bell en Yvonne van der Meulen voor het delen van hun kennis van imaging protocollen.
- Sibrand Houtman, Maria Hopman, Berend Oeseburg, Cees Tack, Paul Smits, Gerald Vervoort, Arnoud Janssen van Roosendaal voor hun expertise.
- Yvonne Wolbert-Heidkamp voor de speciale spectroscopie software.
- Marietta Domensino voor haar inzet.
- Leon van Erning voor zijn kritische blik en zijn positieve opstelling.
- Wim Guyt en Arnoud van Gemert voor de informatietechnologische ondersteuning.

- Theo Arts en Gerrie Grutters voor hun deskundigheid bij het uitvoeren van experimenten met proefdieren.
- Michel Pawlicz.
- De technici Piet ten Bhömer en Barry van Haaren voor het 'in shape' houden van de MR.
- Marijke en Marijke, de ene voor de Afrikaanse cd's de andere voor het ATB'en.
- Udo Engelke en verder iedereen van het CKSL betrokken bij de opwerking van plasmamonsters.
- Alle medewerkers secretariaat Radiologie.
- Jos Joordens en alle anderen bij de hf-NMR faciliteit voor het meten op de 600 MHz.
- Peter van Zijl, Delphine Davis and Dimitri Artemov at the Johns Hopkins Medical School.
- Joost den Otter voor zijn relativering van *de wetenschap* tijdens de vele sportieve uren en daarop volgende 'koffiesessies'.
- Iedereen die zichzelf heeft laten verleiden tot een MR onderzoek.
- Mijn ouders die mij de mogelijkheid hebben geboden te studeren. Zij hebben mij geleerd af te maken waar ik aan begonnen ben. Daarnaast dank ik hun voor hun doorlopende interesse in de vaak moeilijke materie.
- Tenslotte blijkt de niet wetenschappelijke steun de belangrijkste te zijn voor de voltooiing van een proefschrift, **Esther bedankt!**

Curriculum vitae

Adrianus Johannes van den Bergh werd geboren op 20 oktober 1966 te Breda. In 1984 behaalde hij zijn HAVO-diploma aan de Katholieke Scholengemeenschap Markenhage. Datzelfde jaar begon hij aan de opleiding tot analytisch chemicus/biochemicus aan de HLO te Breda, waarvoor in 1988 met succes het examen werd afgelegd. Als stage binnen deze opleiding verrichtte hij bij Gist Brocades te Delft (dr. ir. O. Misset) en Organon International b.v. te Oss (dr. C.W. Funke) onderzoek wat zich richtte op de stabiliteit en activiteit van biologische vlekoplossers (proteasen) en op de toepassingen van fourier transform infrarood spectroscopie. In een afstudeeropdracht bij de laatstgenoemde organisatie deed hij onder leiding van dr. J-R. Mellema structuur analyse onderzoek naar enkele oligopeptiden met behulp van geavanceerde 2D NMR-spectroscopie.

In aansluiting op de vervulling van de dienstplicht in 1989 te Roosendaal als hospik, vervolgde hij zijn opleiding in de vorm van een doctoraalstudie aan de Katholieke Universiteit Nijmegen. In de studierichting Scheikunde koos hij als hoofdvak Farmaco-Chemie. Onder begeleiding van prof. dr. C.A.M. van Ginneken ✞, dr. F.G.M. Russel, dr. R. de Miranda, dr. P. Cox en mevrouw dr. S. Boom werd onderzoek verricht naar organisch aniontransport in proximale tubuluscellen uit de rattenier. In januari 1992 werd het doctoraal examen afgelegd.

Vanaf februari 1992 tot februari 1997 was hij als assistent in opleiding werkzaam bij de afdeling Radiologie van het Academisch Ziekenhuis Nijmegen St. Radboud. Het tijdens deze periode uitgevoerde onderzoek, begeleid door prof. dr. A. Heerschap, staat beschreven in dit proefschrift.

De heer A.J. van den Bergh heeft in 1994 een stipendium ontvangen voor een korte wetenschappelijk stage aan de Johns Hopkins Medical School, Department of Radiology, in Baltimore USA. Aldaar werden diverse dubbel resonantie technieken en protocollen voor de humane toediening van 13C gelabeled materiaal bestudeerd.

In de periode na het AIO-schap tot oktober 1998 was A.J. van den Bergh als onderzoeker werkzaam aan een onderzoek gesubsidieerd door Glaxo Wellcome. Dit project is totstandgekomen in samenwerking met de vakgroep Farmacologie (prof. dr. P. Smits), de afdeling Interne Geneeskunde (dr. C.J.J. Tack en drs. G. Vervoort) en de afdeling Radiologie (prof. dr. A. Heerschap) van het Academisch Ziekenhuis Nijmegen St. Radboud.

Thans is A.J. van den Bergh als onderzoeker betrokken bij een project met als doel het meten van foetale hersenen met behulp van 1H MR spectroscopie.

List of Publications

Articles

1. R. Masereeuw, A. J. van den Bergh, R. J. Bindels, F. G. Russel, Characterization of fluorescein transport in isolated proximal tubular cells of the rat: evidence for mitochondrial accumulation. *J. Pharmacol. Exp. Ther.,* **269,** 1261-1267, (1994).
2. A. J. van den Bergh, S. Houtman, A. Heerschap, N. J. Rehrer, H. J. van den Boogert, B. Oeseburg, M. T. Hopman, Muscle glycogen recovery after exercise during glucose and fructose intake monitored by 13C-NMR. *J. Appl. Physiol.,* **81,** 1495-1500, (1996).
3. A. J. van den Bergh, H. J. van den Boogert, A. Heerschap, Calibration of the 1H decoupling field strength and experimental evaluation of the specific RF absorption rate in 1H-decoupled human 13C- MRS. *Magn. Reson. Med.,* **39,** 642-646, (1998).
4. A. J. van den Bergh, H. J. van den Boogert, A. Heerschap, Heteronuclear cross polarization for enhanced sensitivity of in vivo 13C MR spectroscopy on a clinical 1.5 T MR system. *J. Magn. Reson.,* **135,** 93-98, (1998).
5. A. Heerschap, C. Houtman, H. J. A. in 't Zandt, A. J. van den Bergh, B. Wieringa, Introduction to in vivo 31P MR spectroscopy of (human) skeletal muscle. *Proc. Nutr. Soc.,* (1999). **In Press**

Abstracts

1. S. Houtman, A. J. van den Bergh, N. J. Rehrer, H. J. van den Boogert, A. Heerschap, B. Oeseburg, M. T. E. Hopman, Muscle glycogen resynthesis using 13C-NMR spectroscopy following depletion: a comparison between glucose and fructose feeding. *Med. Sci. Sports. Exerc.,* **27(5),** s168, (1995).
2. A. J. van den Bergh, H. J. van den Boogert, A. Heerschap. Spatially localized calibration of the decoupler radio frequency field strength, *in* "SMR 2nd Meeting, San Francisco, 1994," p. 760.
3. A. J. van den Bergh, H. J. van den Boogert, A. Heerschap. Natural abundance 13C CSI of the human brain, *in* "SMR 2nd Meeting, San Francisco, 1994," p. 567.

4. A. J. van den Bergh, S. Houtman, A. Heerschap, N. J. Rehrer, H. J. van den Boogert, B. Oeseburg, M. T. Hopman. Muscle glycogen resynthesis during glucose and fructose feeding, monitored by in vivo 13C-MR spectroscopy, *in* "SMR 3rd Meeting, ESMRMB 12th Meeting, Nice, 1995," p. 423.
5. A. J. van den Bergh, H. J. van den Boogert, A. Heerschap, Dubbelresonantie technieken voor in vivo 13C NMR. *Klinische fysica* **2,** 32, (1995).
6. A. J. van den Bergh, H. J. van den Boogert, A. Heerschap, Nieuwe RF-spoel ontwerp voor multi-nucleaire MRI/MRS. *Klinische fysica* **4,** 31, (1995).
7. A. J. van den Bergh, H. J. van den Boogert, A. Heerschap. Evaluation of the SAR for broadband proton decoupled 13C MRS in humans, *in* "ESMRMB 13th Annual Meeting, Prague, 1996," p. 69.
8. A. J. van den Bergh, H. J. van den Boogert, A. Heerschap. In vivo three dimensional 13C chemical shift imaging of the human brain, *in* "ISMRM 4th Annual Meeting, New York, 1996," p. 1215.
9. A. J. van den Bergh, C. J. J. Tack, A. Heerschap, P. Smits. In vivo 13C-MR-spectroscopische metabole flux meting bij de mens, *in* "Nederlandse vereniging voor diabetes onderzoek, Breda, 1996
10. A. J. van den Bergh, H. J. van den Boogert, A. Heerschap. Euglycemic-hyperinsulinemic clamp in healthy volunteers and insulin resistant obese subjects monitored with in vivo 13C-MR spectroscopy, *in* "ISMRM 5th Annual Meeting, Vancouver, 1997," p. 365.
11. A. J. van den Bergh, H. J. van den Boogert, H. Heerschap. In vivo 13C-NMR spectroscopy of humans: a comparison between WALTZ-4 and adiabatic broadband 1H decoupling schemes, *in* "ISMRM 5th Annual Meeting, 1997," p. 1347.
12. A. J. van den Bergh, C. J. J. Tack, H. J. van den Boogert, P. Smits, A. Heerschap. Glycogen synthesis rate, as monitored by 13C MRS during an euglycemic-hyperinsulinemic clamp, reflects insulin sensitivity, *in* "ESMRMB 14th annual meeting, Brussels, 1997," p. 95.
13. A. J. van den Bergh, L. VanHamme, S. van Huffel, A. Heerschap. Improving the SNR of glycogen detection in 13C MRS by multiexponential signal fitting using prior knowledge, *in* "ESMRMB 14th annual meeting, Brussels, 1997," p. 571.

14. A. J. van den Bergh, C. J. J. Tack, P. Smits, A. Heerschap. Glycogen synthesis rate as monitored by 13C MR spectroscopy reflects insulin sensitivity, *in* "Nederlandse vereniging voor diabetes onderzoek, Den Haag, 1997,"
15. A. J. van den Bergh, C. J. J. Tack, P. Smits, A. Heerschap, Euglycemic-hyperinsulinemic clamp in healthy volunteers and insulin resistant obese subjects monitored with in vivo 13C-MR spectroscopy. *Netherlands Journal of Medicine* **50,** a45, (1997).
16. A. J. van den Bergh, H. J. van den Boogert, A. Heerschap. Skin temperature in humans remains below 40 C during local exposure of high power RF levels applied by a surface coil as used during proton decoupled MRS, *in* "ESMRMB 15th Annual Meeting, Geneva, 1998," p. 99.
17. H. J. van den Boogert, A. J. van den Bergh, H. Heerschap. A multipurpose coil configuration for 1H decoupled 31P or 13C MRS, *in* "ISMRM 4th Annual Meeting, New York, 1996," p. 1423.

MISSIE

Glaxo Wellcome is een op wetenschappelijk onderzoek gebaseerd bedrijf waarvan de werknemers zich inzetten voor de bestrijding van ziekten. Zij doen dit door het ontwikkelen van innovatieve medicijnen en services, voor patiënten en hun zorgaanbieders overal ter wereld.